NASA CR-54573
MARCH 1971
Allison EDR 6060

Single-Stage Experimental Evaluation of Boundary Layer Bleed Techniques for High Lift Stator Blades

V. — Final Report

Prepared for

NATIONAL AERONAUTICS AND SPACE ADMINISTRATION

Contract NAS3-7619 and NAS3-7900

Detroit Diesel Allison
Division of General Motors Corporation

CONTRACTOR REPORT

SINGLE-STAGE EXPERIMENTAL EVALUATION OF BOUNDARY LAYER BLOWING AND BLEED TECHNIQUES FOR HIGH LIFT STATOR BLADES

V. Final Report

By R. J. Loughery, R. A. Horn, Jr., and P. C. Tramm

Prepared under Contracts NAS3-7619 and NAS3-7900

General Motors Corporation

Indianapolis, Indiana

Technical Management

Lewis Project Manager: William L. Beede

Lewis Research Advisor: L. Joseph Herrig

Detroit Diesel Allison Division EDR 6060

Lewis Research Center Cleveland, Ohio

NATIONAL AERONAUTICS AND SPACE ADMINISTRATION

ABSTRACT

Tests were conducted on a single-stage compressor rig to determine the feasibility of increasing stator blade loading beyond current levels by bleeding or blowing the suction surface boundary layer. The compressor rig employed stator hub and tip end wall boundary layer bleeds. Six highly loaded stator configurations were tested. One of the configurations employed no suction surface boundary layer bleeding or blowing features and was used to establish a performance base line. Two stator configurations provided for suction surface boundary layer bleed and the other three stator configurations employed features to reenergize the suction surface boundary layer by blowing.

A significant improvement in stator performance was achieved with suction surface boundary layer bleed compared to the base line configuration. Performance with suction surface boundary layer blowing was generally inferior to that of the base line configuration.

TABLE OF CONTENTS

LIST OF ILLUSTRATIONS

LIST OF TABLES

SINGLE-STAGE EXPERIMENTAL EVALUATION OF BOUNDARY LAYER BLOWING AND BLEED TECHNIQUES FOR HIGH LIFT STATOR BLADES

V. FINAL REPORT*

By
R. J. Loughery, R. A. Horn, Jr., and P. C. Tramm

Detroit Diesel Allison Division, GM

SUMMARY

The objective of this program was to determine experimentally the feasibility of increasing stator blade loading beyond current levels by bleeding or blowing the suction surface boundary layer.

Tests were conducted on a single-stage compressor rig. Six stator configurations were tested. The stator design conditions were selected to be typical of those found in middle and latter stages of a highly loaded multistage compressor. Stator hub and tip wall bleed was employed in these comparative tests to remove the possibility of end wall boundary layer separation. Flow into the stator was generated by a row of inlet guide vanes and a state-of-the-art flow generating rotor.

The six stator configurations differed with respect to design loading level and the suction surface boundary layer control features used in the designs. A summary of the six stator configurations follows:

Stator hub (D_t)	Stator blade type (bleed-blowing)	No. of slots	Slot location (% chord along suction surface)
0.65	Bleed	1	60
0.65	Blowing	1	42
0.75	Bleed	3	25, 41, 61
0.75	Blowing	1	39.25
0.75	Blowing	2	40, 69.5
0.75	Unslotted	---	---

*This report supersedes NASA CR54565, CR54571, CR54570, CR54572, CR54566, and CR54567. Measurement errors have been found in data presented in these reports.

The unslotted stator configuration was used to establish a performance base line for the 0.75 D_f slotted bleed and blowing configurations.

Each stator configuration was tested in the single-stage rig to determine stator blade element performance and stage overall performance. The intent was to determine stator blade element performance at 10, 30, 50, 70, and 90% span locations. Because of measurement errors, much of the data was deleted and comparison of the configurations was made at the 50% span location only. Blade element performance at the midspan location is presented as loss coefficient, deviation angle, and diffusion factor versus incidence angle, and loss parameter versus diffusion factor.

A summary of results based on a midspan blade element performance comparison follows.

1. A significant improvement in blade element performance was achieved with suction surface boundary layer bleed compared with the unslotted stator configurations.
2. Blade element performance with suction surface boundary layer blowing was generally inferior to that of the unslotted stator configuration.
3. The data suggest that design of the slotted blowing stator configurations may not have been optimum. Possible improvements could be obtained by a modified choice of suction surface slot location and by modifications to the blade leading edge.

Stator end wall bleed improved stage overall efficiency by about 2%. This gain was a result of bleeding the hub end wall; the tip end wall did not respond to bleed.

INTRODUCTION

For future gas turbine power plants, higher compressor stage pressure ratios are desired and adequate stage flow range must be achieved at these increased work levels. Increased stage pressure ratio can lead to increased turning and diffusion for the rotor and stator blades. The result is an increase in diffusion locally near blade suction surfaces which, when increased sufficiently, causes the useful operation of the airfoils to be terminated by severe suction surface boundary layer separation. There is considerable analytical and empirical evidence that boundary layer separation can be delayed by energizing or removing the low energy fluid near the airfoil surface. In view of these considerations, an experimental program was undertaken involving a single-stage compressor rig. The objective of the program was to determine experimentally the feasibility of increasing stator blade loading beyond current levels by bleeding or blowing the suction surface boundary layer.

Six stator configurations—one unslotted, three slotted blowing, and two slotted bleed—were tested in combination with an inlet guide vane and flow generating rotor. Design information for the two slotted bleed stator configurations and the three slotted blowing stator configurations is contained in References 1 and 2, respectively. The compressor rig incorporated special features to remove low energy fluid from the boundary layer adjacent to the stator hub and tip. These features were incorporated to preclude a possibility of stator hub and tip boundary layer separation. Performance of the inlet guide vane and flow generating rotor is reported in Reference 3. Performance of the six stator configurations is reported in References 3, 4, 5, 6, 7, and 8. A review of the stator test data and data reduction procedures has shown that the results reported in References 3, 4, 5, 6, 7, and 8 are in error. The sources of error are reported in the Apparatus and Procedures section of this report. A reevaluation of the data has shown that a valid and reasonably complete comparison of performance for the six stator configurations could be made at the 50% streamline station only.

This report presents a summary and comparison of the performance of the six stator configurations at the 50% streamline station. Data presented in this report supersedes all blade element and overall performance data in References 3, 4, 5, 6, 7, and 8.

SYMBOLS

A_e Elemental area, ft^2

C_f Skin friction coefficient, $\frac{\tau_w}{q}$

c Blade chord, in.

D_f Diffusion factor

H_i Boundary layer shape parameter, $\left(\frac{\text{incompressible displacement thickness}}{\text{incompressible momentum thickness}}\right)$

i Incidence angle, degrees (See Figure 3.)

M Mach number

$\dot{m}$ Bleed rate per blade, lb_m/sec

N Rotational speed, rpm

n	Number of blades
P	Total or stagnation pressure, psia
p	Static or stream pressure, psia
q	Dynamic pressure, psia ($1/2\ \rho V^2$)
R	Radius, in.
R_c	Total pressure ratio
S	Airfoil surface pressure coefficient, $\left(\frac{P_2 - p}{q_2}\right)$
s	Blade spacing, in.
T	Total temperature, °R
t	Blade thickness, in.
t/c	Blade thickness chord ratio
U	Rotor tangential velocity, ft/sec
V	Velocity, ft/sec (See Figure 2.)
W_a	Compressor airflow, lb_m/sec

Greek

α	Streamline angle, degrees (See Figure 2.)
β	Airflow angle, degrees (See Figure 2.)
γ	Ratio of specific heats
$\gamma°$	Blade chord angle, degrees (See Figure 3.)
Δi	Range angle, degrees (See Figure 20.)
$\Delta\beta$	Turning angle, degrees ($\Delta\beta_R = \beta'_1 - \beta'_2$, $\Delta\beta_S = \beta_2 - \beta_3$)
δ	Ratio of stage inlet total pressure to standard sea level pressure of 14.7 psia

δ°	Deviation angle, degrees (See Figure 3.)
ϵ	Circumferential rake setting angle, degrees
η	Efficiency
θ	Ratio of stage inlet total temperature to standard sea level temperature of 518.6°R
κ	Blade metal angle, degrees (See Figure 3.)
ρ	Static or stream density, lb_m/ft^3
σ	Blade row solidity, (c/s)
τ_w	Wall shear stress, lb_f/ft^2
ϕ	Camber angle, degrees (See Figure 3.)
ω	Local total pressure loss coefficient (See Equation A6.)
$\bar{\omega}$	Blade element total pressure loss coefficient (See Equation A7.)

Subscripts

ad	Adiabatic
fs	Free stream
h	Hub
ma	Mass flow averaged
min	Minimum
neg	Negative
pos	Positive
R	Rotor
S	Stator
ST	Stage
t	Tip

z	Axial direction
θ	Tangential direction
θz	Tangential-axial plane
0	Guide vane inlet
1	Rotor inlet or guide vane exit
2	Stator inlet or rotor exit
3	Stator exit

Superscripts

'	Relative to rotor

DESIGN

The test rig used in this program was designed to test stators with hub loading levels of 0.65 and 0.75 D_f.

A row of inlet guide vanes and a flow generating rotor were designed within the current state of the art to provide the selected inlet conditions to the stators. The flow path dimensions are shown in Figure 1. The design values of the flow generating rotor were:

$W_a\sqrt{\theta}/\delta$	= 88.2 lb/sec
$R_{c,R}$	= 1.37
$\eta_{ad,R}$	= 88.8%
$N/\sqrt{\theta}$	= 8367 rpm (1095 ft/sec tip speed)
R_h/R_t (rotor inlet)	= 0.683
D_f rotor tip	= 0.414

The design of the inlet guide vane and rotor is reported in Reference 2.

The stator inlet hub Mach number was 0.75 at an inlet flow angle of 54 degrees and the stator inlet hub-to-tip radius ratio was 0.696. The stator blade airfoil section selected was a 65-series thickness distribution with a circular arc mean-line shape. Stators were designed at hub loading levels of both 0.65 and 0.75 D_f.

Nomenclature used for velocity diagrams and blade description is shown in Figures 2 and 3. The rotor design velocity diagrams are shown in Figure 4. The design velocity diagrams for the 0.65 D_f and 0.75 D_f stators are shown in Figures 5 and 6. Since the radial component of velocity is relatively small, values of V are shown in velocity diagrams in places where $V_{\theta z}$, literally, should be shown.

Stator blade airfoil properties are given in Table I. These properties were used for both slotted and unslotted configurations. One unslotted and five slotted stator configurations were designed. A summary of these configurations follows:

Stator hub (D_f)	Stator blade type (bleed-blowing)	No. of slots	Slot location (% chord along suction surface)
0.65	Bleed	1	60
0.65	Blowing	1	42
0.75	Bleed	3	25, 41, 61
0.75	Blowing	1	39.25
0.75	Blowing	2	40, 69.5
0.75	Unslotted	---	---

Blade sections for these configurations are shown in Figure 7. These stators were cast with a hollow core and only two basic designs were made, i.e., 0.65 and 0.75 D_f. For the blowing slotted configurations, high pressure air was ingested on the pressure surface at the blade leading edge. This air passed through a cored section of the blade and was discharged through a slot or slots on the suction surface. The design of the blowing slotted stators is reported in more detail in Reference 2. For the bleed slotted configurations, air from the suction surface of the blade was bled through a slot or slots into the core which was connected to an external pumping source. The design of the bleed slotted stators is reported in more detail in Reference 1.

APPARATUS AND PROCEDURES

TEST FACILITY

A general arrangement of the test facility is shown in Figure 8. Air entered the test compressor after passing through the test facility filter house, an inlet duct, plenum, and bell mouth, and was exhausted to the atmosphere through a diffuser. Provisions existed for maintaining compressor inlet pressures above or below atmospheric, if necessary.

COMPRESSOR TEST RIG

The mechanical arrangement of the compressor test rig was similar for all testing. The only differences were the stator configuration incorporated in the rig and, in the case of the slotted bleed stator tests, a connection to a vacuum source to remove the bleed air. A typical layout of the compressor test rig for a slotted bleed stator test is shown in Figure 9. Provision was also made in the rig for bleeding the wall boundary layers at stator tip and hub. This was accomplished by fabricating the stator flow passage walls

from 0.010 in. thick perforated sheet metal. Manifolds behind the perforated metal surfaces were connected by multiple tubes to separate vacuum headers for tip and hub wall bleeds. A pressure drop was maintained across the porous wall during all testing to ensure the structural integrity of the perforated metal.

INSTRUMENTATION

Instrumentation was provided to obtain blade element performance for the stator and stage overall performance. Figure 1 defines the axial location of the various instrumentation planes. The following is a summary of the instrumentation* used in each plane:

- Inlet plenum
  - 6 single-element total pressure probes
  - 2 six-element radial total temperature rakes
  - 2 outer wall static pressure taps
- Rotor inlet (Station 1)
  - 3 radial traverse combination total pressure and yaw angle probes
  - 1 radial traverse wedge static pressure probe
  - 4 outer wall static pressure taps
  - 4 inner wall static pressure taps
- Stator inlet (Station 2)
  - 3 radial traverse combination total pressure, total temperature, and yaw angle probes
  - 2 radial traverse wedge static pressure probes
  - 4 outer wall static pressure taps
  - 4 inner wall static pressure taps
  - 2 fixed hot wire annemometers
  - 1 radial traverse hot wire annemometer
- Stator exit (Station 3)
  - 1 radial traverse 16-element circumferential total pressure rake
  - 1 radial traverse combination total pressure, total temperature, and yaw angle probe
  - 2 radial traverse wedge static pressure probes
  - 4 five-element radial total temperature rakes
  - 1 outer wall five-element total pressure boundary layer rake
  - 1 inner wall five-element total pressure boundary layer rake
  - 4 outer wall static pressure taps
  - 4 inner wall static pressure taps

OVERALL AND BLADE ELEMENT PERFORMANCE DATA

Overall and blade element performance data were obtained at five points per speed line to define rotor or stage performance between choke and stall. The stage stall point was defined as the onset of a steady stall cell indication on the hot wire anemometers. One of the five points on each speed line was a near-stall setting which permitted a full data point recording. At each full data point, fixed and traverse pressure and temperature data were recorded at five radial locations at the stator inlet and exit measurement planes.

*This instrumentation is discussed in Reference 3.

DATA EDITING

Review of the data obtained during the stator testing indicated that an error exists in the information presented in References 3, 4, 5, 6, 7, and 8. The circumferential rake at stator discharge was designed to survey a passage between adjacent blades with the leading edge of the rake perpendicular to the compressor axis. Preliminary test results indicated that the air angle at stator exit was considerably different from the design intent. A decision was made to rotate the wake probe to provide better alignment of the probe with the stator exit air angle. The rake angle used in each test is shown in Table II. Unfortunately, the fact that the probe had been reset was not accounted for in the reduction of data. This resulted in an error in the mass averaging of the data circumferentially. Also, for a large part of the testing the yaw probe at stator exit was in the blade wake, making its angle reading of doubtful accuracy. These inequities in the data resulted in a complete reevaluation of all data obtained. The following data editing criteria were used to establish the validity of the data.

1. Air angle at stator exit measured by the yaw probe was not used when the yaw probe was in the stator wake. This condition was determined by identifying the yaw probe with a circumferential rake element in the same relative circumferential location. The wake was defined as an area of steep total pressure gradient as measured by the circumferential rake.
2. Total pressure at the stator exit measured by the circumferential rake was not used when the element of the rake corresponding to the same relative circumferential position as the yaw probe differed in reading by more than 0.5 in. Hg from the yaw probe reading.

At the 50% streamline station about one-half of the data met the first criterion and about three-fourths of the data met the second criterion. At the 30 and 70% streamline stations about one-tenth of the data met both criteria. At the 10 and 90% streamline stations about one-seventh of the data met both criteria. The results of the data editing led to the decision to present only the blade element data obtained at the 50% streamline station. The data at the 50% streamline station which satisfied both criteria are given in Table III. The effect of exit air angle on the calculation of $\bar{\omega}$ is minimal. Therefore, additional data at the 50% streamline station which met only the second criterion are included in the $\bar{\omega}$ vs incidence plots to provide a more complete picture of the stator loss characteristics.

DATA REDUCTION

Data reduction was performed by two separate computer programs. The first program was used to calculate overall stage performance, stator

blade element performance and wall bleed flow rate. Calculations were carried out for the five streamlines which passed through the 10, 30, 50, 70, and 90% span stations at the stator inlet measurement plane. The second program was used to determine the stator blade static pressure distribution and calculate the blade boundary layer control blowing and bleed flow rates. Calculations were performed at the 10, 50, and 90% span station which corresponded to the locations of the blade static pressure instrumentation. A summary of the equations used in these two programs is given in the Appendix.

In many cases, redundant data were obtained. When redundant information was available for a particular quantity, the consequences of selecting the various options were investigated and a judgment was made as to the best option. The following is a list of sources of data used in the data reduction programs to calculate velocity triangles:

- Stator inlet (Station 2)
  - Static pressure (p_2) vs radius—The four static pressure readings were arithmetically averaged at the outer and inner walls; static pressure was obtained as a linear interpolation from these average wall static pressures. Since wall curvature and convergence were small, linear interpolation was a good approximation. Reference 3 presents a discussion of the merits of this procedure in comparison with the use of readings from the radial traverse wedge static pressure probes.
  - Total pressure (P_2), total temperature (T_2), and yaw angle (β_2) vs radius—An arithmetic average of the readings from the three radial traverse combination probes was used.
- Stator exit (Station 3)
  - Static pressure (p_3) vs radius—The four static pressure readings were arithmetically averaged at the outer and inner walls, and static pressure was obtained as a linear interpolation from these average wall static pressures.
  - Total pressure ($P_{3,\ ma}$) vs radius—The radial traverse 16-element circumferential total pressure rake data were used to obtain total pressure at each radial location. The rake data were mass flow averaged across one blade gap according to Equation (A8) in the Appendix.
  - Total temperature (T_3) vs radius—The readings from the four five-element radial total temperature rakes were arithmetically averaged at each of the five radial locations.
  - Yaw angle (β_3) vs radius—The radial traverse combination probe was used to obtain yaw angle.

Stator Blade Element Performance

Synthesis of the velocity triangles at stator inlet and exit provided the required information to calculate diffusion factor, deviation angle, and

incidence angle according to Equations (A3), (A4), and (A5) of the Appendix. Blade element total pressure loss coefficient was calculated by Equation (A7) of the Appendix. The numerator of Equation (A7) is one minus stator total pressure recovery. The choice was made to define recovery as mass flow averaged total pressure at stator exit—Equation (A8)—divided by the maximum total pressure as read by the 16-element circumferential rake, $P_{3,fs}$. Using $P_{3,fs}$ in preference to an arithmetic average of the three radial traverse combination probes at stator inlet, P_2, is a difference which exists in the stator blade element data presented in this report and the data previously presented in References 3, 4, 5, 6, 7, and 8.

Total Pressure Loss Coefficient Contour Plots

Stator local total pressure loss coefficient for contour plots was obtained using Equation (A6) of the Appendix. The quantity P_3 is a function of both radius and tangential location. It was obtained from the radial traverse 16-element circumferential rake and was divided by P_2, the average of the three radial traverse combination probes at stator inlet. A preference was made for P_2 rather than $P_{3,fs}$ in these presentations of data to give a more accurate evaluation of the end-wall effects.

Stage Overall Performance

The quantities required to define stage overall performance were obtained by use of the following procedures.

- Stage exit total pressure ($P_{3,ma}$)—Circumferentially mass flow averaged total pressure at stator exit ($P_{3,ma}$ vs radius) was mass flow averaged radially to obtain the required average stage exit total pressure.
- Stage exit total temperature ($T_{3,ma}$)—The arithmetically averaged total temperature rake data at stator exit (T_3 vs radius) was mass flow averaged radially to obtain the required average stage exit total temperature.
- Stage inlet total pressure (P_0)—The six single-element total pressure probes in the inlet plenum were at varying radial depths. The total pressure was assumed to be uniform circumferentially, and stage inlet total pressure was obtained by radially mass flow averaging the total pressure as measured by these six probes.
- Stage inlet total temperature (T_0)—Inlet plenum total temperature was averaged for the two rakes at each of the six radial locations, and stage inlet total temperature was obtained by radially mass flow averaging the inlet plenum total temperature.

The stage inlet airflow was measured with an ASME orifice located in each branch of the triple inlet header upstream of the inlet plenum. Weight flow was corrected to stage inlet conditions according to Equation (A1), and stage efficiency was calculated according to Equation (A2) of the Appendix.

DISCUSSION OF RESULTS

The following discussion is divided into categories of overall stage performance, stator blade element performance, and evaluation of stator blade boundary layer control methods. Stator end-wall bleed was in effect for all data being discussed. Selection of optimum stator hub and tip end-wall bleed rates was accomplished in an early phase of the test program. Data from this phase of testing are presented in the discussion of overall stage performance and demonstrates the effect of three stator end-wall bleed flow rates on performance. All data discussed under stator blade element performance were obtained with optimum stator end-wall bleed flow rate. In this portion of the discussion, stator blade element data at the 50% streamline location for the six stator blade configurations are compared to determine relative performance merits. The unslotted 0.75 D_f stator is used as a performance base line for the 0.75 D_f slotted stator comparisons. The final portion of the discussion, evaluation of stator blade boundary layer control methods, is a brief evaluation of the design of the stator blade bleed and blowing configurations using current boundary layer prediction methods.

OVERALL STAGE PERFORMANCE

Figures 10 and 11 show the overall stage performance for the unslotted 0.75 hub diffusion factor stator at three stator end-wall bleed flow rates. Performance of this configuration is considered representative of all configurations tested. The optimization of wall bleed (Reference 3) was performed only on this configuration and only at design speed.

Overall stage performance at design speed for this configuration and for the three stator end-wall bleed rates compares with the design performance as follows:

	Stage design	Optimum wall bleed	Mean wall bleed	Min wall bleed
$W_a\sqrt{\theta}/\delta$ at design $R_{c,ST}$ — lb_m/sec	88.2	93.6	94.0	93.1
$R_{c,ST}$ at design $W_a\sqrt{\theta}/\delta$	1.35	1.39	1.40	1.38
$\eta_{ad,ST}$ at design $R_{c,ST}$ — %	85.5	86.8	85.8	84.7
Tip bleed as % of W_a inlet	---	2.00	1.44	0.87
Hub bleed as % of W_a inlet	---	2.45	2.09	1.18

Within instrumentation accuracy, there was no significant trend of stage inlet corrected airflow with bleed rate. However, measured stage inlet corrected airflow was approximately 6% higher than the design value. The unexpected high flow was a consequence of actual rotor blade deviation angle being less than design values and actual rotor minimum loss incidence angle being more negative than design values. Peak stage efficiency at design speed occurred near design pressure ratio. Stator end wall bleed improved stage overall efficiency by about 2%. This gain was a result of bleeding the hub end wall; the tip end wall did not respond to bleed.

Figures 12, 13, and 14 are contour plots of stator local total pressure loss coefficient at design speed with minimum, mean, and optimum stator end-wall bleed. It is evident from these loss coefficient contour plots that the increase in overall stage efficiency was almost entirely the result of hub wall bleed. Stator loss coefficients in the outer one third of annulus were essentially unresponsive to bleed flow rate over the range of values investigated. Because the method of bleed at the hub and tip wall was the same, the different character of response to bleed is attributed to flow conditions near the stator tip being dissimilar to flow conditions near the stator hub.

STATOR BLADE ELEMENT PERFORMANCE

The stator blade element performance results in the following discussion are those obtained at the 50% streamline position and were obtained with optimum stator end-wall bleed. Corrected airflow was modulated at a given corrected speed to produce a range of stator incidence angle. Data were recorded over a range of incidence angle at 60, 80, 90, 100 and 110% of design speed. Stator blade element inlet Mach number was relatively constant at a given corrected speed over the range of flows for which data were recorded. The range of stator blade inlet Mach number for the 50% streamline for all data recorded at a given corrected speed is as follows:

Corrected speed (% of design)	M_2 at 50% streamline
60	0.40 - 0.44
80	0.54 - 0.59
90	0.59 - 0.66
100	0.64 - 0.75
110	0.71 - 0.79

Stator blade element performance is presented in figures as the variation of loss coefficient, deviation angle, and diffusion factor with incidence angle and as the variation of loss parameter with diffusion factor. Lines have been drawn through the data at design speed in these figures to highlight data trends. Because the data from the various configurations generally

show a consistent trend with corrected speed, the discussion of results will refer to data at design speed unless otherwise specified. In the figures which present loss parameter as a function factor, a line is provided which represents two-dimensional cascade data (Figure 149 of Reference 9).

Design point values of incidence angle, loss coefficient, loss parameter, deviation angle, and diffusion factor are denoted in the figures which present stator blade element performance. In comparing data with these design point quantities, it may be helpful to review briefly the background for selection of these design point quantities. Design point incidence was selected to provide flow stagnation at the leading edge. This selection was considered to be a desirable condition for the bleed and blowing configurations and not necessarily optimum for the unslotted configuration. The values of design point loss coefficient and loss parameter were selected to provide a target level of loss which was between one-half and two-thirds of that predicted for unslotted stator blade elements. The design point diffusion factor at the 50% streamline was somewhat lower than at the hub as a consequence of the radial variation in velocity diagrams and stator blade solidity. Design point deviation represented an estimate of stator blade element deviation with boundary layer control. Additional detail on considerations relative to selection of these design point quantities may be obtained from the design reports (References 1 and 2).

The stators in the following discussion are identified by their design hub diffusion factor, number of slots, and type of boundary layer control (suction surface bleed or blowing). A summary of the six stator configurations, including slot location, and design slot flow is as follows:

Stator loading (D_f at hub)	No. of slots (type)	Slot location (% chord along suction surface)	Design slot flow (% stage inlet flow)
0.75	Unslotted	---	---
0.75	3—bleed	1—25.0 2—41.0 3—61.0	1.50
0.75	1—blowing	39.25	1.34
0.75	2—blowing	1—40.0 2—69.5	1.92
0.65	1—bleed	60.0	1.80
0.65	1—blowing	42.0	1.08

There was no provision for measurement of slot flow during testing of the three blowing stator configurations. Slot flow was measured during testing of the two bleed stator configurations.

During testing of the 0.75 D_f triple-slotted bleed stator, three levels of suction surface boundary layer bleed rates were applied to the stator. These were classified as the optimum bleed rate, mean bleed rate, and zero bleed rate. The optimum bleed rate is defined as that which analytically removes one-third of the local boundary layer at each slot location (Reference 1). Optimum and mean bleed rates expressed as a percent of stage inlet flow are shown in Figures 15 and 16 as a function of stage pressure ratio and percent of design corrected speed. In the discussion of results for the 0.75 D_f triple-slotted bleed stator, bleed rate used was the optimum rate unless otherwise specified.

During testing of the 0.65 D_f single-slotted bleed stator, three levels of suction surface boundary layer bleed rates were applied to the stator. These were classified as optimum bleed rate, 2/3 optimum bleed rate, and 1/3 optimum bleed rate. Optimum, 2/3 optimum, and 1/3 optimum bleed rates expressed as a percent of stage inlet flow are shown in Figures 17, 18, and 19 as a function of stage pressure ratio and percent of design corrected speed. In the discussion of results for the 0.65 D_f single-slotted stator, bleed rate used was the optimum rate unless otherwise specified.

Quantities which are used in the following discussion to assess the relative merits of the various stator configurations are illustrated in Figure 20. They are defined as follows:

$\bar{\omega}_{3,\ min}$—minimum value of $\bar{\omega}_3$ at a given corrected speed

$i_{2,\ min}$—value of i_2 at which $\bar{\omega}_{3,\ min}$ occurs

$D_{f_{3,\ min}}$—value of D_{f_3} at $i_{2,\ min}$

$\delta^\circ_{3,\ min}$—value of δ°_3 at $i_{2,\ min}$

$i_{2,\ neg}$—value of i_2 less than $i_{2,\ min}$ at which $\bar{\omega}_3 = \bar{\omega}_{3,\ min} + 0.05$

$i_{2,\ pos}$—value of i_2 greater than $i_{2,\ min}$ at which $\bar{\omega}_3 = \bar{\omega}_{3,\ min} + 0.05$

$D_{f_{3,\ pos}}$—value of D_{f_3} at $i_{2,\ pos}$

Δi_2—quantity $(i_{2,\ pos} - i_{2,\ neg})$

The quantities $i_{2,\ neg}$ and $i_{2,\ pos}$ are chosen to indicate the onset of high loss coefficients at incidences more negative and more positive than $i_{2,\ min}$, respectively. The definition of $i_{2,\ neg}$ and $i_{2,\ pos}$ is arbitrary and is intended to represent approximately the useful limits of operation of the stator blade element. The quantity Δi_2 is referred to as range in the following discussion.

Values of the eight quantities, $\bar{\omega}_{3,\ min}$, $i_{2,\ min}$, $D_{f_{3,\ min}}$, $\delta^{\circ}_{3,\ min}$, $i_{2,\ neg}$, $i_{2,\ pos}$, $D_{f_{3,\ pos}}$, and Δi_2, have been listed in Table IV for design speed blade element performance of the six stator configurations. In some cases, definition of values for Table IV has required extrapolation of data. Where extrapolations have been required, an asterisk has been placed adjacent to the value. Values in Table IV which have been left blank were judged to require excessive extrapolation.

Comparison of Slotted vs Unslotted Stators

The 0.75 D_f unslotted stator will be used as a base line for comparing the three 0.75 D_f slotted stators in the following paragraphs.

0.75 D_f Triple-Slotted Bleed Stator vs 0.75 D_f Unslotted Stator

The performance of these two configurations is shown in Figures 21a and 21b. Performance at design speed may be compared as follows:

Configuration	$i_{2,\ min}$ (deg)	$\bar{\omega}_{3,\ min}$	$D_{f_{3,\ min}}$	$\delta^{\circ}_{3,\ min}$ (deg)	$i_{2,\ neg}$ (deg)	$i_{2,\ pos}$ (deg)	$D_{f_{3,\ pos}}$	Δi_2 (deg)
0.75 D_f unslotted	-5.0	0.042	0.64	13.0	-14.4*	1.5	0.71*	15.9
0.75 D_f triple-slotted bleed (optimum)	-0.5	0.014	0.70	10.0	-13.5*	7.0	0.77	20.5
Design	-3.0	0.042	0.70	18.0				

*These values have been extrapolated from the data in Figure 21a.

This comparison shows that the triple-slotted stator had a lower minimum loss coefficient, a lower deviation angle, higher D_f at minimum loss incidence, and larger range than the unslotted stator. Increased range was achieved principally by increased ability to operate at more positive incidence (increased $i_{2,\ pos}$). Compared to design values, the triple-slotted bleed stator achieved design loading at about 2.5 degrees more positive incidence angle and was accompanied by a lower-than-design loss coefficient. Deviation angle was less than the design value by about 8 degrees.

Figure 21b illustrates that the triple-slotted stator had generally lower loss parameter and higher diffusion factor than the unslotted stator. Loss parameter of the triple-slotted bleed stator at $i_{2,\ min}$ was approximately one-half of the reference value for two-dimensional cascades.

The comparisons of Figure 21a and 21b indicate that the 0.75 D_f triple-slotted bleed stator was far superior to the 0.75 D_f unslotted stator.

0.75 D_f Triple-Slotted Bleed Stator With Zero Bleed vs 0.75 D_f Unslotted Stator

The 0.75 D_f triple-slotted bleed stator was evaluated for blade element performance at three suction surface boundary layer bleed rates. One of these was zero bleed rate. Blade element performance at zero bleed rate for the 0.75 D_f triple-slotted bleed stator provides an interesting comparison with the 0.75 D_f unslotted stator. Unfortunately, yaw probe data at the stator exit were generally in error for the zero bleed rate investigation and data were obtained only at design corrected speed. With these limitations, the comparison is made on the basis of loss coefficient versus incidence angle only and is shown in Figure 22. A summary of the comparison shown in Figure 22 follows:

Configuration	$i_{2,\ min}$ (deg)	$\bar{\omega}_{3,\ min}$	$i_{2,\ neg}$ (deg)	$i_{2,\ pos}$ (deg)	Δi_2 (deg)
0.75 D_f unslotted	-5.0	0.042	-14.4*	1.5	15.9
0.75 D_f triple-slotted bleed (zero)	1.0	0.091	-9.1	5.3	14.4

*These values have been extrapolated from the data in Figure 22.

This summary shows that minimum loss coefficient of the triple-slotted stator at zero bleed was about twice as high as for the unslotted stator. Range of the two configurations was about the same. Values of $i_{2,\ min}$, $i_{2,\ neg}$, and $i_{2,\ pos}$ for the triple-slotted stator at zero bleed occurred at about five degrees more positive incidence angle compared with corresponding values for the unslotted stator.

The comparison in Figure 22 shows that the 0.75 D_f triple-slotted bleed stator operating with zero net suction surface boundary layer bleed had about twice the loss of the 0.75 D_f unslotted stator. This comparison suggests that substantial detrimental recirculation existed into and out of the slots of the 0.75 D_f triple-slotted bleed stator when operated with zero net bleed.

0.75 D_f Single-Slotted Blowing Stator vs 0.75 D_f Unslotted Stator

Performance of these two configurations is shown in Figures 23a and 23b. There is insufficient data to define $i_{2,\ pos}$ and, therefore, Δi_2 of the blowing stator. With these exceptions, the two configurations may be compared at design corrected speed from Figure 23a as follows:

Configuration	$i_{2,\ min}$ (deg)	$\bar{\omega}_{3,\ min}$	$D_{f_{3,\ min}}$	$\delta^{\circ}_{3,\ min}$ (deg)	$i_{2,\ neg}$ (deg)
0.75 D_f unslotted	-5.0	0.042	0.64	13.0	-14.4*
0.75 D_f single-slotted blowing	2.0	0.078	---	---	-5.6
Design	-3.0	0.042	0.70	18.0	

*These values have been extrapolated from the data in Figure 23a.

This comparison shows that the single-slotted blowing stator had a higher minimum loss coefficient and a more positive $i_{2,\ neg}$ than the unslotted stator. Figure 23a shows that the single-slotted blowing stator exhibited a trend of decreasing deviation with increased incidence unlike the unslotted stator and achieved a somewhat lower loss coefficient at incidences greater than about one degree. Figure 23b also indicates that the single-slotted blowing stator had generally higher loss than the unslotted stator.

The comparison given in Figures 23a and 23b indicates that the 0.75 D_f single-slotted blowing stator was generally inferior to the 0.75 D_f unslotted stator. Note also, that minimum loss occurs at a much higher incidence with the single-slotted stator. The poorer performance of the single-slotted blowing stator at negative incidence angle may be an indication of a problem with flow in the region of the blade leading edge associated with the source of the blowing stream also located in the region of the blade leading edge.

0.75 D_f Double-Slotted Blowing Stator vs 0.75 D_f Unslotted Stator

Figures 24a and 24b show the performance of these two configurations. A comparison of the two configurations at design corrected speed from Figure 24a follows:

Configuration	$i_{2,\ min}$ (deg)	$\bar{\omega}_{3,\ min}$	$D_{f_{3,\ min}}$	$\delta^{\circ}_{3,\ min}$ (deg)	$i_{2,\ neg}$ (deg)	$i_{2,\ pos}$ (deg)	$D_{f_{3,\ pos}}$	Δi_2 (deg)
0.75 D_f unslotted	-5.0	0.042	0.64	13.0	-14.4*	1.5	0.71*	15.9
0.75 D_f double-slotted blowing	1.2	0.052	0.70	15.5	-6.8	4.9	0.74*	11.7
Design	-3.0	0.042	0.70	18.0				

*These values have been extrapolated from the data in Figure 24a.

This comparison shows that the double-slotted blowing stator had on the order of 25% higher minimum loss coefficient, achieved higher loading at minimum loss incidence angle, and had about 4 degrees lower range than the unslotted stator. Qualitatively similar to the previous comparison, the blowing stator in this comparison exhibited poorer performance at more negative incidence angles and a shift in the minimum loss point to a positive incidence compared with the unslotted stator. The markedly poorer performance of the double-slotted blowing stator at more negative incidence accounted for its reduced range compared with the unslotted stator. Figure 24b also shows that loss of the double-slotted blowing stator was somewhat higher than the unslotted stator.

The comparison of Figures 24a and 24b indicate that the 0.75 D_f double-slotted blowing stator was generally somewhat inferior to the 0.75 D_f unslotted stator. As in the previous comparison, the unslotted blowing stator exhibited poorer characteristics at more negative incidence angles and a shift in the minimum loss point toward more positive incidence as compared with the unslotted stator. The recurrence of this characteristic confirms the indication of a leading edge flow problem for blowing stators of this type.

Cross-Comparison of Various Slotted Stator Configurations

The following paragraphs present comparisons of stator blade element performance on the basis of the effects of the number of slots, the effects of suction surface boundary layer bleed rate, the effects of bleed vs blowing slots, and the effect of loading level.

0.75 D_f Single-Slotted Blowing Stator vs 0.75 D_f Double-Slotted Blowing Stator

The performance of these two configurations is shown in Figures 25a and 25b. There is insufficient data to define $i_{2,\ pos}$ and range for the single-slotted blowing stator. With these exceptions, the two configurations may be compared at design corrected speed from Figure 25a as follows:

Configuration	$i_{2,\ min}$ (deg)	$\bar{\omega}_{3,\ min}$	$D_{f_{3,\ min}}$	$\delta^*_{3,\ min}$ (deg)	$i_{2,\ neg}$ (deg)
0.75 D_f single-slotted blowing	2.0	0.078	---	---	-5.6
0.75 D_f double-slotted blowing	1.2	0.052	0.70	15.5	-6.8
Design	-3.0	0.042	0.70	18.0	

Both configurations had approximately the same value of $i_{2,\ min}$, $i_{2,\ neg}$, and $\delta^{\circ}_{3,\ min}$. The primary difference between the configurations was that the single-slotted stator had about 50% higher minimum loss coefficient than the double-slotted stator. The generally higher loss of the single-slotted stator is shown by data presented in Figures 25a and 25b.

The comparison given in Figures 25a and 25b indicates that the 0.75 D_f double-slotted blowing stator was superior to the 0.75 D_f single-slotted blowing stator. The slot arrangement of these two configurations is shown in Figure 7. Both stator blades had a slot located at approximately 40% of chord. The double-slotted blades had an added slot located at about 70% of chord. The performance comparison given by Figures 25a and 25b suggests that the added slot located at 70% of chord improved blade element performance.

Effect of Bleed Rate for 0.65 D_f Single-Slotted Stator

The blade element performance of this configuration as affected by suction surface boundary layer bleed rate is shown in Figures 26a and 26b. A summary at design corrected speed of the comparison shown in Figure 26a follows:

Bleed rate	$i_{2,\ min}$ (deg)	$\bar{\omega}_{3,\ min}$	$Df_{3,\ min}$	$\delta^{\circ}_{3,\ min}$ (deg)	$i_{2,\ neg}$ (deg)	$i_{2,\ pos}$ (deg)	$Df_{3,\ pos}$	Δi_2 (deg)
Optimum	3.0	0.007	0.58	8.0	-3.6	9.0*	0.68*	12.6
2/3 optimum	2.7	0.014	0.54	---	-6.2*	8.8*	0.63*	15.0
1/3 optimum	2.0	0.010	0.52	8.0*	-2.8*	8.4*	0.63	11.2
Design	3.0	0.040	0.60	10.0				

*These values have been extrapolated from data in Figure 26a.

This summary does not indicate any strong or consistent trends of stator blade element performance with variation in suction surface boundary layer bleed rate over the range tested. The losses are low compared to design and variations with bleed flow rate are within data accuracy. Figure 26b does not illustrate any significant trend of loss parameter with bleed flow rate.

Figures 26a and 26b indicate that the performance of the 0.65 D_f single-slotted bleed stator was relatively independent of suction surface boundary layer bleed rate over the range of bleed rates tested.

0.65 D_f Single-Slotted Blowing Stator vs 0.65 D_f Single-Slotted Bleed Stator

No unslotted 0.65 D_f stator was evaluated. The only comparison available at 0.65 D_f is between a bleed and a blowing stator. This comparison is shown in Figures 27a and 27b. A summary at design corrected speed of the comparison given by Figure 27a follows:

Configuration	$i_{2,\ min}$ (deg)	$\bar{\omega}_{3,\ min}$	$D_{f_{3,\ min}}$	$\delta^*_{3,\ min}$ (deg)	$i_{2,\ neg}$ (deg)	$i_{2,\ pos}$ (deg)	$D_{f_{3,\ pos}}$	Δi_2 (deg)
0.65 D_f single-slotted blowing	3.7	0.042	0.47	16.5	0*	8.0	0.62	8.0
0.65 D_f single-slotted bleed (optimum)	3.0	0.007	0.58	8.0	-3.6	9.0*	0.68*	12.6
Design	3.0	0.040	0.60	10.0				

*These values have been extrapolated from the data in Figure 27a.

This summary indicates that the 0.65 D_f single-slotted bleed stator had lower minimum loss coefficient, a more negative $i_{2,\ neg}$, a larger range, higher loading at minimum loss incidence angle, and lower deviation angle than the 0.65 D_f single-slotted blowing stator. The 0.65 D_f single-slotted bleed stator blade element performance compared closely with design values of incidence angle, diffusion factor, and deviation angle. Minimum loss coefficient of the bleed stator was in the order of one-sixth of the design loss coefficient. Data presented in Figures 27a and 27b show that the 0.65 D_f single-slotted bleed stator had much lower loss than the 0.65 D_f single-slotted blowing stator. Minimum loss parameter of the 0.65 D_f single-slotted bleed stator was lower than the reference line for two-dimensional cascades.

The comparison given in Figures 27a and 27b indicates that the 0.65 D_f single-slotted bleed stator was superior in performance to the 0.65 D_f single-slotted blowing stator.

Effect of Bleed Rate for 0.75 D_f Triple-Slotted Bleed Stator

The blade element performance of this configuration as affected by suction surface boundary layer bleed rate is shown in Figure 28a and 28b. A summary at design corrected speed of the comparison shown in Figure 28a follows:

Bleed rate	i_2, min (deg)	$\bar{\omega}_3$, min	D_{f_3}, min	δ^*_3, min (deg)	i_2, neg (deg)	i_2, pos (deg)	D_{f_3}, pos	Δi_2 (deg)
Optimum	-0.5	0.014	0.70	10.0	-13.5*	7.0	0.77	20.5
Mean	-1.4	0.026	0.68	11.0*	-13.6*	6.3	0.76	19.9
Zero	1.0	0.091	---	---	-9.1	5.3	---	14.4
Design	-3.0	0.042	0.70	18.0				

*These values have been extrapolated from the data in Figure 28a.

This summary indicates that optimum bleed rate resulted in about one half the minimum loss coefficient as compared with the mean bleed rate. Minimum loss coefficient at both optimum and mean bleed rate was well below the design loss coefficient. Comparison of optimum with mean bleed rate for other blade element performance quantities in this summary indicates no significant trend within the accuracy of the data. Blade element performance at zero bleed rate was greatly deteriorated. Minimum loss coefficient was about twice the design loss coefficient and the range was about six degrees lower than the range obtained with optimum bleed rate. The data at 80% of design corrected speed in Figure 28b also shows that the loss coefficient of this stator configuration was lower when optimum suction surface bleed rate was applied as compared to mean bleed rate.

Figures 28a and 28b indicate that best blade element performance of the 0.75 D_f triple-slotted bleed stator was obtained at optimum bleed rate. A mild deterioration of performance resulted when bleed flow rate was reduced from the optimum level to the mean level, and a large deterioration of performance resulted when bleed flow rate was further reduced from the mean level to zero. In fact, at zero bleed, losses were higher than for the unslotted blade.

0.75 D_f Double-Slotted Blowing Stator vs 0.75 D_f Triple-Slotted Bleed Stator

The better of the two 0.75 D_f slotted blowing stators has been chosen to compare with the 0.75 D_f triple-slotted bleed stator. Figures 29a and 29b show the performance of these two configurations. The two configurations may be compared at design corrected speed from Figure 29a as follows:

Configuration	i_2, min (deg)	$\bar{\omega}_3$, min	D_{f_3}, min	δ^*_3, min (deg)	i_2, neg (deg)	i_2, pos (deg)	D_{f_3}, pos	Δi_2 (deg)
0.75 D_f double-slotted blowing	1.2	0.052	0.70	15.5	-6.8	4.9	0.74*	11.7
0.75 D_f triple-slotted bleed (optimum)	-0.5	0.014	0.70	10.0	-13.5*	7.0	0.77	20.5
Design	-3.0	0.042	0.70	18.0				

*These values have been extrapolated from the data in Figure 29a.

The 0.75 D_f triple-slotted bleed stator had performance equal to or better than the performance of the 0.75 D_f double-slotted blowing stator for all quantities compared from Figure 29a. Particularly outstanding quantities to compare are loss coefficient and range. Data presented in Figure 29a and 29b indicate that the 0.75 D_f triple-slotted bleed stator had a much lower loss than the 0.75 D_f double-slotted blowing stator.

The comparison presented in Figures 29a and 29b indicates that the 0.75 D_f triple-slotted bleed stator was superior in performance to the 0.75 D_f double-slotted blowing stator.

Effect of Loading—0.65 D_f Single-Slotted Blowing Stator vs 0.75 D_f Single-Slotted Blowing Stator

The performance of these two configurations is shown in Figures 30a and 30b. Comparison of the two configurations is made by relating blade element performance of each configuration to its design performance. A summary of blade element performance at design corrected speed as shown in Figure 30a follows:

Configuration	$i_{2,\ min}$ (deg)	$\omega_{3,\ min}$	$D_{f_{3,\ min}}$	$\delta^*_{3,\ min}$ (deg)	$i_{2,\ neg}$ (deg)
0.65 D_f single-slotted blowing	3.7	0.042	0.47	16.5	0*
0.65 D_f design	3.0	0.040	0.60	10.0	
0.75 Df single-slotted blowing	2.0	0.078	---	---	-5.6
0.75 D_f design	-3.0	0.042	0.70	18.0	

*These values have been extrapolated from data in Figure 30a.

From this summary, the 0.65 D_f single-slotted blowing stator demonstrated a minimum loss coefficient and a minimum loss incidence angle equal to its design loss coefficient and incidence angle within the data accuracy. Deviation angle at minimum loss incidence angle was much higher than design deviation angle for the 0.65 D_f stator, and diffusion factor at minimum loss incidence angle was much lower than design diffusion factor. The 0.75 D_f single-slotted blowing stator had a minimum loss coefficient approximately twice as high as its design loss coefficient. Deviation angle at minimum loss incidence angle was less than design deviation angle for this 0.75 D_f stator. There are insufficient data presented in Figure 30a to define $i_{2,\ pos}$ and to compare range. Data presented in Figure 30b indicate that the 0.65 D_f single-slotted blowing stator demonstrated a minimum loss parameter about equal to its design loss parameter, while the 0.75 D_f single-slotted blowing stator demonstrated loss parameters much greater than its design loss parameter.

The comparison presented by Figures 30a and 30b indicates that, relative to design values, the 0.65 D_f single-slotted blowing stator had generally better loss characteristics and poorer deviation characteristics than the 0.75 D_f single-slotted blowing stator.

EVALUATION OF BLADE BOUNDARY LAYER CONTROL METHODS

The blade element performance data presented in this report indicate that significant improvements in stator range and loss at a given level of loading can be realized by using an effective means of stator blade boundary layer control. Of the two methods presented here, bleeding off the momentum deficient air adjacent to the blade surface appears to be a more effective method of controlling the boundary layer as compared with reenergizing the air by tangential slot blowing. Although these conclusions appear valid for this particular situation, a generalization regarding the merits of bleed control versus blowing control cannot be made until a valid method for optimizing the slot design and location for maximum effectiveness is available. This will require a more detailed knowledge of the boundary layer parameters for these parameters determine the location and characteristics of the boundary layer control device. These boundary layer parameters, in turn, depend on the static pressure distribution about the airfoil.

Airfoil static pressure distributions are fundamental consequences of airfoil shapes and are usually determined either by direct measurement in cascades or are the result of interpolations and extrapolations of existing cascade data; this was the case for the stator designs reported here. A detailed explanation in Reference 1 describes how the static pressure distributions at design incidence about the 0.65 D_f and 0.75 D_f stator blades were estimated. These static pressure distributions presented in the form of pressure coefficient versus percent chord are shown in Figures 31 and 32 of this report and will be the basis of the analytic investigation that follows. These static pressure distributions at the stated loading levels are based on the premise that some means of boundary layer control exists to prevent separation from occurring and also on the assumption that the presence of a means of boundary layer control would not affect the distributions themselves.

The boundary layer analysis originally used in the slot design procedure was an integral solution as formulated by Truckenbrodt (Reference 10). This basic momentum integral technique was used in conjunction with a compressible transformation to predict the streamwise slot location and related boundary layer parameters. However, in light of the sophistication of current turbulent boundary layer computational techniques, a review and comparison of the slot location as predicted by the Truckenbrodt method was initiated. The methods used here to reassess the points of boundary layer separation are the Mellor-Herring incompressible technique (Reference 11), the Herring compressible technique (Reference 12), and the McNally compressible technique (Reference 13).

The Mellor-Herring incompressible method provides a numerical solution to the boundary layer equations through the use of the effective viscosity hypothesis of Mellor (Reference 14). The basic numerical scheme can be described as an implicit scheme resulting in an ordinary differential equation at each station which is solved according to a Runge-Kutta method adapted to the laminar and turbulent boundary layer equations. The Herring compressible analysis is conceptually similar to the incompressible mode. The coupled equations of mass, momentum, and energy are solved numerically, again using the effective viscosity concept. The McNally calculation is a solution to the momentum integral and moment of momentum integral equations, using a compressible boundary layer transformation. This method is similar in approach to that of Sasman and Cresci (Reference 15). The results of these three more sophisticated methods are compared to the original Truckenbrodt calculations for the 10, 50, and 90% annulus height sections at design conditions as shown in Figures 33 through 35 for the 0.65 D_f stator and Figures 36 through 38 for the 0.75 D_f stator. The criterion used to determine the separation point for the Mellor-Herring incompressible, Herring compressible, and McNally compressible methods is defined as that point where the wall shear stress, τ_w, and, correspondingly, the skin friction coefficient, C_f, approach zero. The Truckenbrodt method assumes that separation occurs when the incompressible shape parameter $H_i = 2.2$.

It can be seen from Figures 33 through 38 that the current techniques are in close agreement and indicate separation about 20% chord further downstream than the original Truckenbrodt prediction. This result implies that when using the same boundary layer control design procedure at design incidence as reported in References 1 and 2, slot location should be further downstream than originally thought. Whether the conservative upstream location of the single slots could have tripped the boundary layer (particularly in the case of tangential blowing) and caused premature separation or whether the blowing slot was located too far upstream to be effective at design conditions can only be speculated. The blade element data do tend to support these possibilities. However, better performance should have been measured at high incidence angles where the upstream location of the slot would be advantageous. Blade surface static pressure measurements were made to better define the points of separation. Unfortunately, this information was, for the most part, rendered useless because of excessive data scatter. This scatter was primarily a result of locating the 12 suction surface static taps on four separate blades. Figures 39a and 39b present two experimental 0.75 D_f unslotted static pressure distributions, and show the points of separation as predicted by the four boundary layer analysis methods considered. The three more sophisticated analysis methods are in close agreement with each other and with experimental observations, while the Truckenbrodt solution appears too conservative. The fact that the pressure distribution shown in Figure 39b indicates severe upstream separation is attributed to its close proximity to the end wall which exhibited a considerable effect on the blade surface flow distributions.

Based on this study, the following conclusions are drawn.

1. Of the current boundary layer methods studied—Mellor-Herring incompressible, McNally compressible, and Herring compressible—all predicted nearly the same location of suction surface separation and were in close agreement with experimental observations. This suggests that the relatively simple Mellor-Herring incompressible method is adequate for freestream Mach numbers up to 0.7.
2. The ability to accurately predict the separation point is highly dependent on possessing a good design or experimental freestream pressure distribution since this distribution supplies most of the information for the boundary layer calculation.
3. The use of current methods of predicting boundary layer separation would increase the chances of successful application of boundary layer control.
4. The leading edge pressure distribution as well as the zone of transition from laminar flow to turbulent flow should be investigated in more detail in order to study their effects on separation.

SUMMARY OF RESULTS

Comparison of the performance of the six stator configurations was restricted to the midspan blade element. Stator hub and tip wall bleeds were used to minimize end wall effects. Comparisons at midspan indicate the following results.

1. A significant improvement in blade element performance was achieved with suction surface boundary layer bleed.

   - Minimum values of loss coefficient for the 0.75 D_f triple-slotted bleed stator were about one-third of those for the 0.75 D_f unslotted stator.
   - The useful operating range of incidence angle for the 0.75 D_f triple-slotted bleed stator was judged to be about 4 degrees larger than that of the 0.75 D_f unslotted stator.
   - The 0.75 D_f triple-slotted bleed stator achieved about 10% higher diffusion factor throughout its useful operating range as compared with the 0.75 D_f unslotted stator.
   - Deviation angle for the 0.75 D_f triple-slotted bleed stator was about 3 degrees lower than that for the 0.75 D_f unslotted stator.

2. Blade element performance with suction surface boundary layer blowing was generally inferior to that of the unslotted stator.

   - Minimum values of loss coefficient for both 0.75 D_f slotted blowing stators were higher than those of the 0.75 D_f unslotted stator.

- The negative incidence limit of useful operating range for the 0.75 D_f unslotted stator extended approximately 8 degrees further in the negative incidence direction than that of either 0.75 D_f slotted blowing stators.
- The minimum loss point for both 0.75 D_f slotted blowing stators was shifted to a much higher incidence angle than that of the 0.75 D_f unslotted stator.

3. Design of the slotted blowing stator configurations may not have been optimum.
   - At relatively negative incidence angle, the inferior performance of both 0.75 D_f slotted blowing stators when compared with the 0.75 D_f unslotted stator suggests a problem with design of the leading edge and/or the blowing flow intake slot located near the leading edge.
   - The current boundary layer prediction methods are in close agreement with experiemental observations. The current methods predict suction surface boundary layer separation about 20% of chord further downstream than the method used for design.

4. Over the range of bleed rates tested, the 0.65 D_f single-slotted bleed stator demonstrated no trend of performance within limits of data accuracy. When bleed rate was reduced from the design level to about one-half of the design level, the 0.75 D_f triple-slotted bleed stator demonstrated a loss in performance but was still superior to the 0.75 D_f unslotted stator. At zero bleed rate the 0.75 D_f triple-slotted bleed stator was inferior to the 0.75 D_f unslotted stator.

An improvement of about 2% in stage efficiency was achieved at design speed as stator end wall bleed was increased. This gain in performance was the result of bleeding the hub end wall; the tip end wall did not respond to bleed.

REFERENCES

1. Chapman, D. C. and Miller, M. L. Single-Stage Experimental Evaluation of Boundary Layer Bleed Techniques for High Lift Stator Blades, I—Compressor Design. NASA CR-54569 (Allison EDR 5658). February 1968.

2. Chapman, D. C. and Miller, M. L. Single-Stage Experimental Evaluation of Boundary Layer Blowing Techniques for High Lift Stator Blades, I—Compressor Design. NASA CR-54564 (Allison EDR 5636). February 1968.

3. Miller, M. L. and Beck, T. E. Single-Stage Experimental Evaluation of Boundary Layer Blowing Techniques for High Lift Stator Blades, II—Data and Performance of Flow Generation Rotor and Single-Slotted 0.75 Hub Diffusion Factor Stator. NASA CR-54565 (Allison EDR 5691). February 1968.

4. Carmody, R. H. and Seren, G. Single-Stage Experimental Evaluation of Boundary Layer Bleed Techniques for High Lift Stator Blades, III—Data and Performance of Unslotted 0.75 Hub Diffusion Factor Stator. NASA CR-54571 (Allison EDR 5863). September 1968.

5. Carmody, R. H. and Seren, G. Single-Stage Experimental Evaluation of Boundary Layer Bleed Techniques for High Lift Stator Blades, II—Data and Performance of Single-Slotted 0.65 Hub Diffusion Factor Stator. NASA CR-54570 (Allison EDR 5862). August 1968.

6. Carmody, R. H., Horn, R. A., and Seren, G. Single-Stage Experimental Evaluation of Boundary Layer Bleed Techniques for High Lift Stator Blades, IV—Data and Performance of Triple-Slotted 0.75 Hub Diffusion Factor Stator. NASA CR-54572 (Allison EDR 5944). October 1968.

7. Miller, M. L. and Seren, G. Single-Stage Experimental Evaluation of Boundary Layer Blowing Techniques for High Lift Stator Blades, III—Data and Performance of Single-Slotted 0.65 Hub Diffusion Factor Stator. NASA CR-54566 (Allison EDR 5759). June 1968.

8. Seren, G. Single-Stage Experimental Evaluation of Boundary Layer Blowing Techniques for High Lift Stator Blades, IV—Data and Performance of Double-Slotted 0.75 Hub Diffusion Factor Stator. NASA CR-54567 (Allison EDR 5861). August 1968.

9. Aerodynamic Design of Axial Flow Compressors. NASA SP-36 (1965).

10. Truckenbrodt, E. A Method of Quadrature for Calculation of the Laminar and Turbulent Boundary Layer in Case of Plane and Rotationally Symmetric Flow. NACA TM-1379 (1955).

11. Herring, H. J. and Mellor, G. L. A Computer Program to Calculate Incompressible Laminar and Turbulent Boundary Layer Development. NASA CR-1564 (1970).

12. Herring, H. J. and Mellor, G. L. A Method of Calculating Compressible Turbulent Boundary Layers. NASA CR-1144 (September 1968).

13. McNally, W. D. Fortran Program for Calculating Compressible Laminar and Turbulent Boundary Layers in Arbitrary Pressure Gradients. NASA TN-D-5681.

14. Mellor, G. L. and Gibson, D. M. "Equilibrium Turbulent Boundary Layers." Journal of Fluid Mechanics: Vol 24, Part 2, pp 225-253 (1966).

15. Sasman, P. K. and Cresci, R. J. "Compressible Turbulent Boundary Layer with Pressure Gradient and Heat Transfer." AIAA Journal, Vol 4, No. 1 (1966).

APPENDIX

PERFORMANCE EQUATIONS

The following overall and blade element performance parameters were calculated for the analysis of test data and the evaluation of the slotted and unslotted stator performance.

WEIGHT FLOW

Overall performance is presented as a function of corrected weight flow defined as

$$\frac{W_a\sqrt{\theta}}{\delta} \tag{A1}$$

ADIABATIC EFFICIENCY

Adiabatic efficiency for the inlet guide vane, rotor, and stator combination is

$$\eta_{ad,\ ST} = \frac{\left(\frac{P_{3,\ ma}}{P_0}\right)^{\frac{\gamma-1}{\gamma}} - 1}{\frac{T_{3,\ ma}}{T_0} - 1} \tag{A2}$$

DIFFUSION FACTOR

The stator diffusion factor is defined as

$$D_{f_3} = 1 - \frac{V_3}{V_2} + \frac{V_{\theta,2} - V_{\theta,3}}{2\sigma V_2} \tag{A3}$$

DEVIATION ANGLE

The stator deviation angle is defined as

$$\delta_3^\circ = \beta_3 - \kappa_3 \tag{A4}$$

INCIDENCE ANGLE

The stator incidence angle is defined as

$$i_2 = \beta_2 - \kappa_2 \tag{A5}$$

TOTAL PRESSURE LOSS COEFFICIENT

a) The local total pressure loss coefficient for the stator is defined as

$$\omega_3 = \frac{1 - \frac{P_3}{P_2}}{1 - \left[1 + \frac{\gamma-1}{2}(M_2)^2\right]^{\frac{-\gamma}{\gamma-1}}} \tag{A6}$$

b) The blade element total pressure loss coefficient for the stator is defined as

$$\bar{\omega}_3 = \frac{1 - \frac{P_{3,ma}}{P_{3,fs}}}{1 - \left[1 + \frac{\gamma-1}{2}(M_2)^2\right]^{\frac{-\gamma}{\gamma-1}}} \tag{A7}$$

MASS AVERAGED TOTAL PRESSURE

Mass averaged total pressure is defined as

$$P_{3,\,ma} = \frac{\sum_{i=1}^{n} (P_3)_i \, (\rho_3 V_3 A_e)_i}{\sum_{i=1}^{n} (\rho_3 V_3 A_e)_i} \tag{A8}$$

where $(A_e)_{i=1}$ is the first partial elemental area between adjacent blades and $(A_e)_{i=n}$ is the last partial elemental area between adjacent blades. The number of elemental areas between adjacent blades and their values depends on rake probe angle ϵ.

PRESSURE COEFFICIENT

Pressure coefficient (S) is defined as

$$S = \frac{P_2 - p}{q_2} \tag{A9}$$

where

p is the stator blade surface static pressure

$$q_2 = \frac{1}{2} \rho_2 V_2^2$$

SKIN FRICTION COEFFICIENT

The skin friction coefficient is defined as

$$C_f = \frac{\tau_w}{\frac{1}{2}\rho V^2} \tag{A10}$$

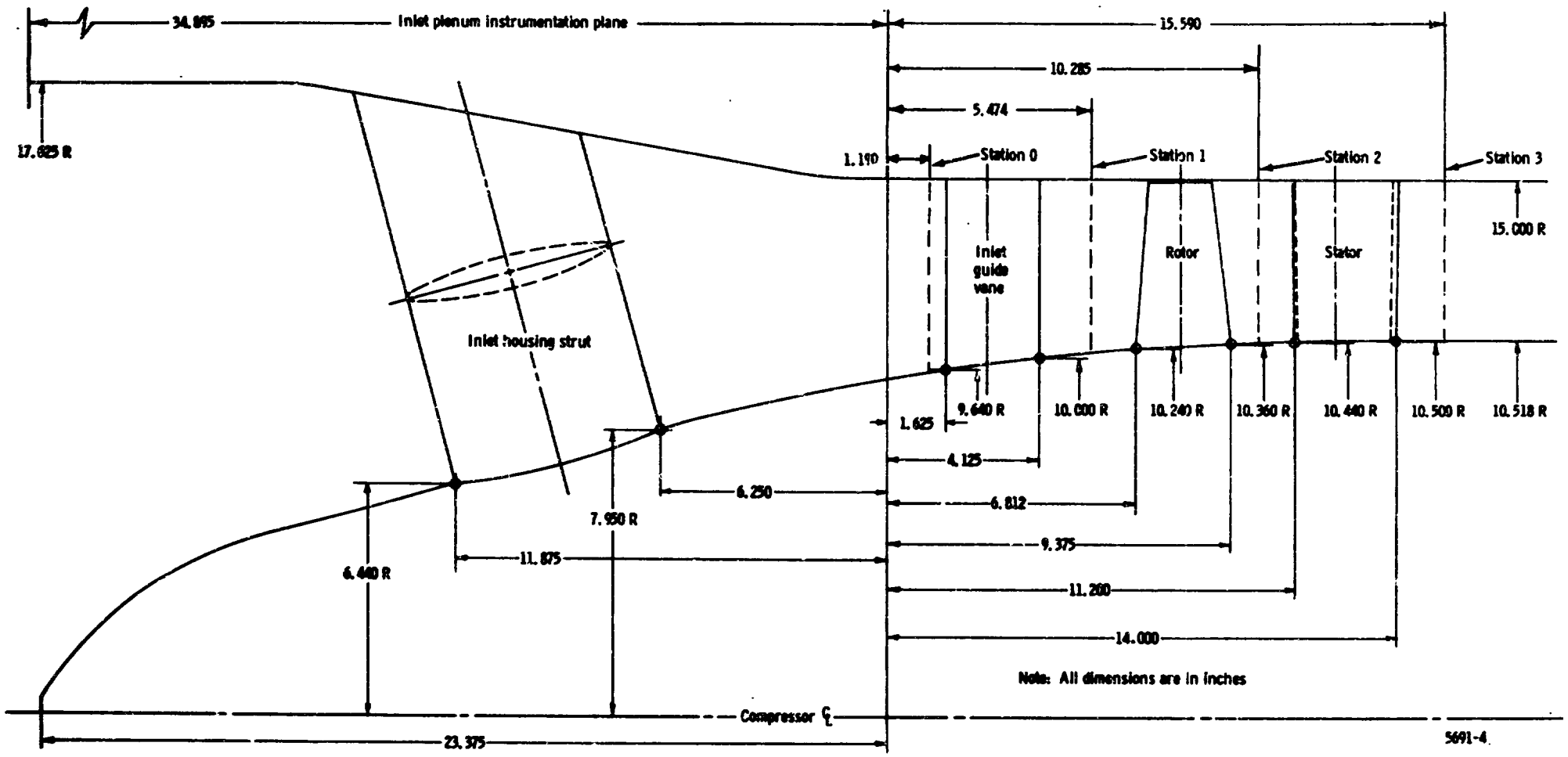

Figure 1. Compressor test rig flowpath.

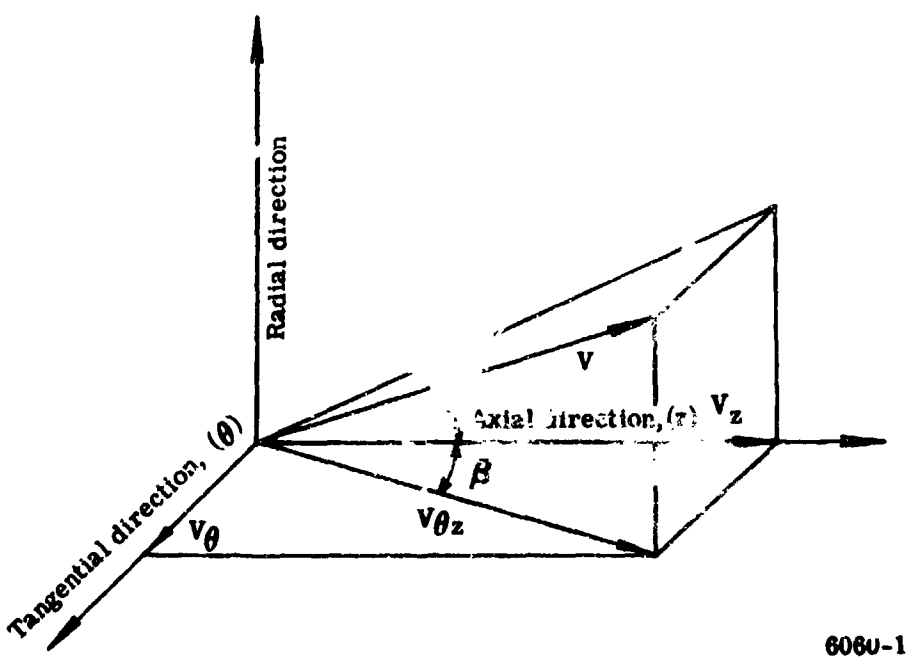

Figure 2. Velocity diagram nomenclature.

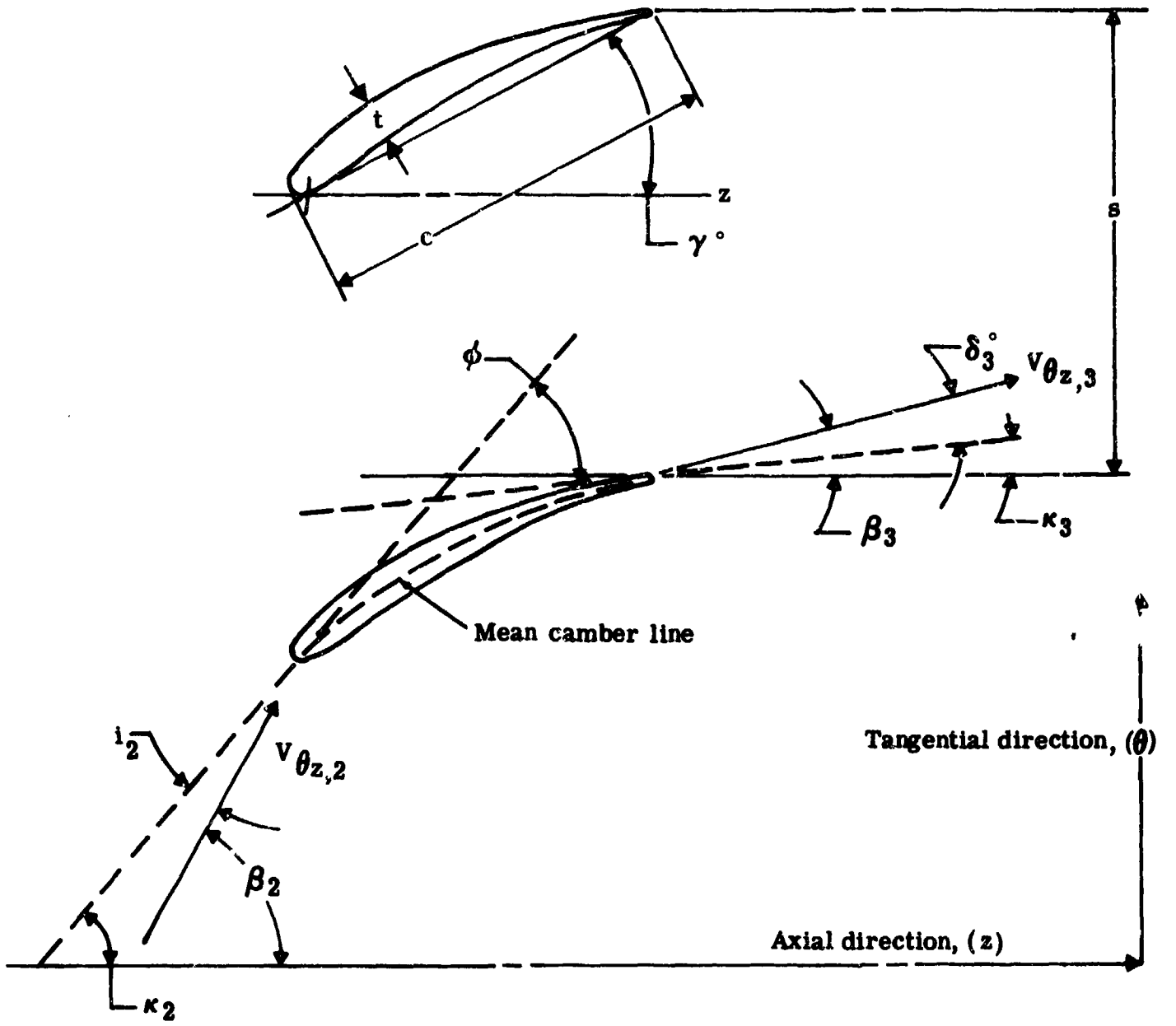

Figure 3. Stator aerodynamic and blade geometric nomenclature.

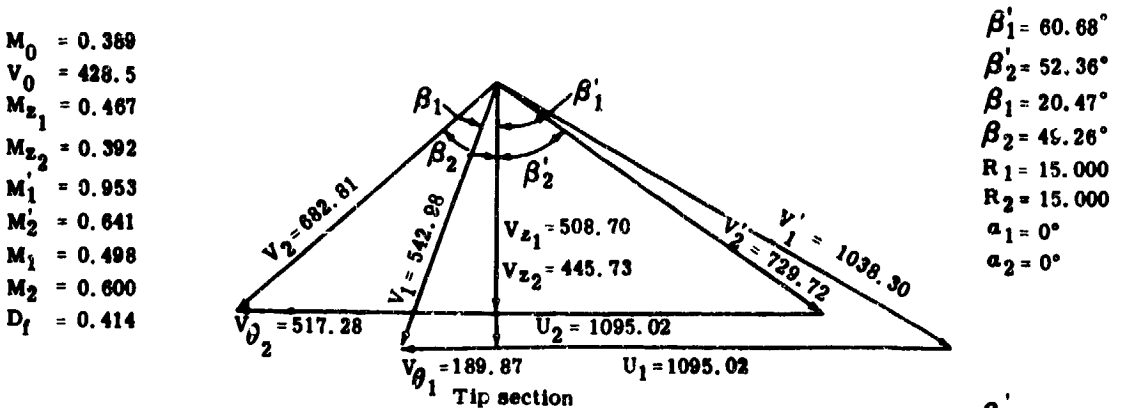

Tip section

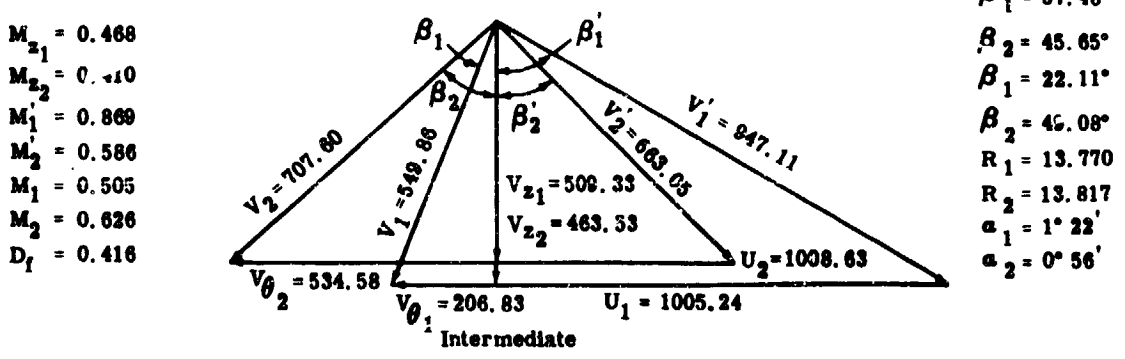

Intermediate

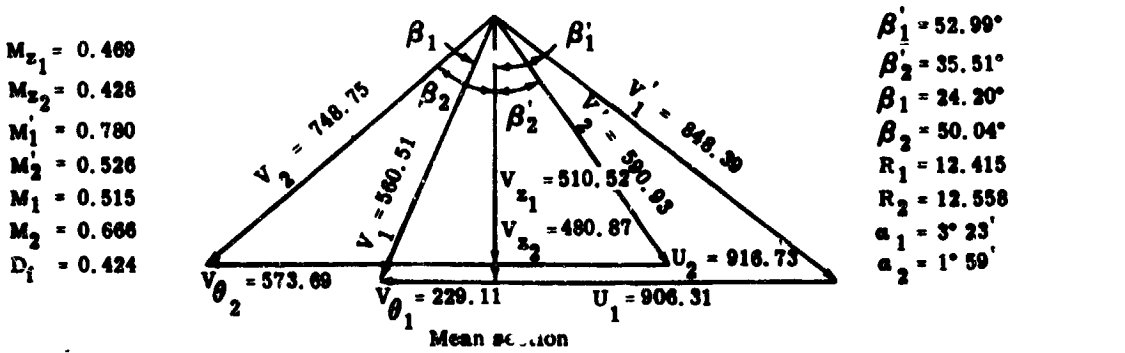

Mean section

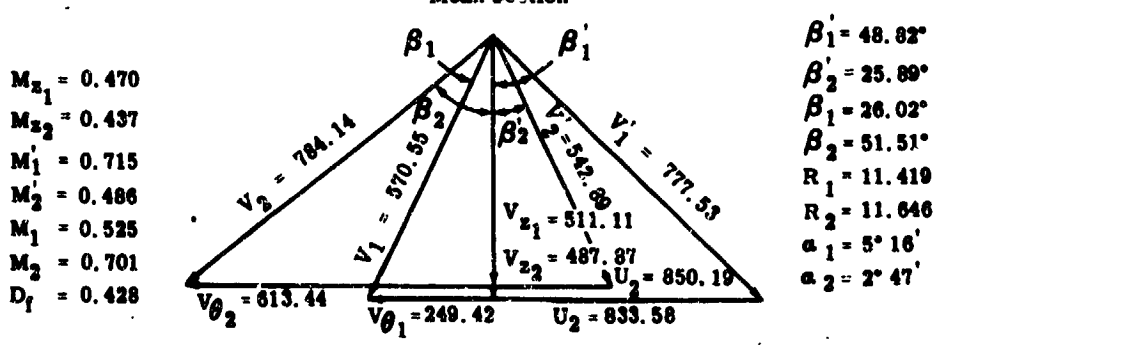

Intermediate

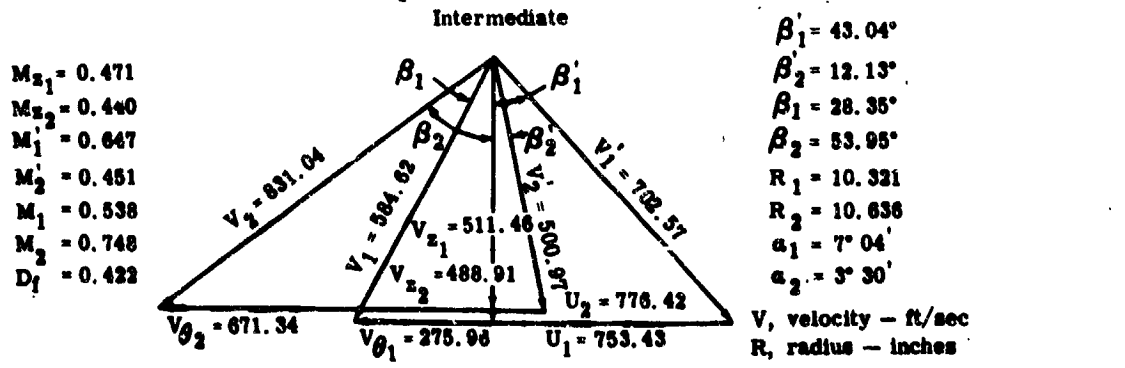

Hub section

Notes: (1) Since the radial component of velocity is relatively small, values of V are shown in velocity diagrams in places where V_{θ_z}, literally, should be shown.

(2) Radii at the hub section include an aerodynamic blockage factor and are not physical dimensions.

6660-4

Figure 4. Velocity diagrams for flow generating rotor.

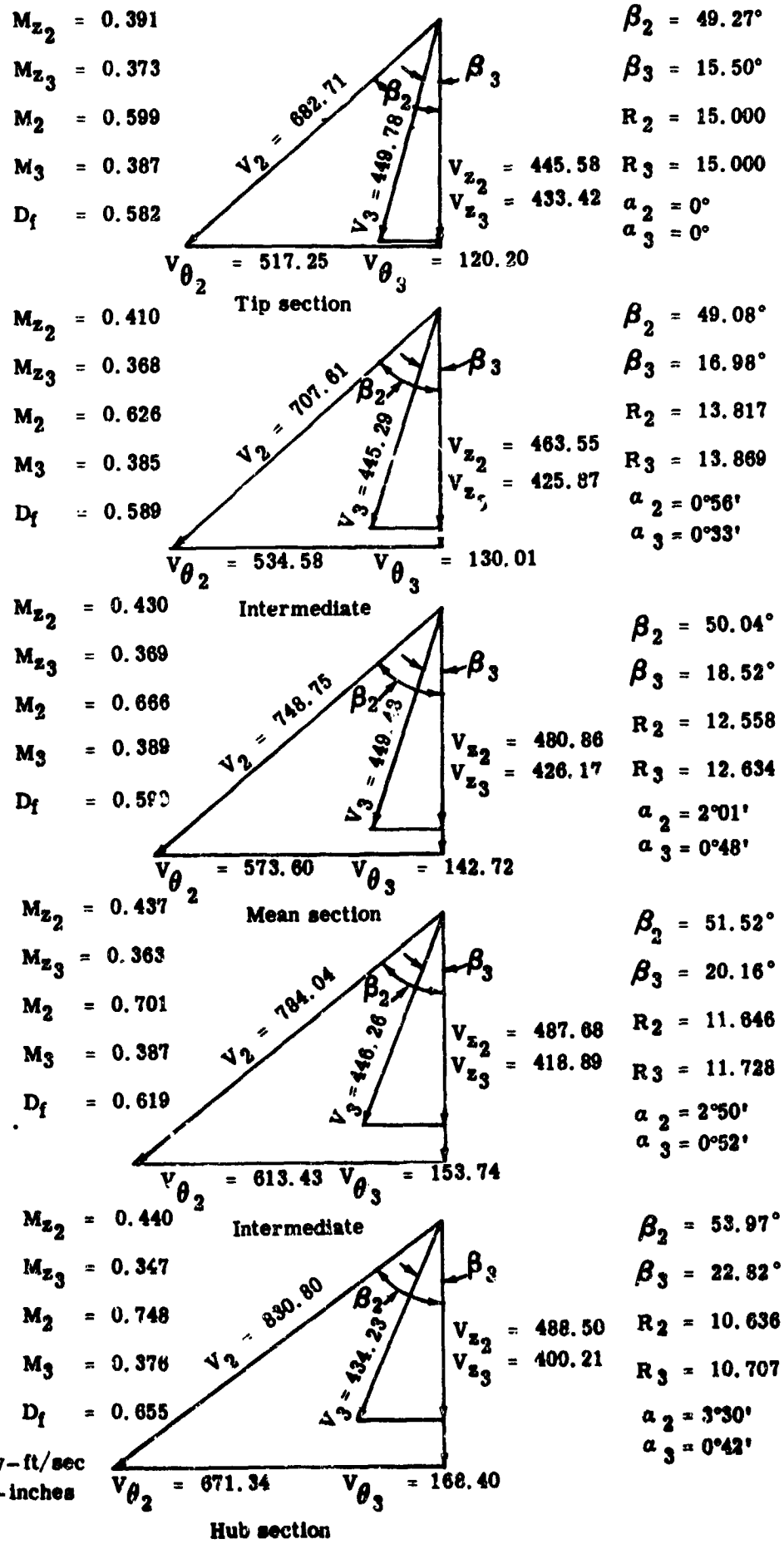

Notes: (1) Since the radial component of velocity is relatively small, values of V are shown in velocity diagrams in places where $V\theta_z$, literally, should be shown.

(2) Radii at the hub section include an aerodynamic blockage factor and are not physical dimensions.

6060-6

Figure 5. Velocity diagrams for 0.65 hub D_f stator.

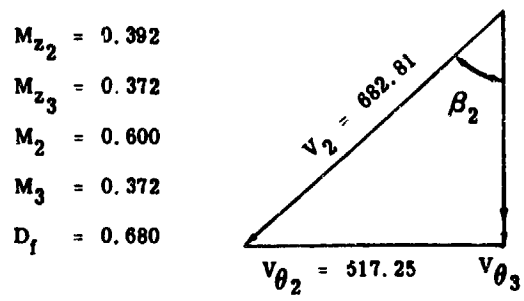

Tip section

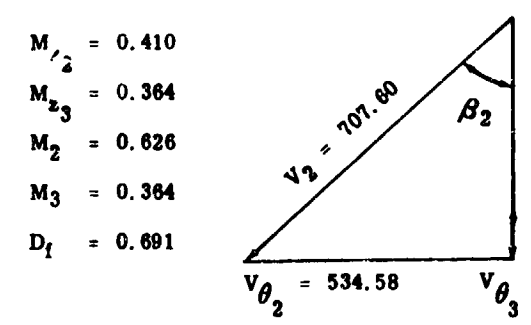

Intermediate

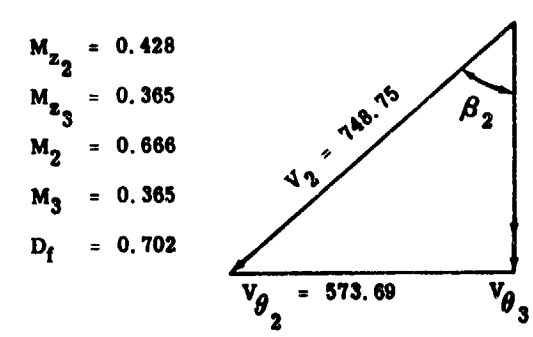

Mean section

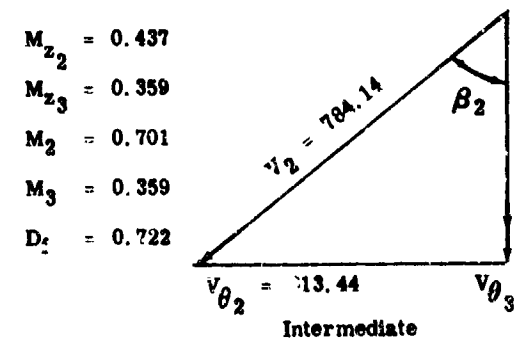

Intermediate

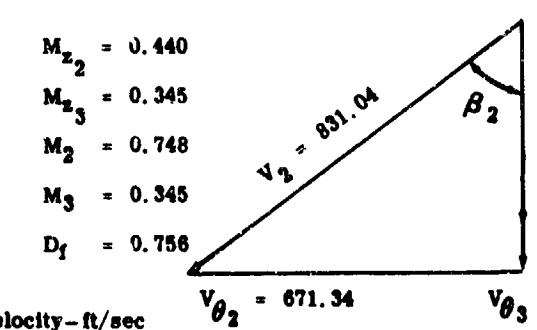

V, velocity – ft/sec
R, radius – inches

Hub section

Notes: (1) Since the radial component of velocity is relatively small, values of V are shown in velocity diagrams in places where V_{θ_z}, literally, should be shown.

(2) Radii at the hub section include an aerodynamic blockage factor and are not physical dimensions.

6060-5

Figure 6. Velocity diagrams for 0.75 hub D_f stator.

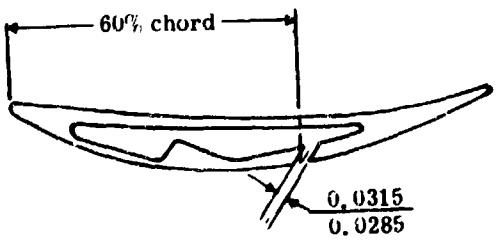

a. 0.65 D_f single-slotted bleed

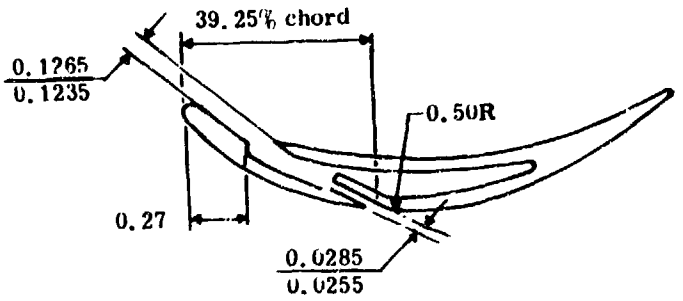

d. 0.75 D_f single-slotted blowing

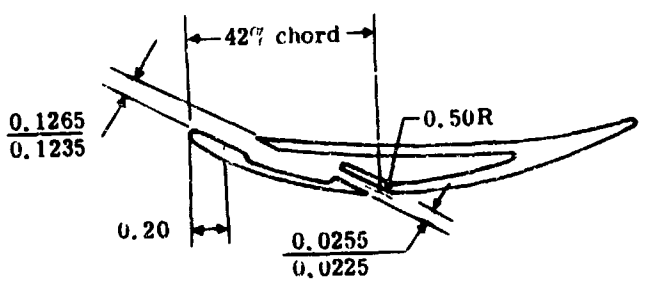

b. 0.65 D_f single-slotted blowing

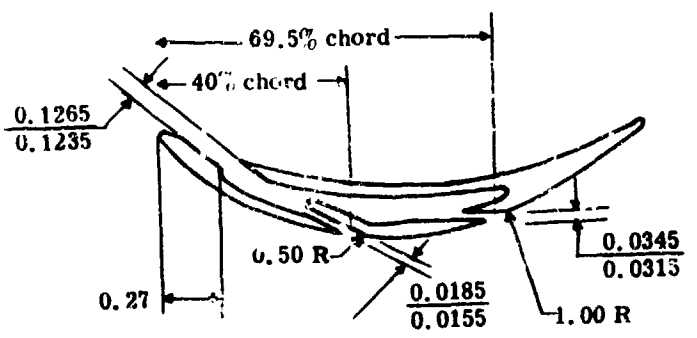

e. 0.75 D_f double-slotted blowing

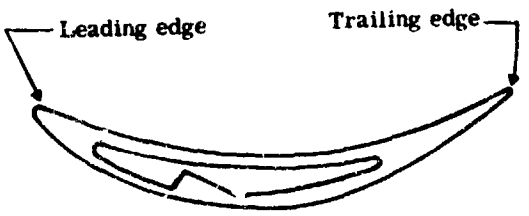

c. 0.75 D_f unslotted

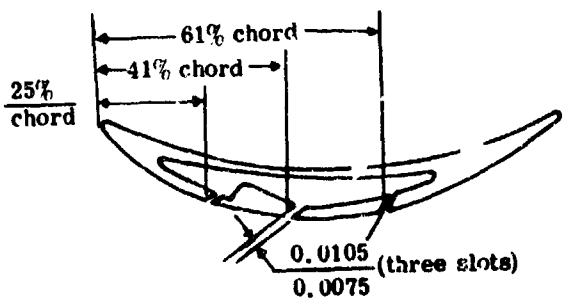

f. 0.75 D_f triple-slotted bleed

6060-79

Figure 7. Typical airfoil sections for slotted and unslotted stators.

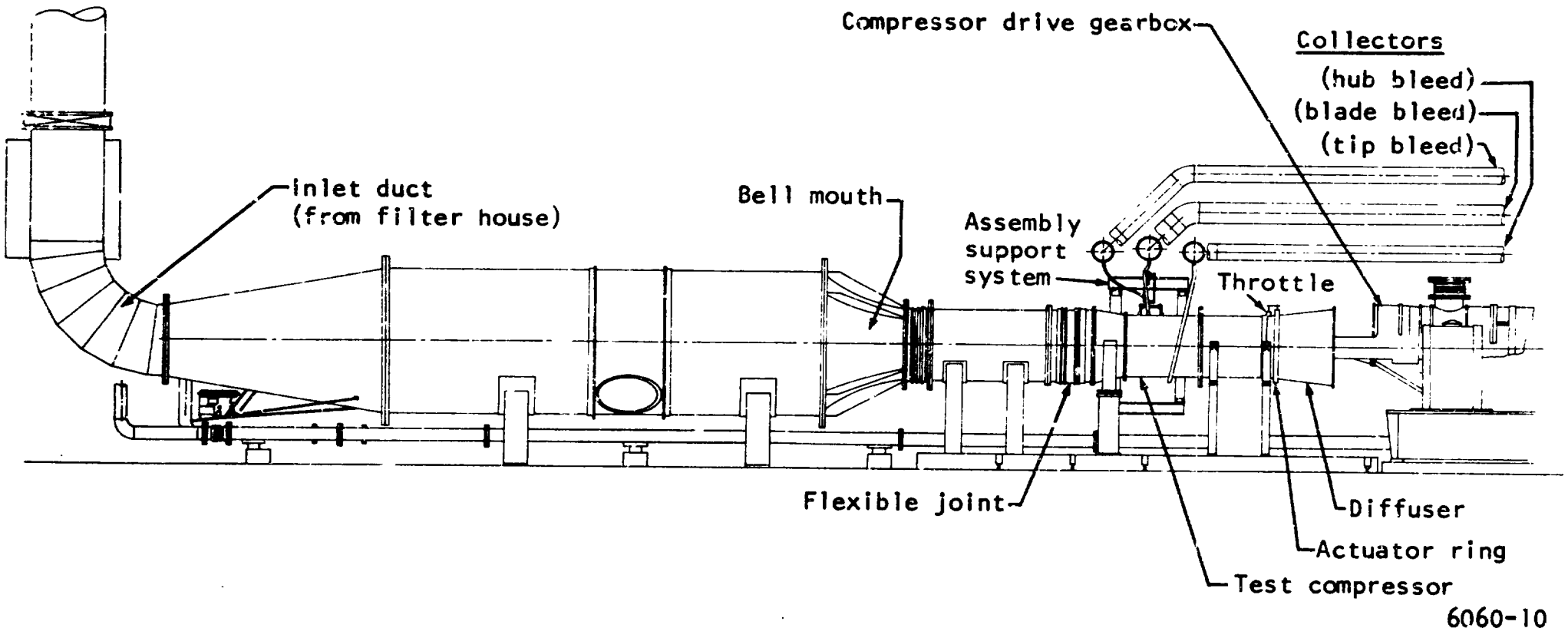

Figure 8. Compressor test facility.

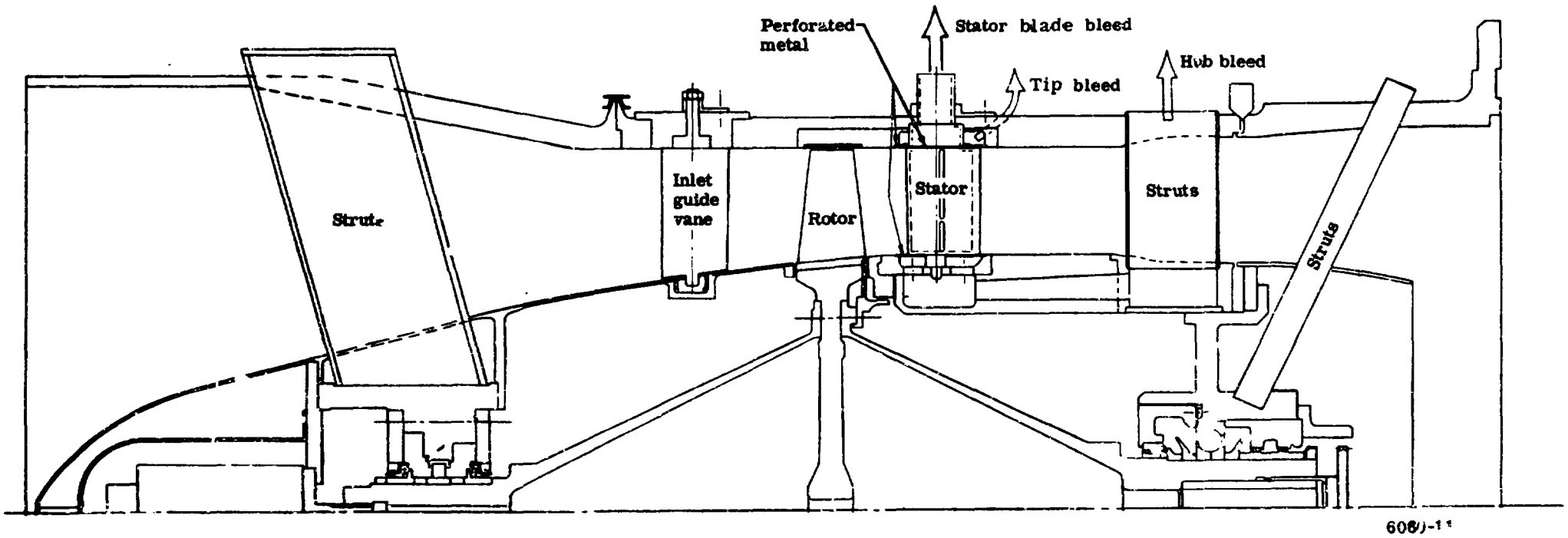

Figure 9. Layout of compressor test rig.

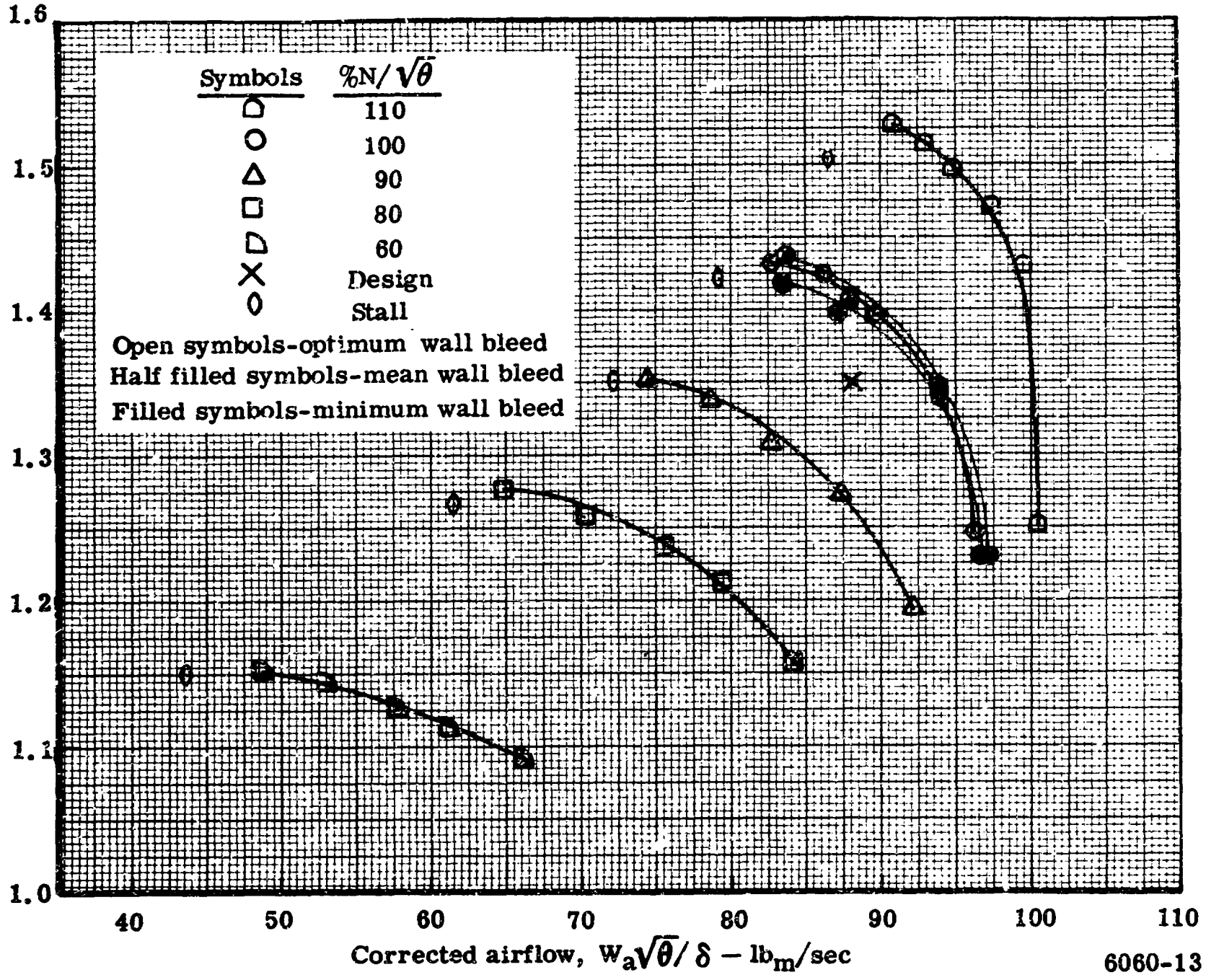

Figure 10. Unslotted 0.75 D_f stator—stage overall performance—pressure ratio.

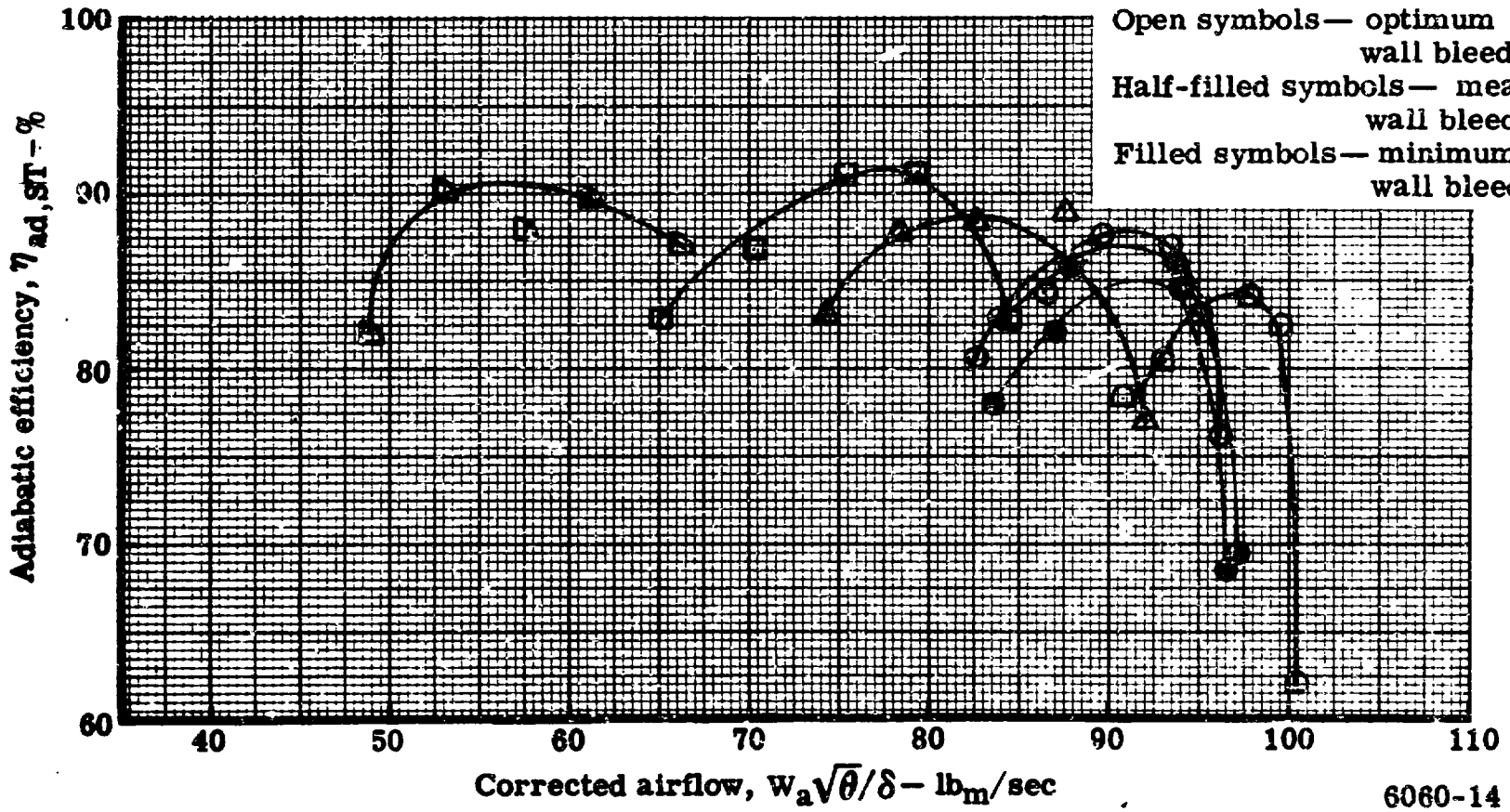

Figure 11. Unslotted 0.75 D_f stator—stage overall performance—adiabatic efficiency.

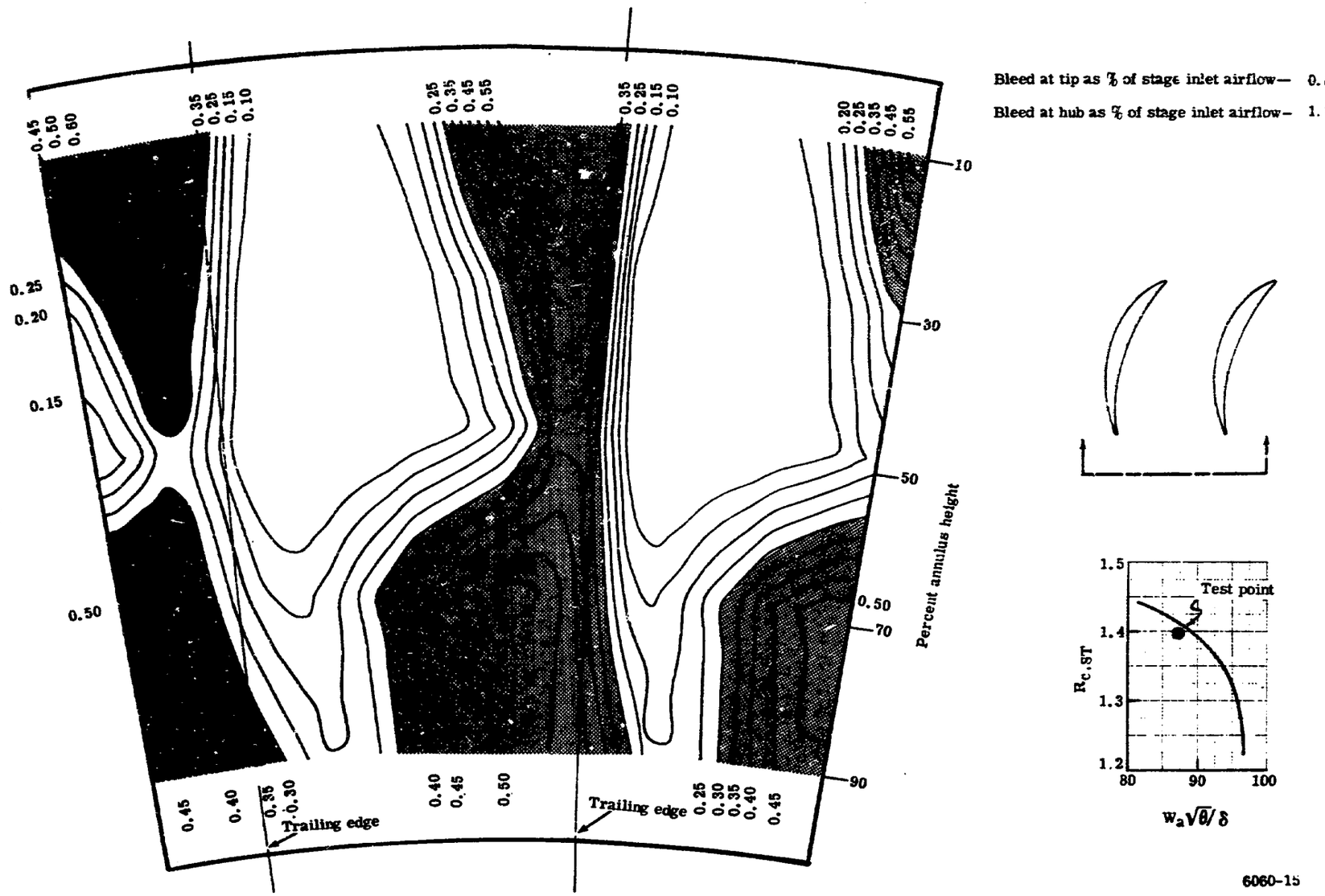

Figure 12. 0.75 D_f unslotted stator—contour plot of local total pressure loss coefficient, (ω_3)—minimum wall bleed.

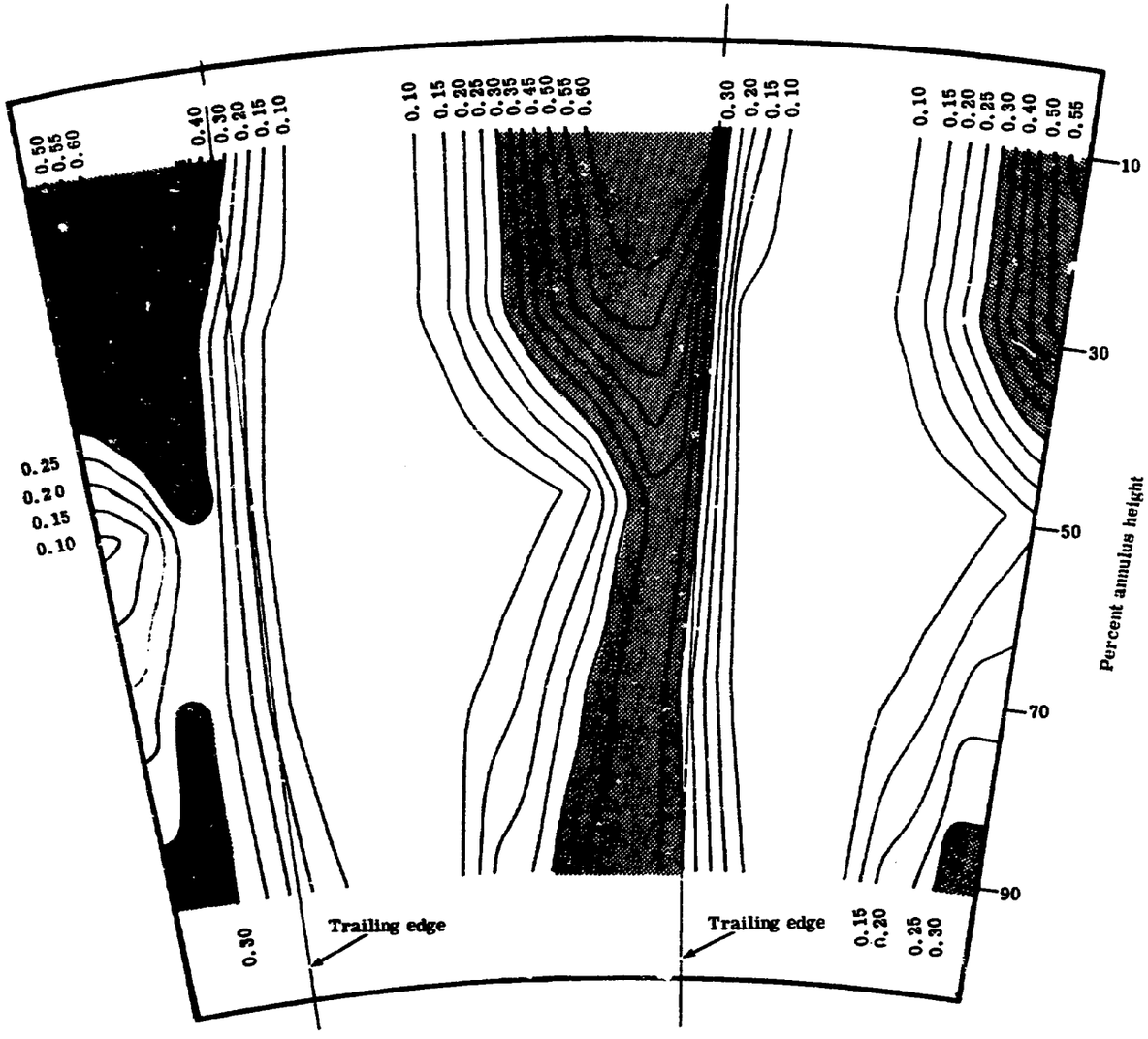

Bleed at tip as % of stage inlet airflow— 1.44

Bleed at hub as % of stage inlet airflow— 2.09

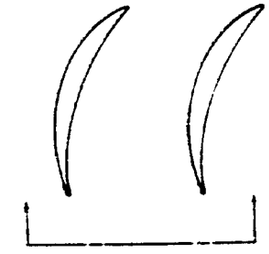

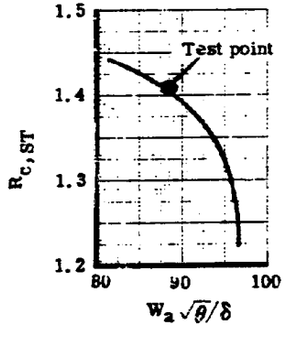

6060-16

Figure 13. 0.75 D_f unslotted stator—contour plot of local total pressure loss coefficient, (ω_3)—mean wall bleed.

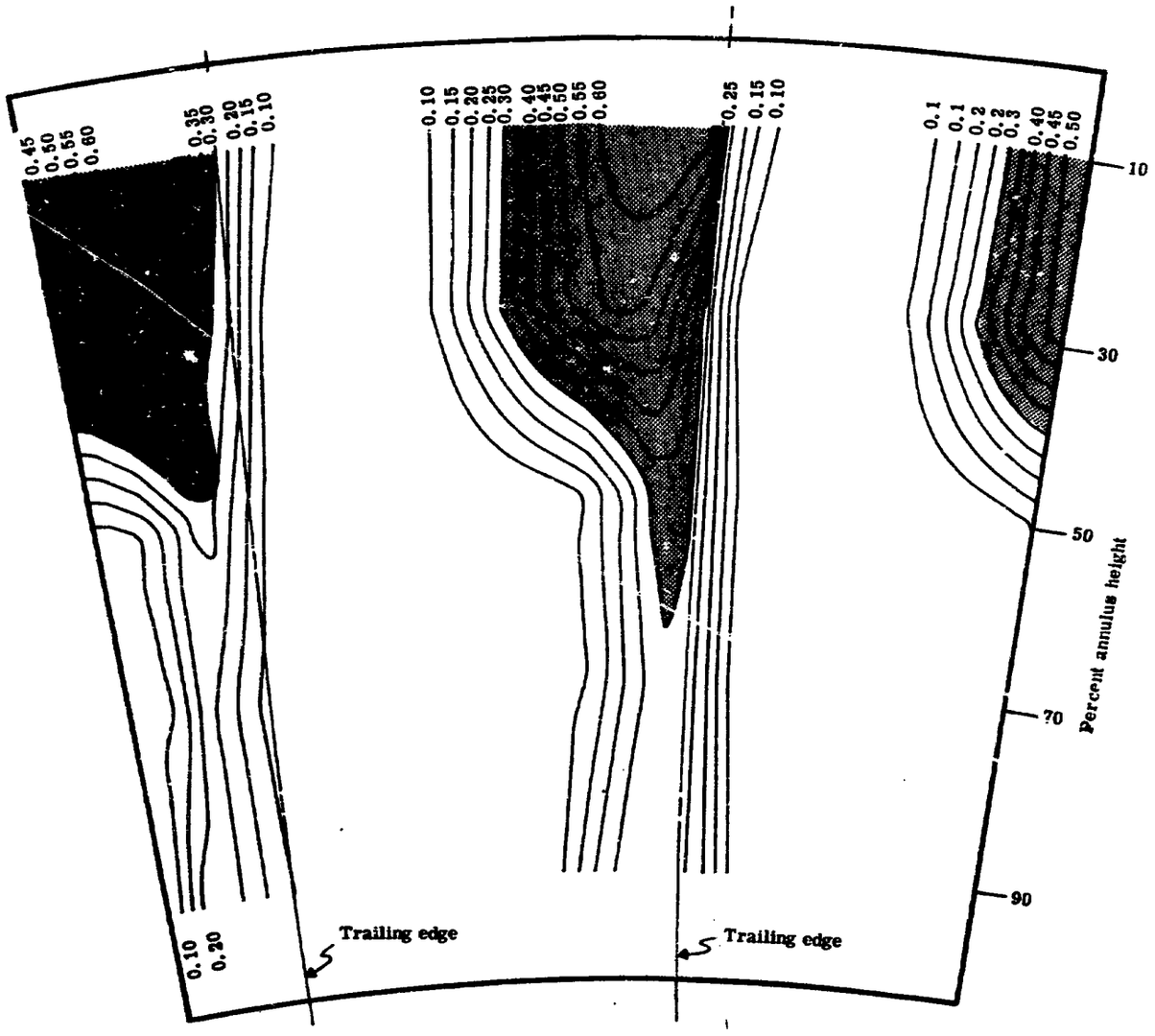

Bleed at tip as % of stage inlet airflow— 2.00

Bleed at hub as % of stage inlet airflow— 2.45

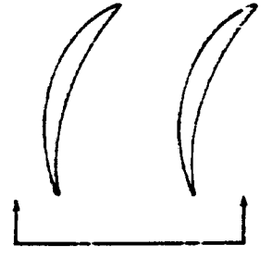

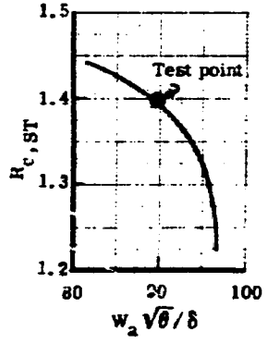

6060-17

Figure 14. 0.75 D_f unslotted stator—contour plot of local total pressure loss coefficient, (ω_3)—optimum wall bleed.

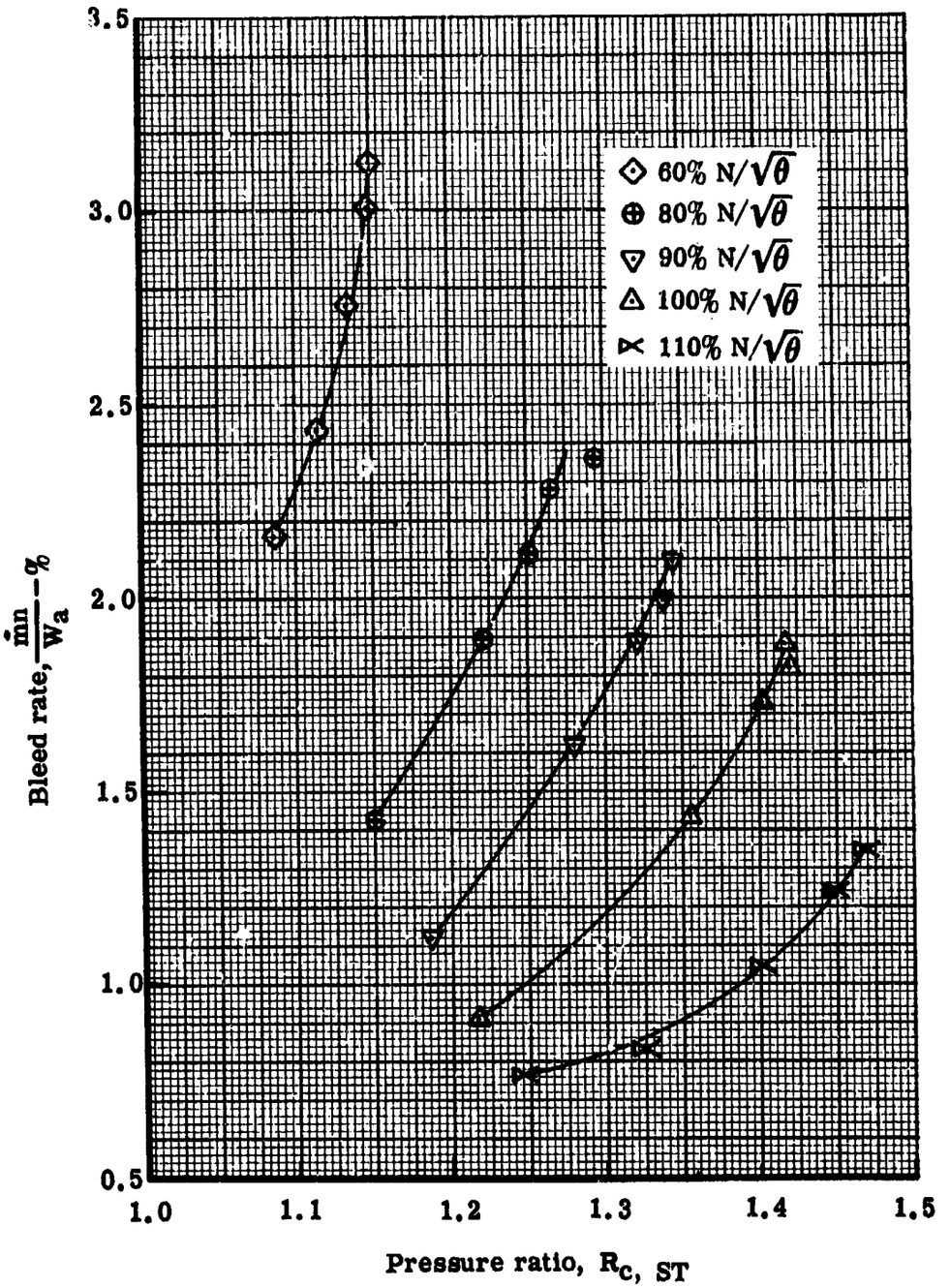

Figure 15. 0.75 D_f triple-slotted stator—bleed rate vs stage pressure ratio—optimum bleed rate.

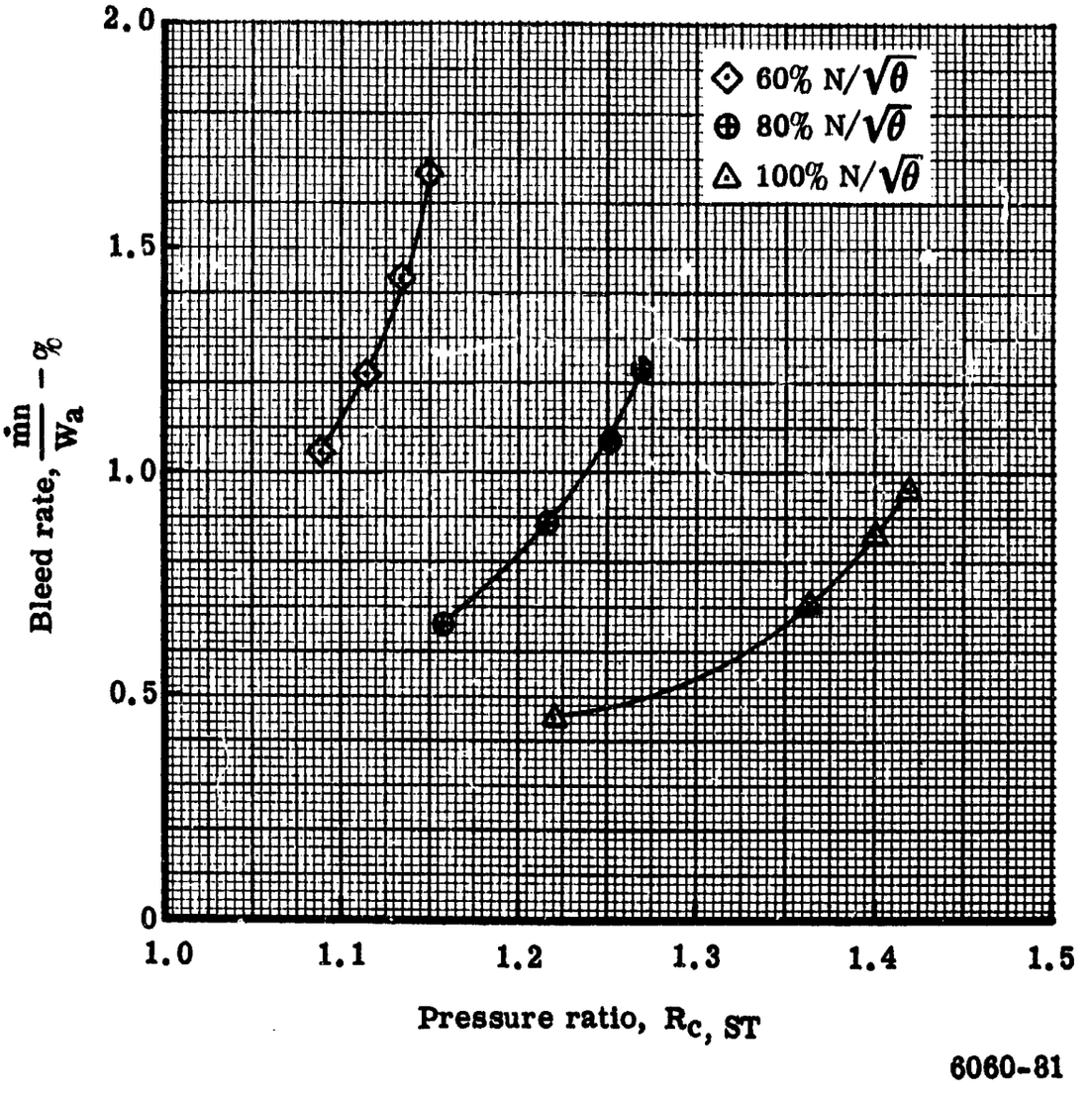

Figure 16. 0.75 D_f triple-slotted stator—bleed rate vs stage pressure ratio—mean bleed rate.

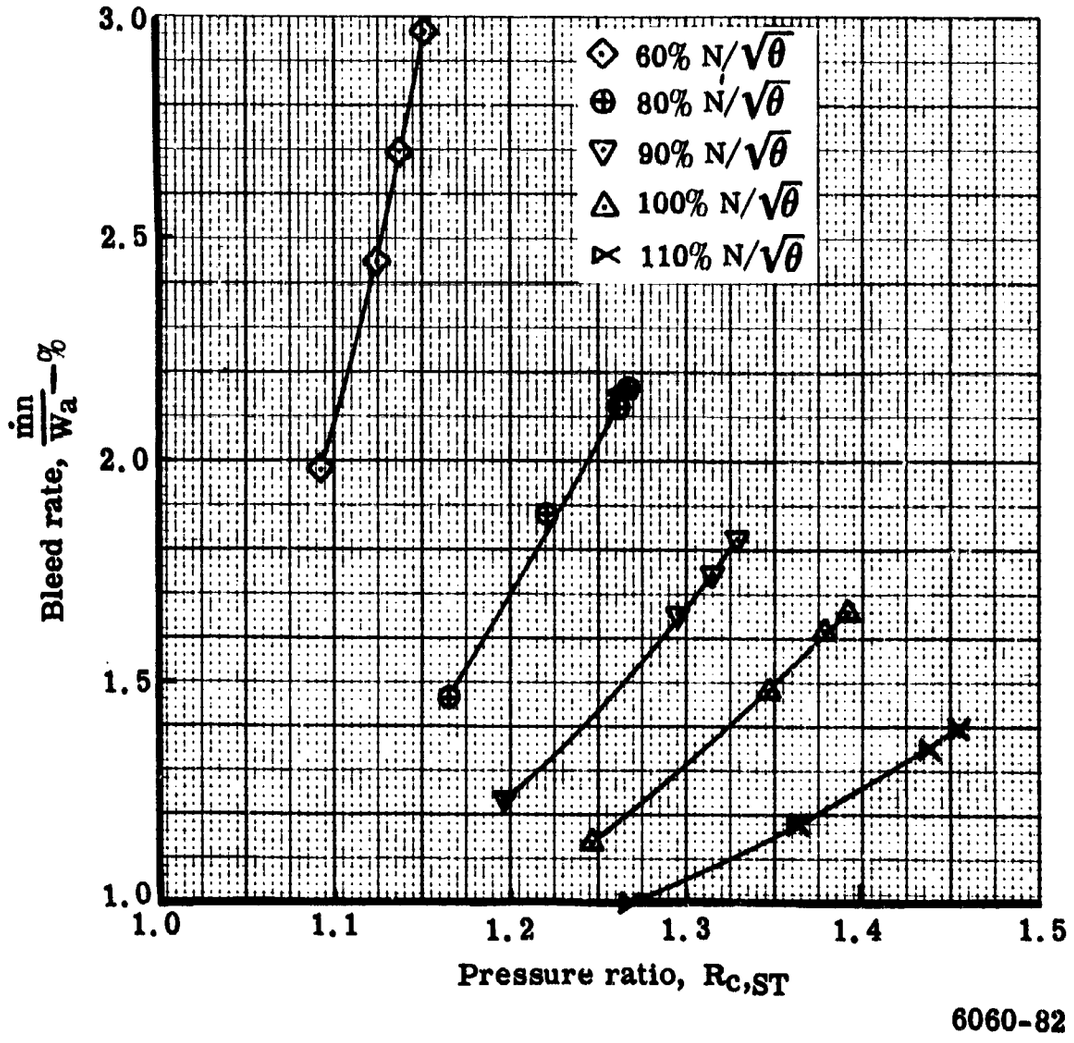

Figure 17. 0.65 D_f single-slotted stator—bleed rate vs stage pressure ratio—optimum bleed rate.

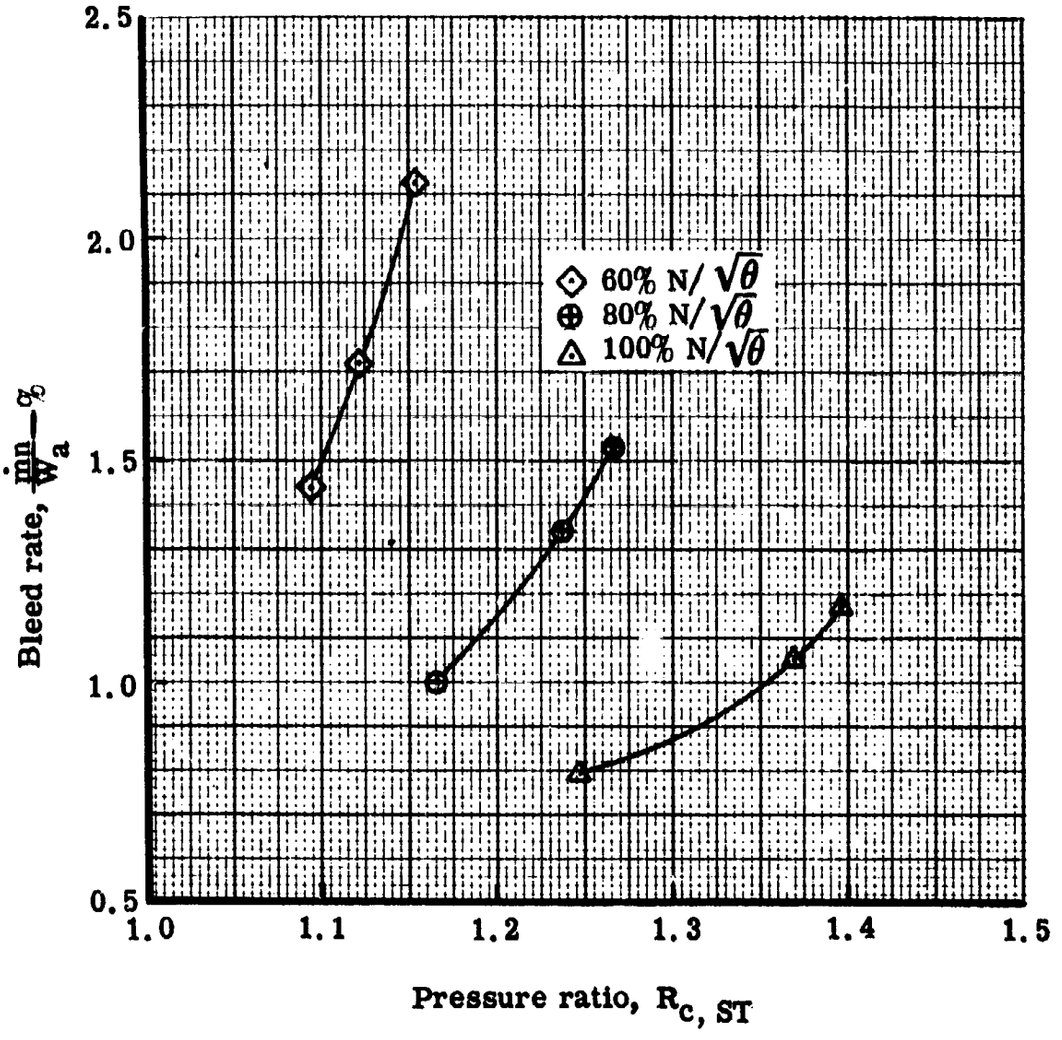

Figure 18. 0.65 D_f single-slotted stator—bleed rate vs stage pressure ratio—2/3 optimum bleed rate.

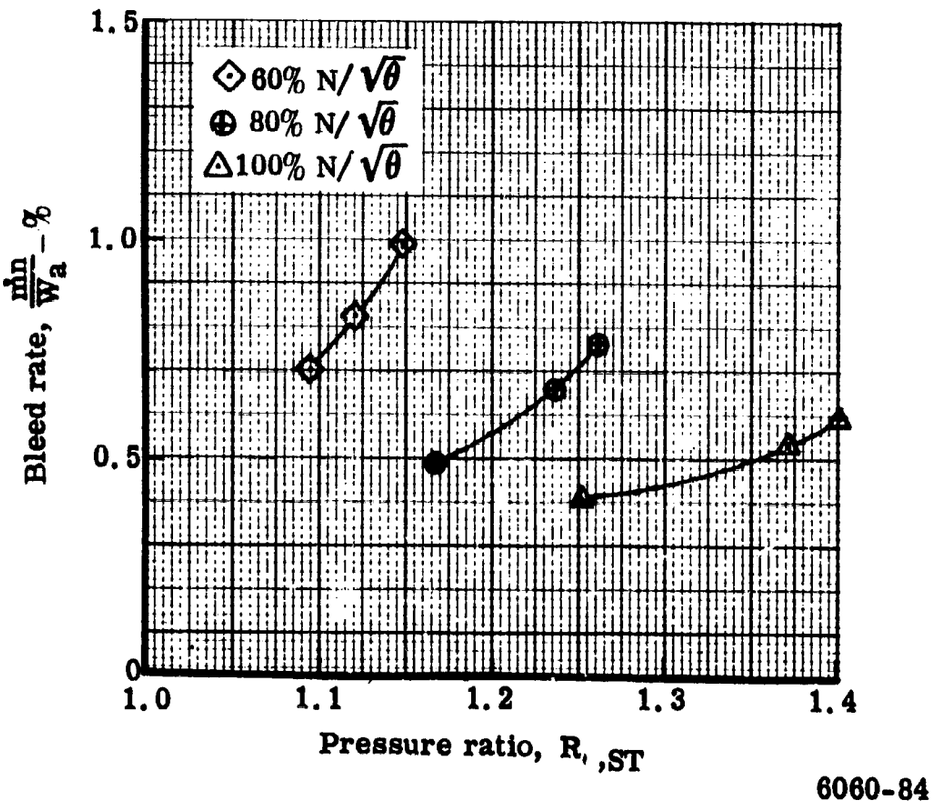

Figure 19. 0.65 D_f single-slotted stator—bleed rate vs stage pressure ratio—1/3 optimum bleed rate.

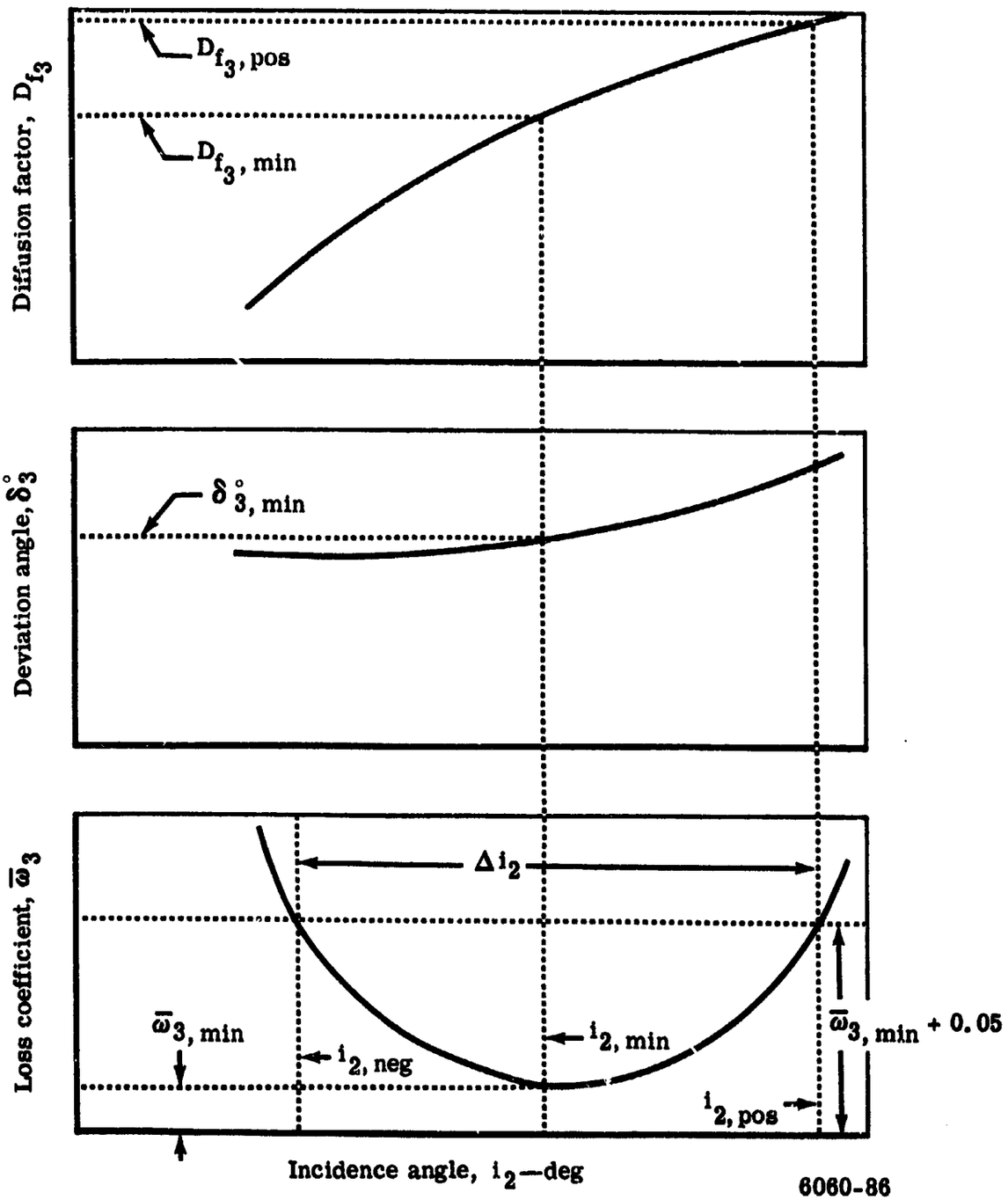

Figure 20. Definition of minimum loss coefficient, range, and related quantities.

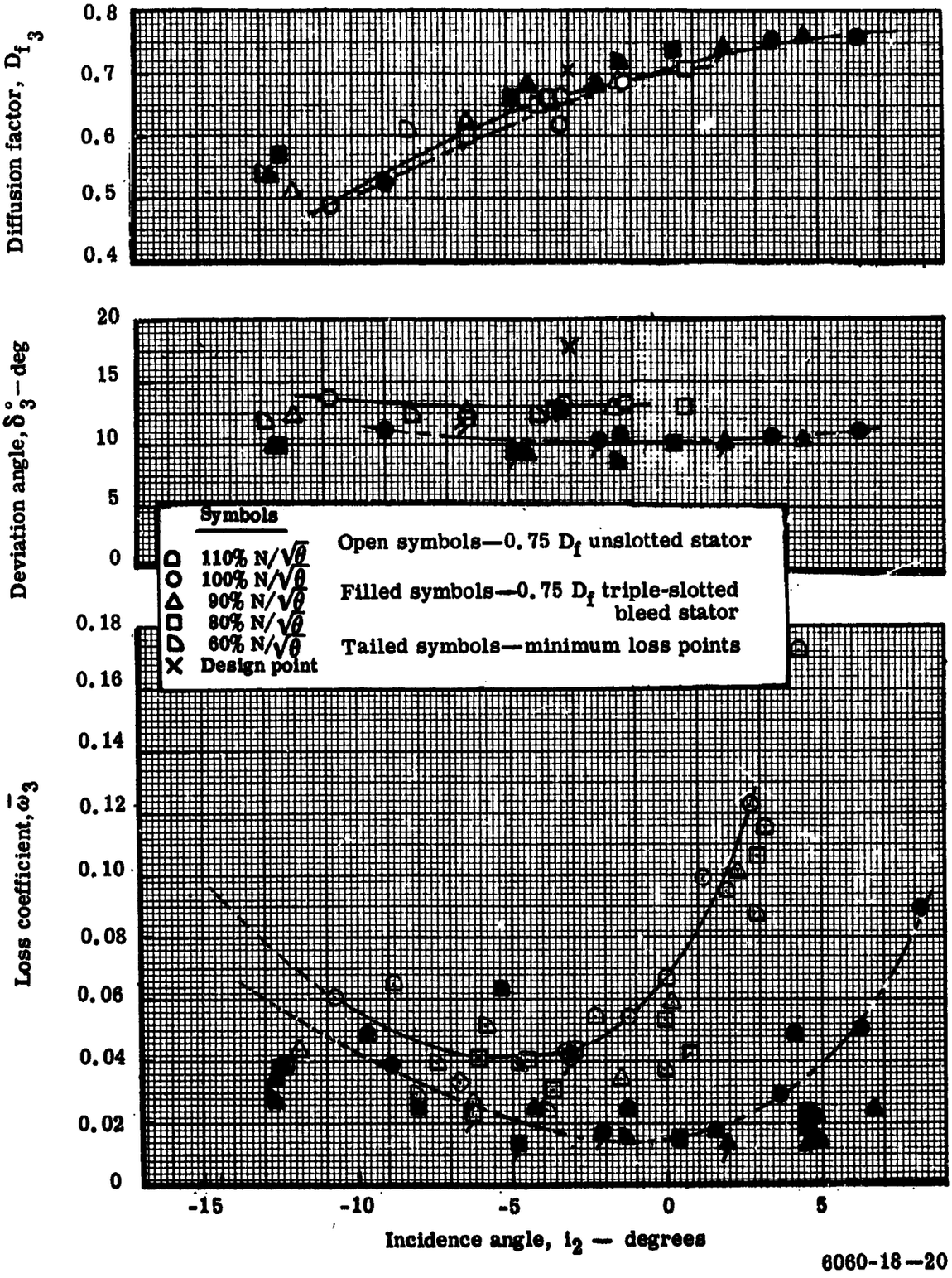

Figure 21a. Blade element performance—comparison of 0.75 D_f triple-slotted bleed stator vs 0.75 D_f unslotted stator at 50% streamline.

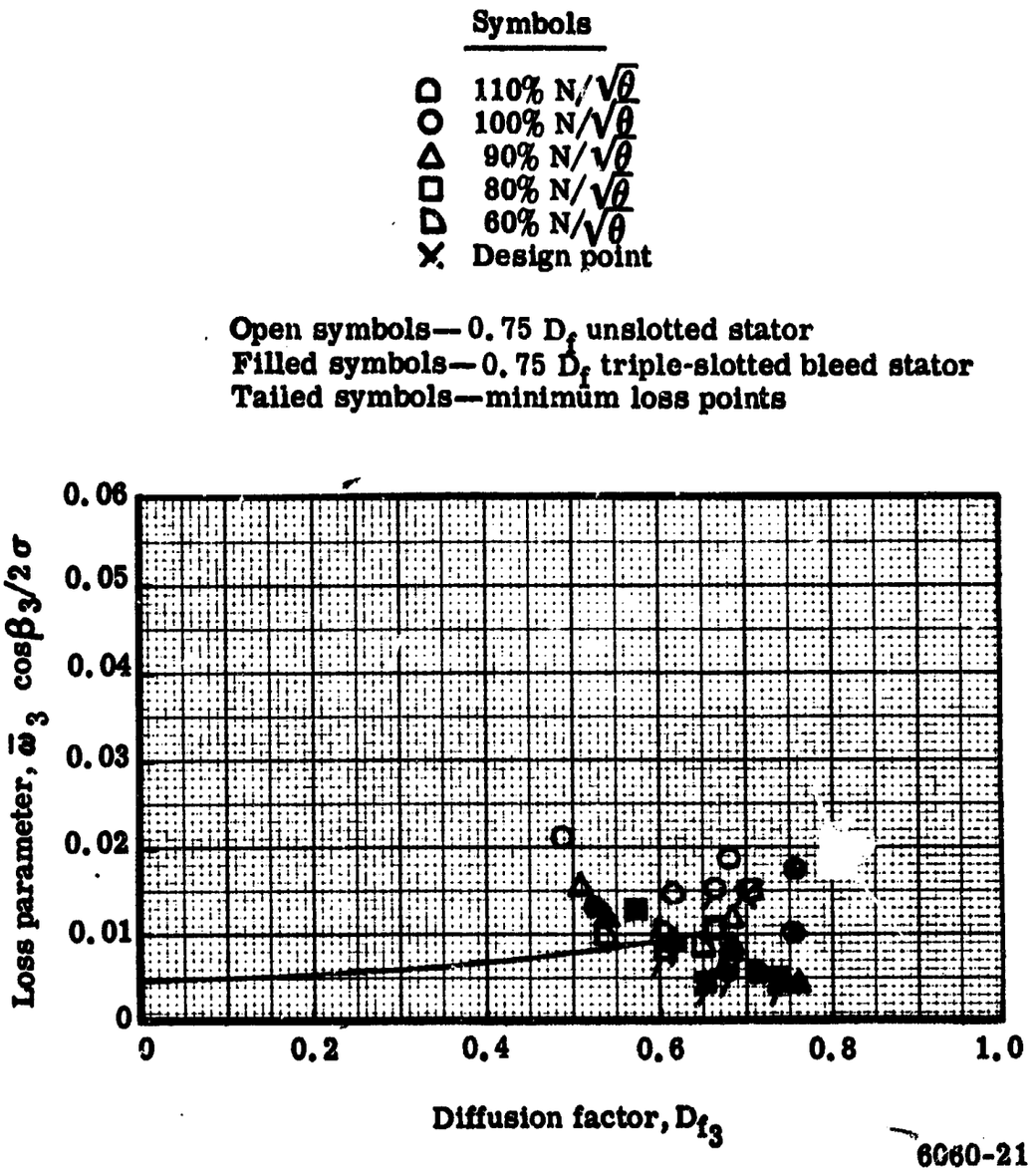

Figure 21b. Loss parameter vs diffusion factor—comparison of 0.75 D_f triple-slotted bleed stator with 0.75 D_f unslotted stator at 50% streamline.

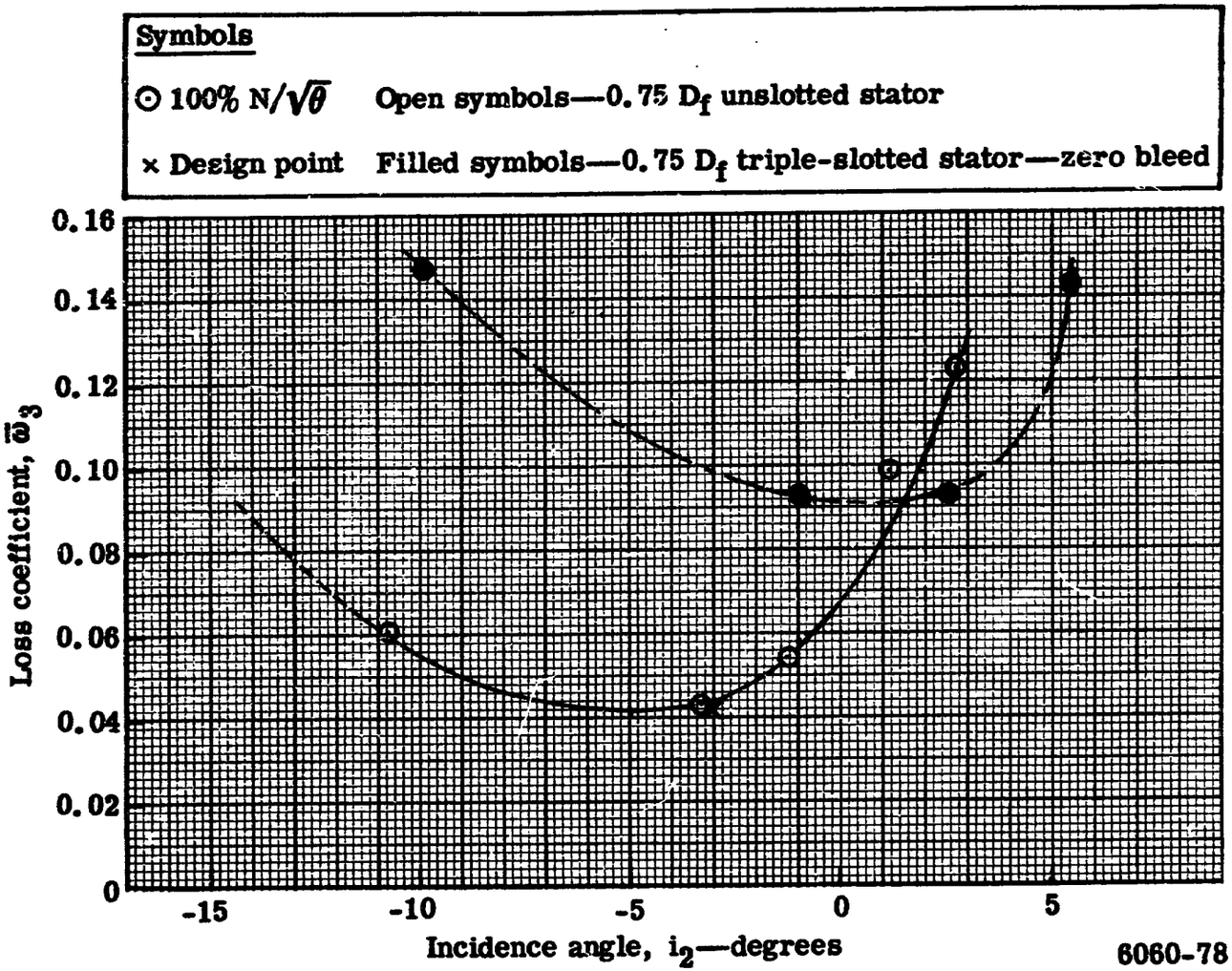

Figure 22. Blade element performance—comparison of 0.75 D_f triple-slotted bleed stator with zero bleed vs 0.75 D_f unslotted stator at 50% streamline.

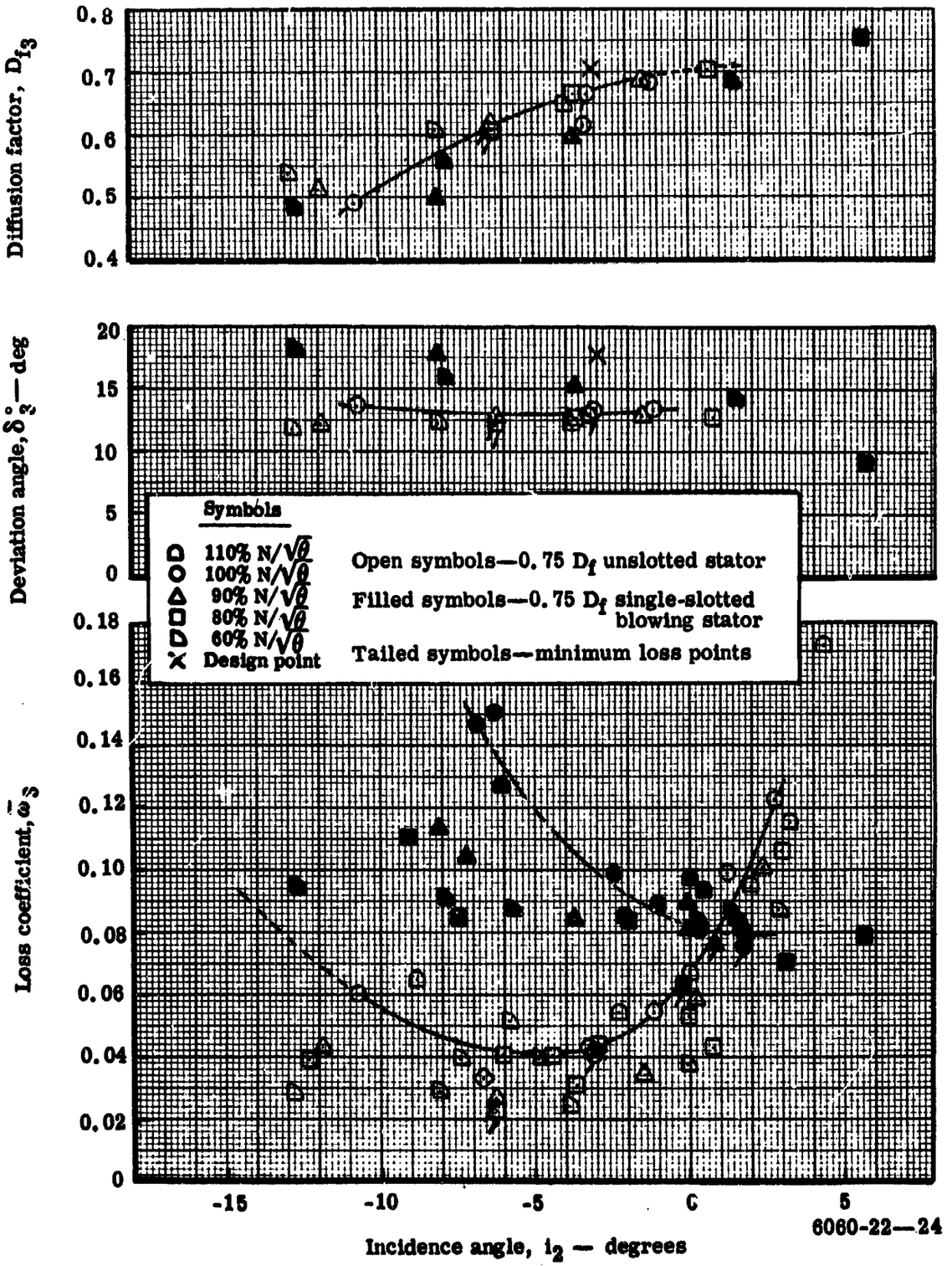

Figure 23a. Blade element performance—comparison of 0.75 D_f single-slotted blowing stator vs 0.75 D_f unslotted stator at 50% streamline.

Symbols

◻	110% N/$\sqrt{\theta}$
○	100% N/$\sqrt{\theta}$
△	90% N/$\sqrt{\theta}$
□	80% N/$\sqrt{\theta}$
▽	60% N/$\sqrt{\theta}$
×	Design point

Open symbols—0.75 D_f unslotted stator
Filled symbols—0.75 D_f single-slotted blowing stator
Tailed symbols—minimum loss points

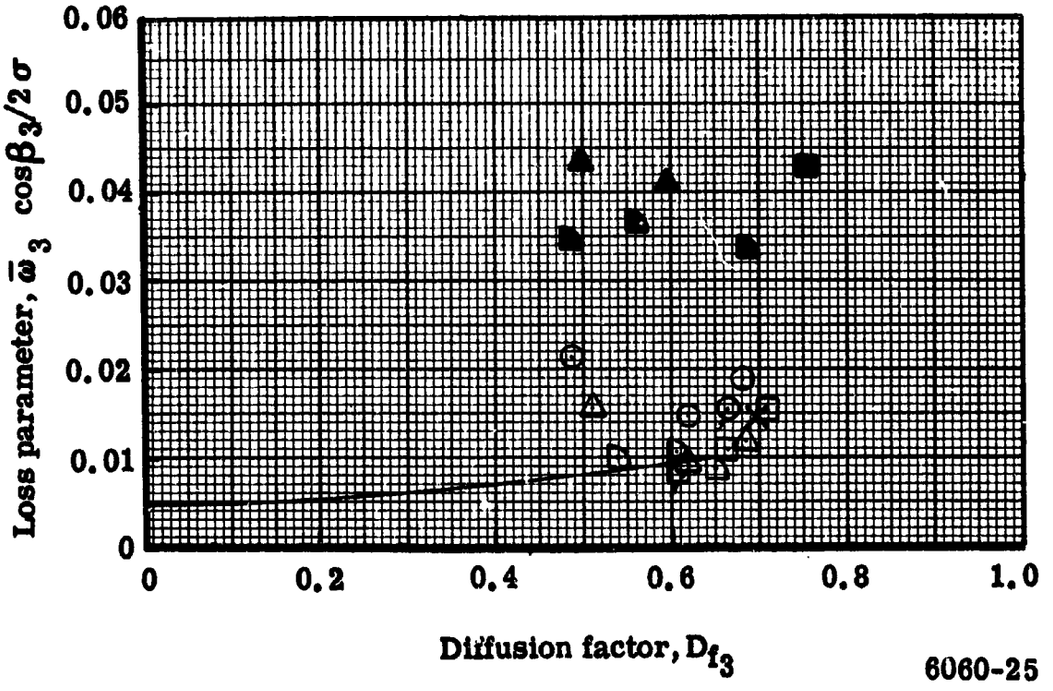

Figure 23b. Loss parameter vs diffusion factor—comparison of 0.75 D_f single-slotted blowing stator with 0.75 D_f unslotted stator at 50% streamline.

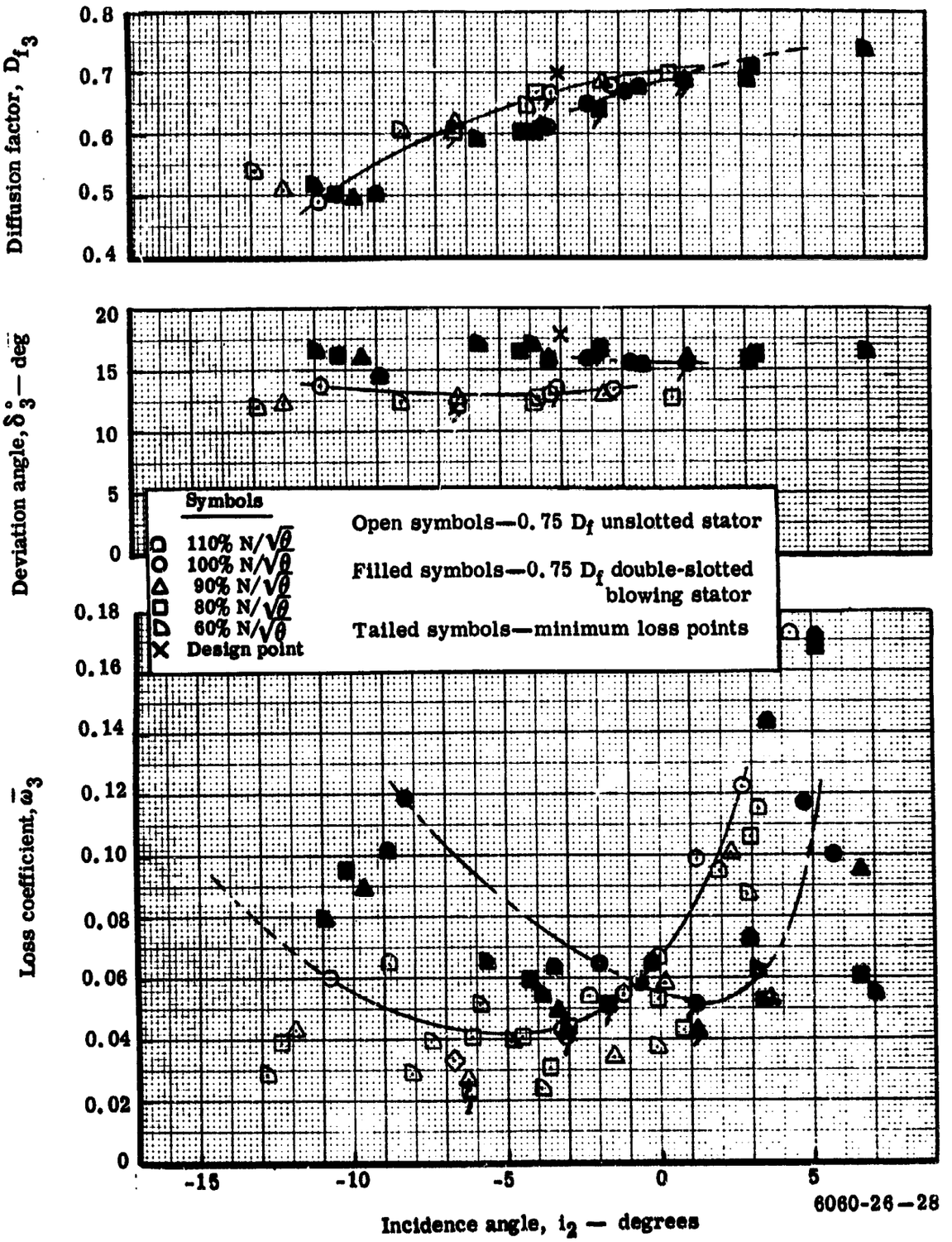

Figure 24a. Blade element performance—comparison of 0.75 D_f double-slotted blowing stator vs 0.75 D_f unslotted stator at 50% streamline.

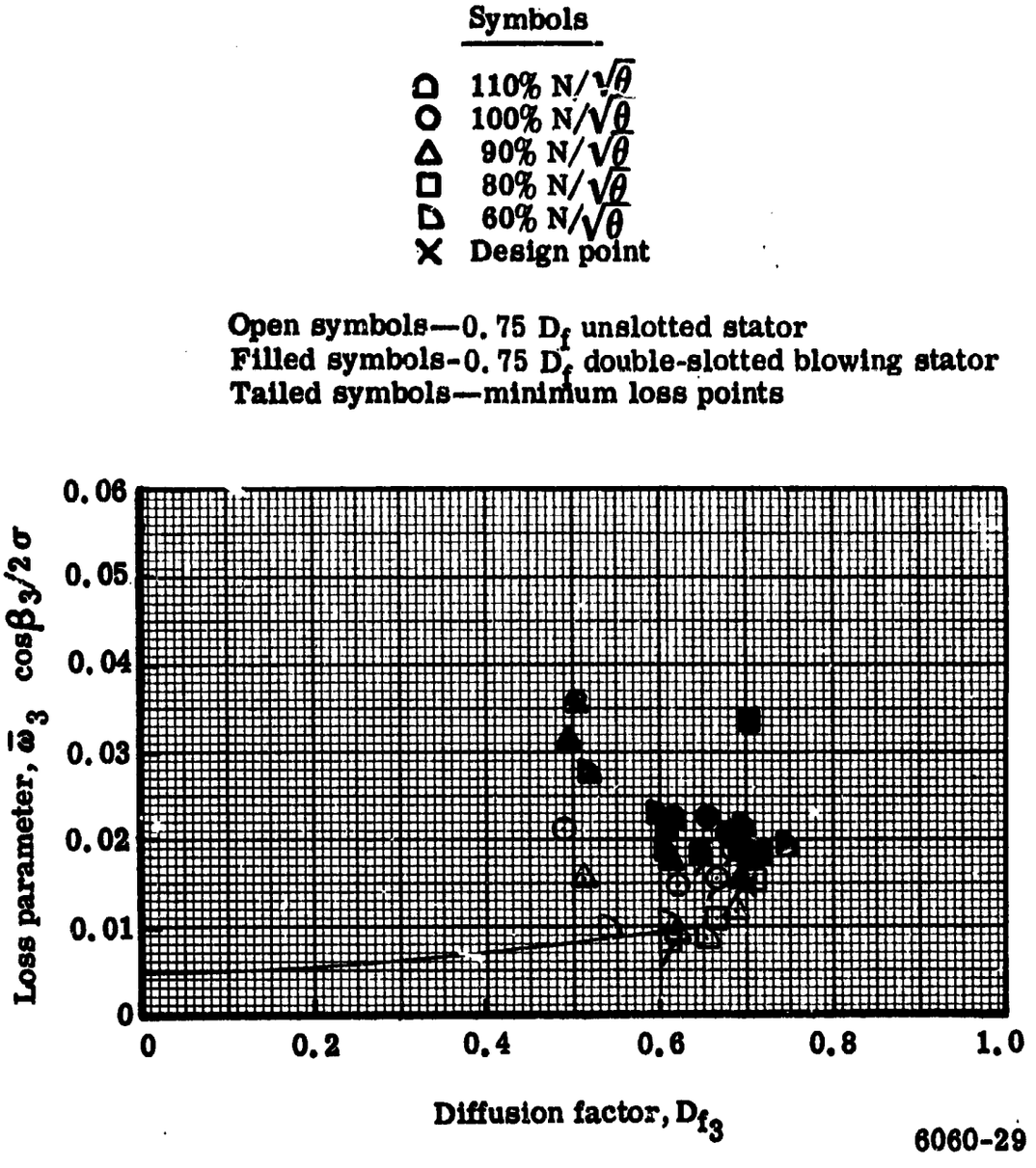

Figure 24b. Loss parameter vs diffusion factor—comparison of 0.75 D_f double-slotted blowing stator with 0.75 D_f unslotted stator at 50% streamline.

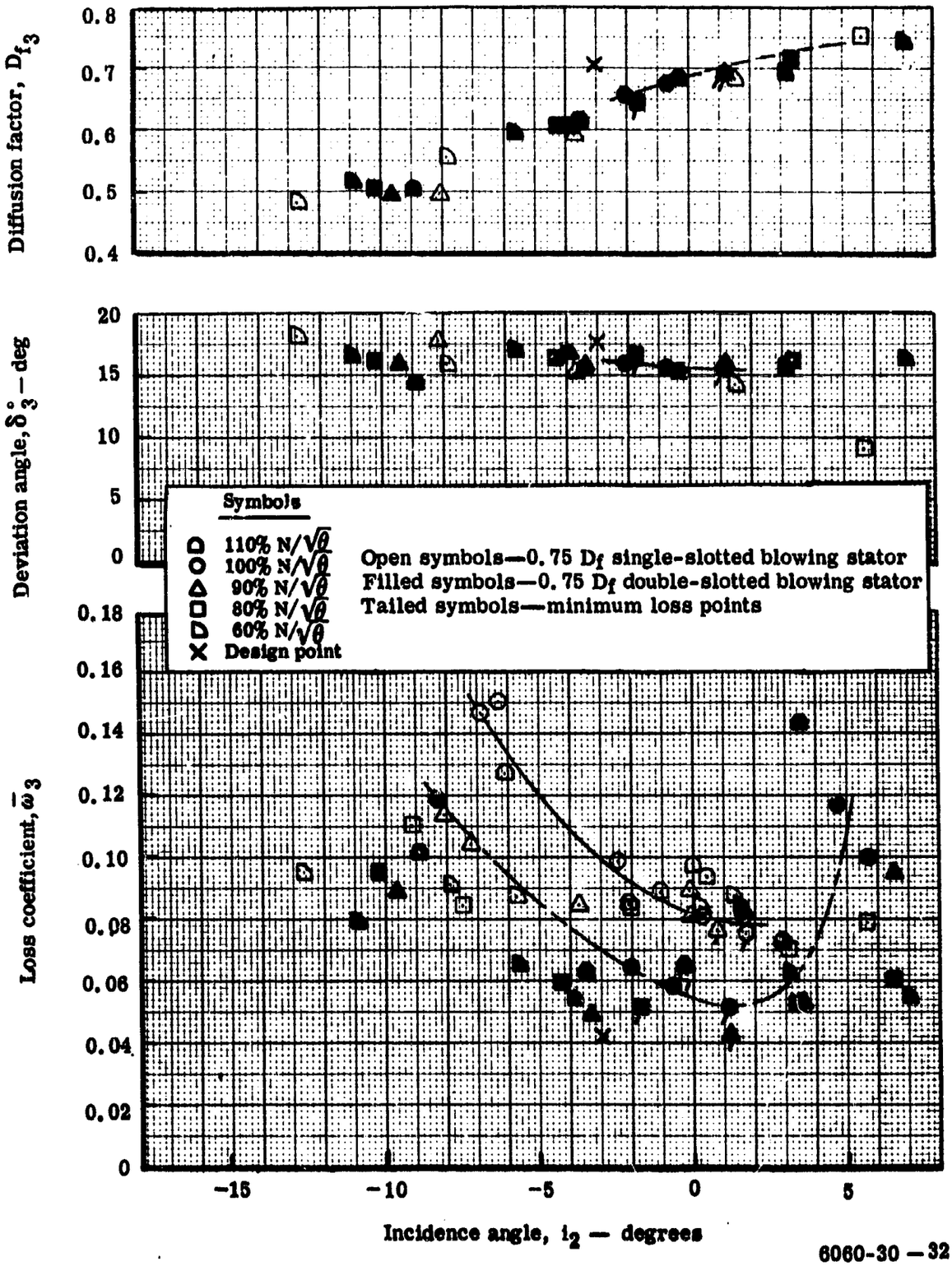

Figure 25a. Blade element performance—comparison of 0.75 D_f single-slotted blowing stator vs 0.75 D_f double-slotted blowing stator at 50% streamline.

Symbols

◻	110% $N/\sqrt{\theta}$
○	100% $N/\sqrt{\theta}$
△	90% $N/\sqrt{\theta}$
□	80% $N/\sqrt{\theta}$
▷	60% $N/\sqrt{\theta}$
✕	Design point

Open symbols— 0.75 D_f single-slotted blowing stator
Filled symbols— 0.75 D_f double-slotted blowing stator
Tailed symbols—minimum loss points

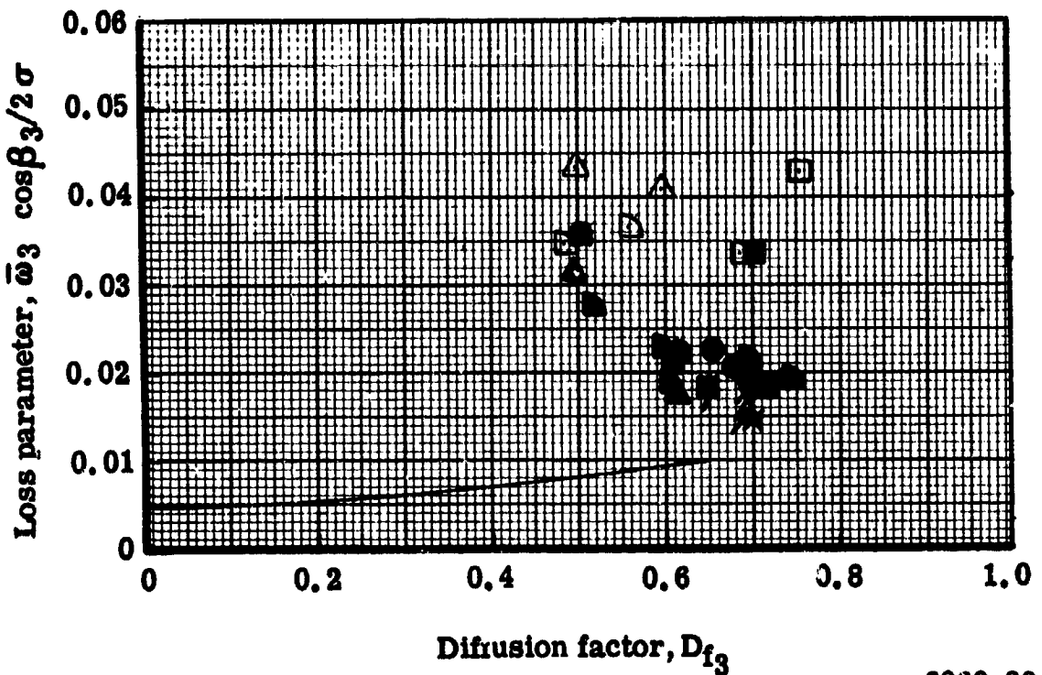

Figure 25b. Loss parameter vs diffusion factor—comparison of 0.75 D_f single-slotted blowing stator with 0.75 D_f double-slotted blowing stator at 50% streamline.

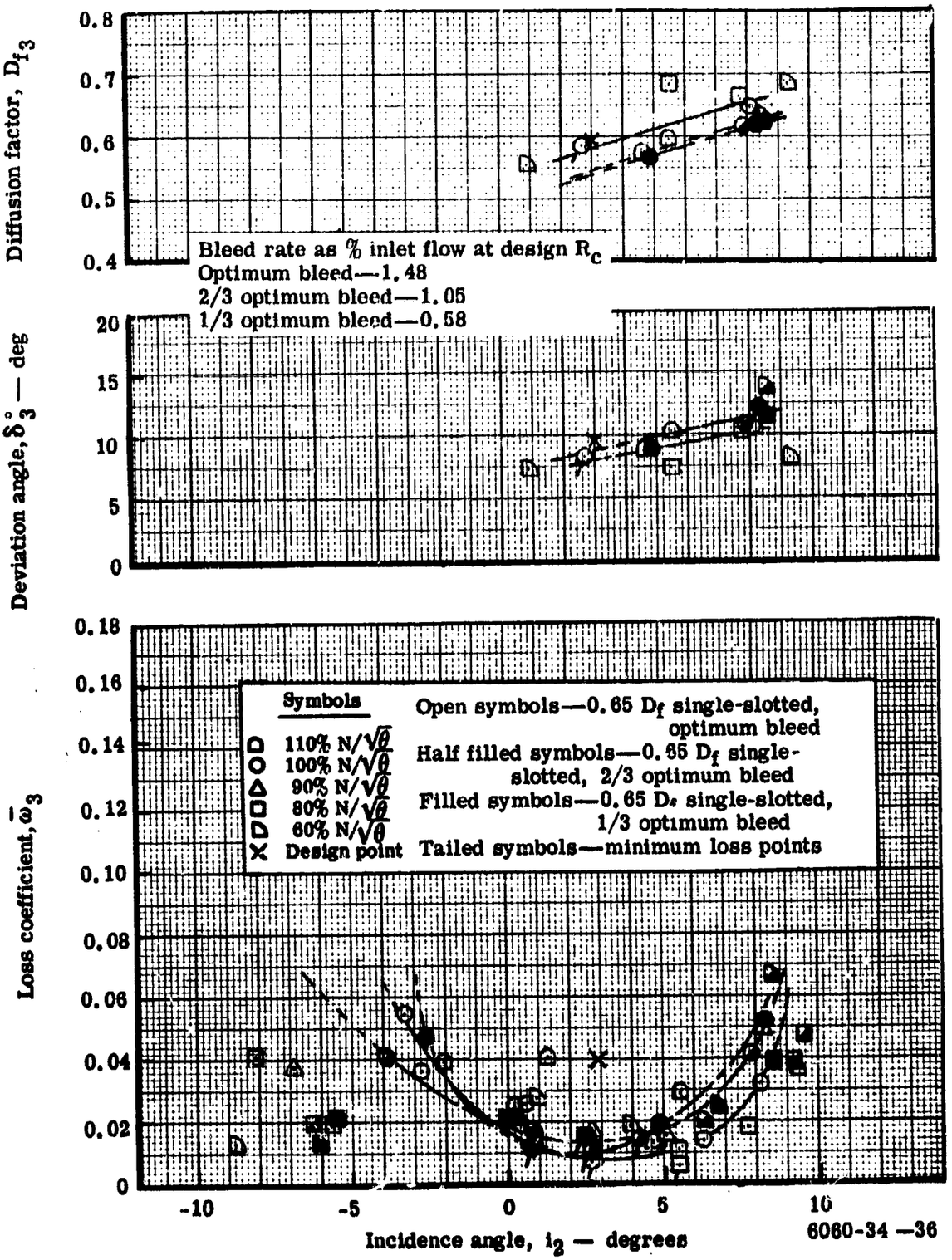

Figure 26a. Blade element performance—comparison of 0.65 D_f single-slotted stator at three bleed rates at 50% streamline.

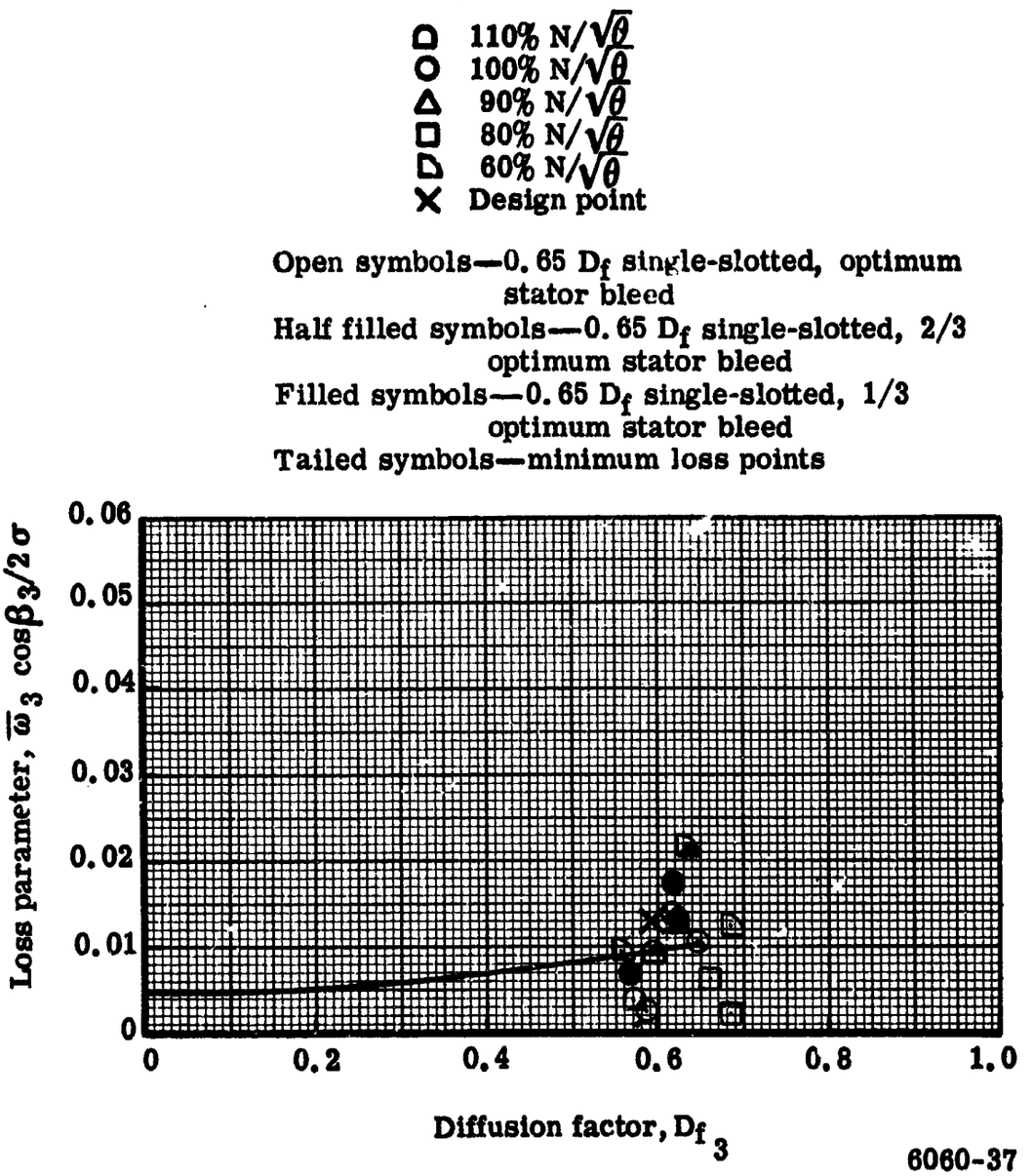

Figure 26b. Loss parameter vs diffusion factor—comparison of 0.65 D_f single-slotted stator at three bleed rates at 50% streamline.

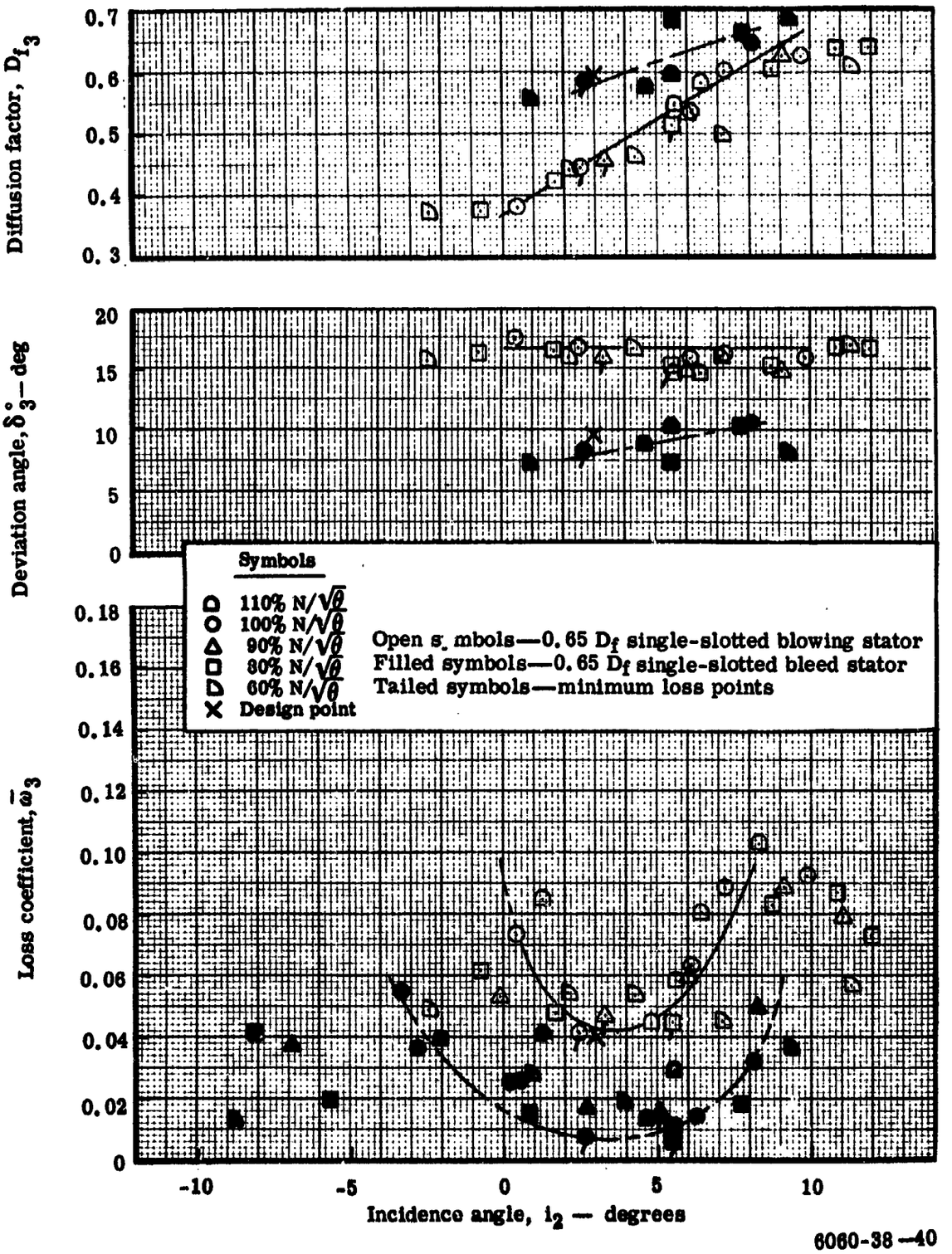

Figure 27a. Blade element performance—comparison of 0.65 D_f single-slotted blowing stator vs 0.65 D_f single-slotted bleed stator at 50% streamline.

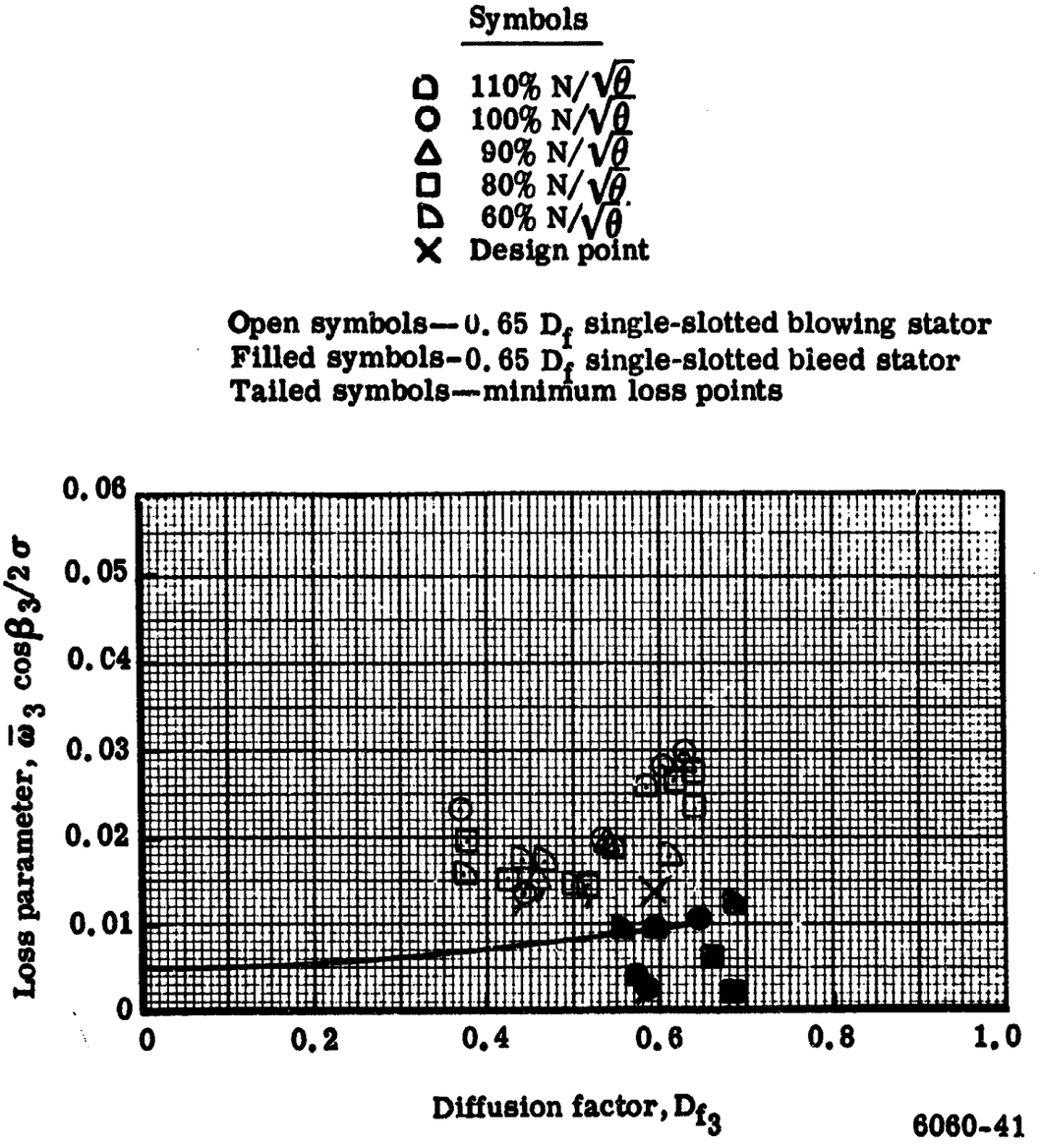

Figure 27b. Loss parameter vs diffusion factor—comparison of 0.65 D_f single-slotted blowing stator with 0.65 D_f single-slotted bleed stator at 50% streamline.

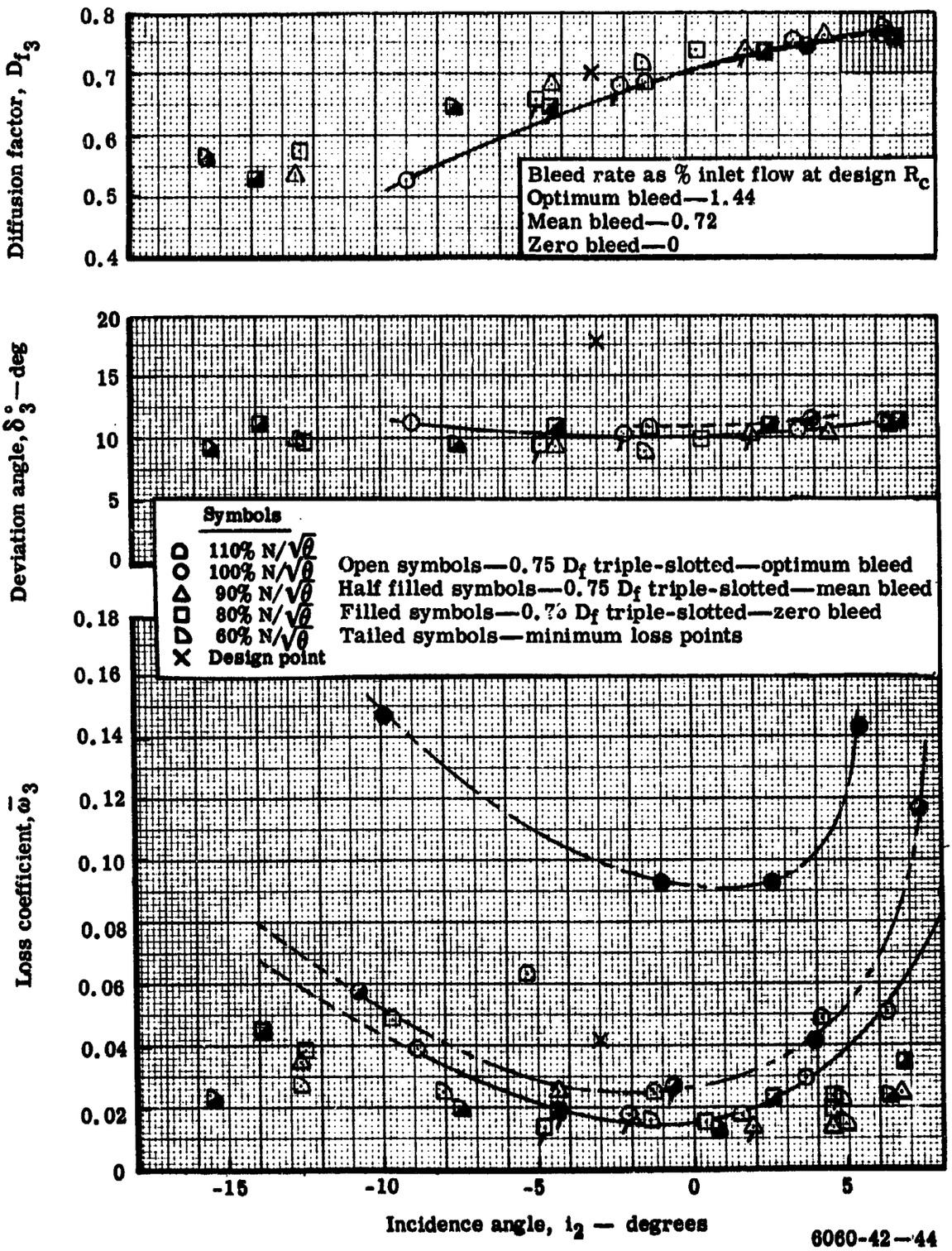

Figure 28a. Blade element performance—comparison of 0.75 D_f triple-slotted stator at three bleed rates at 50% streamline.

Symbols

◻	110% $N/\sqrt{\theta}$
○	100% $N/\sqrt{\theta}$
△	90% $N/\sqrt{\theta}$
◻	80% $N/\sqrt{\theta}$
▽	60% $N/\sqrt{\theta}$
×	Design point

Open symbols—0.75 D_f triple-slotted—optimum bleed
Half filled symbols—0.75 D_f triple-slotted—mean bleed
Filled symbols—0.75 D_f triple-slotted—zero bleed
Tailed symbols—minimum loss points

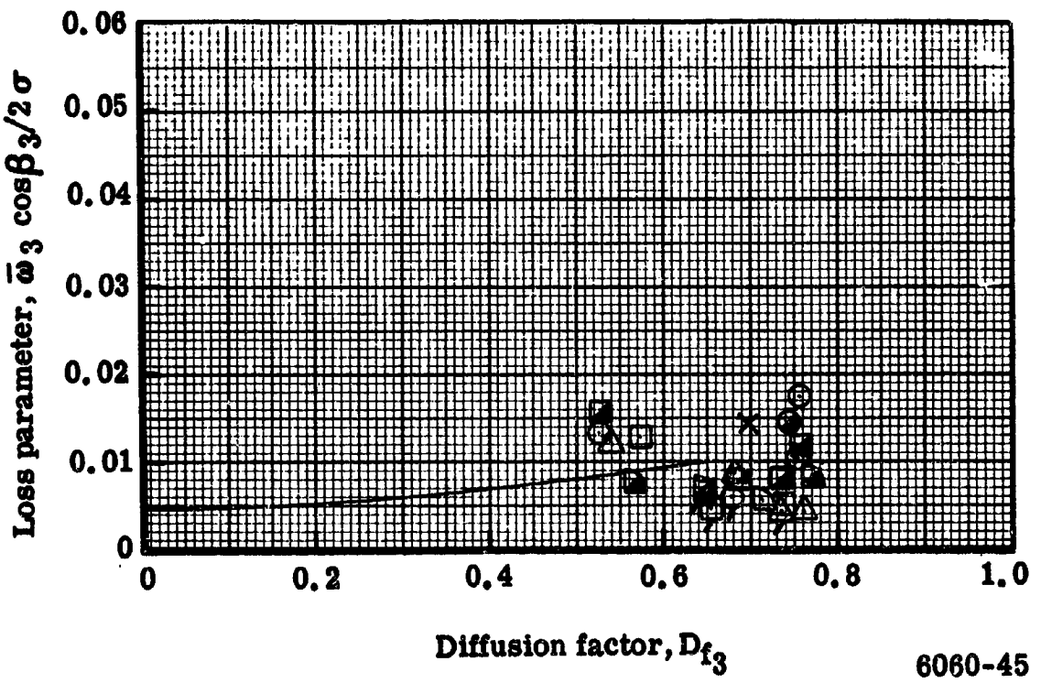

Figure 28b. Loss parameter vs diffusion factor—comparison of 0.75 D_f triple-slotted stator at three bleed rates at 50% streamline.

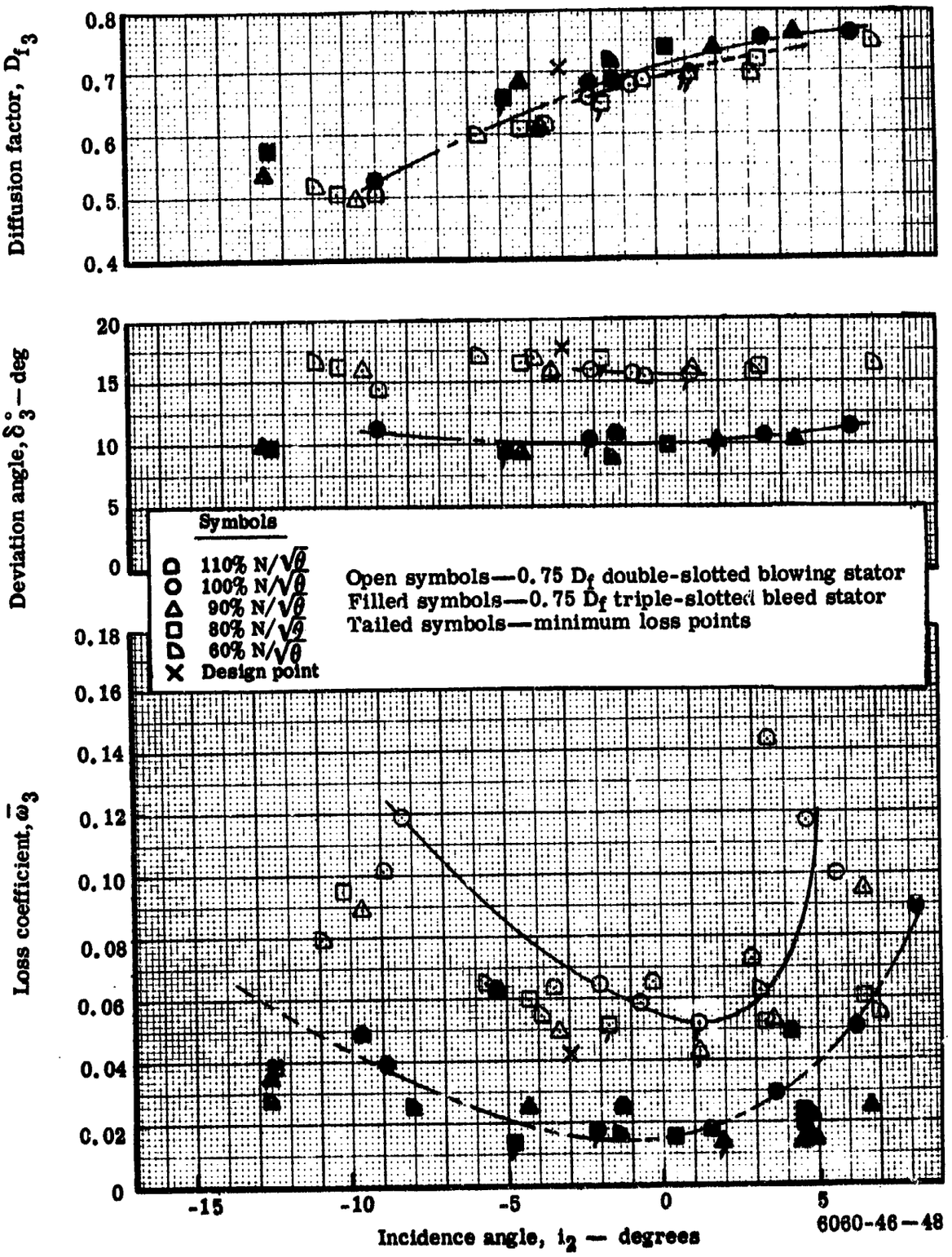

Figure 29a. Blade element performance—comparison of 0.75 D_f double-slotted blowing stator vs 0.75 D_f triple-slotted bleed stator at 50% streamline.

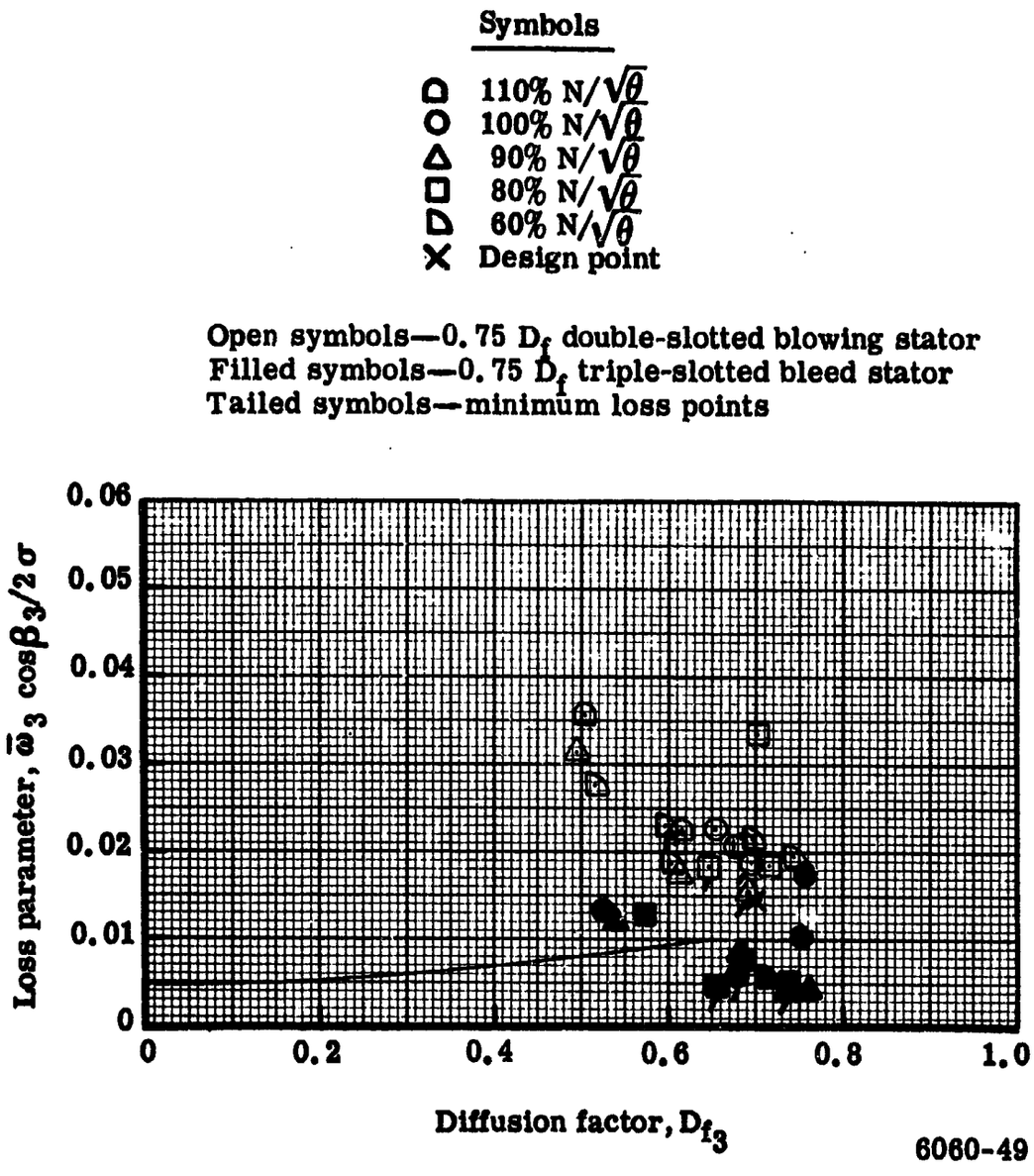

Figure 29b. Loss parameter vs diffusion factor—comparison of 0.75 D_f double-slotted blowing stator with 0.75 D_f triple-slotted bleed stator at 50% streamline.

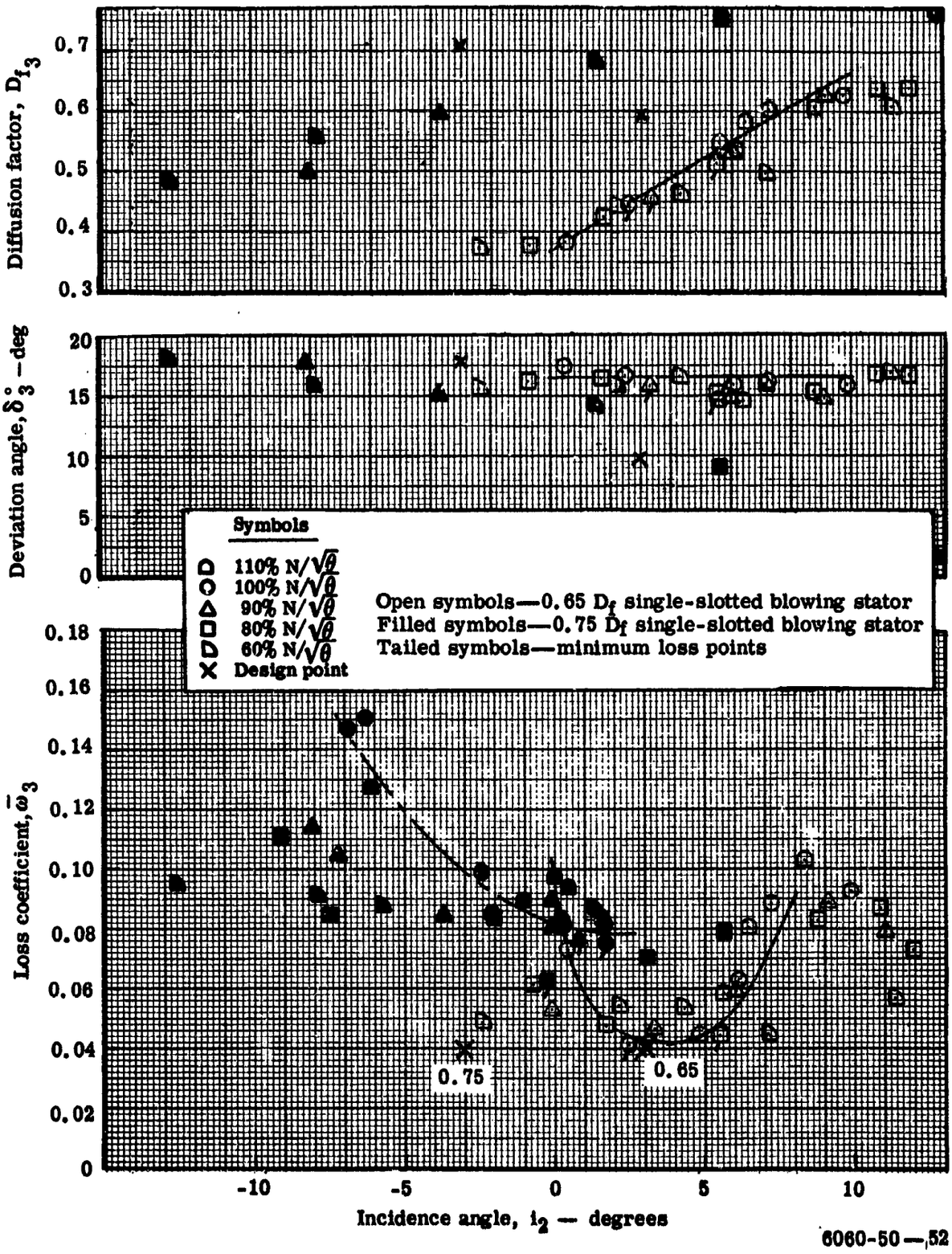

Figure 30a. Blade element performance—effect of loading—0.65 D_f single-slotted blowing stator vs 0.75 D_f single-slotted blowing stator at 50% streamline.

Symbols

- 110% $N/\sqrt{\theta}$
- 100% $N/\sqrt{\theta}$
- 90% $N/\sqrt{\theta}$
- 80% $N/\sqrt{\theta}$
- 60% $N/\sqrt{\theta}$
- Design point

Open symbols—0.65 D_f single-slotted blowing stator
Filled symbols—0.75 D_f single-slotted blowing stator
Tailed symbols—minimum loss points

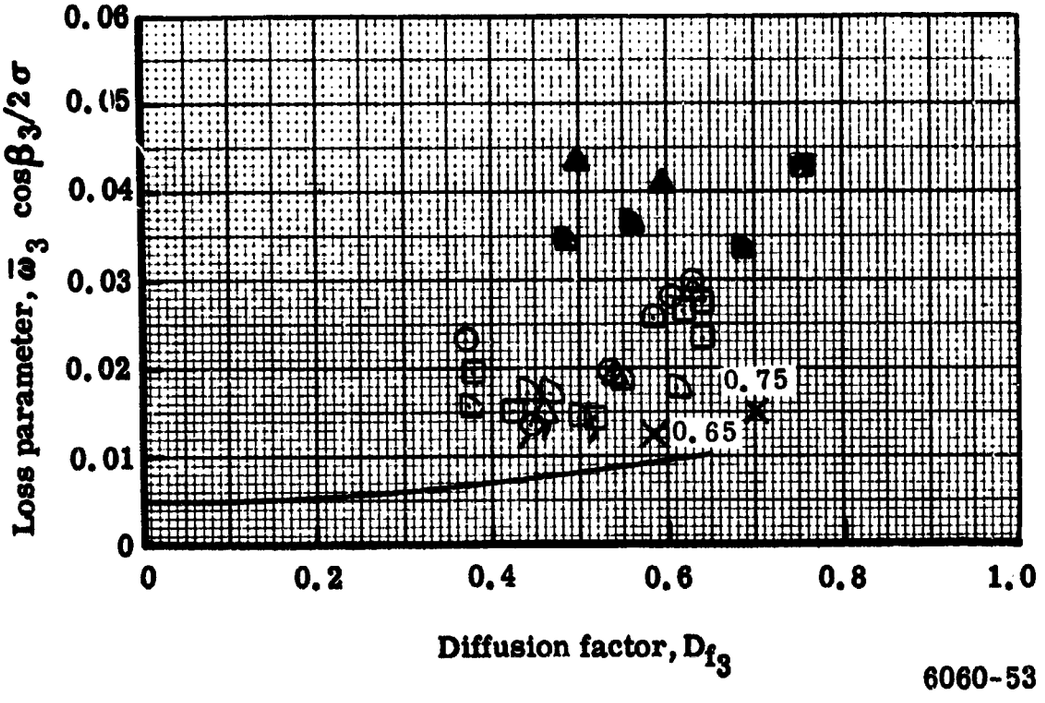

Figure 30b. Loss parameter vs diffusion factor—effect of loading—0.65 D_f single-slotted blowing stator vs 0.75 D_f single-slotted blowing stator at 50% streamline.

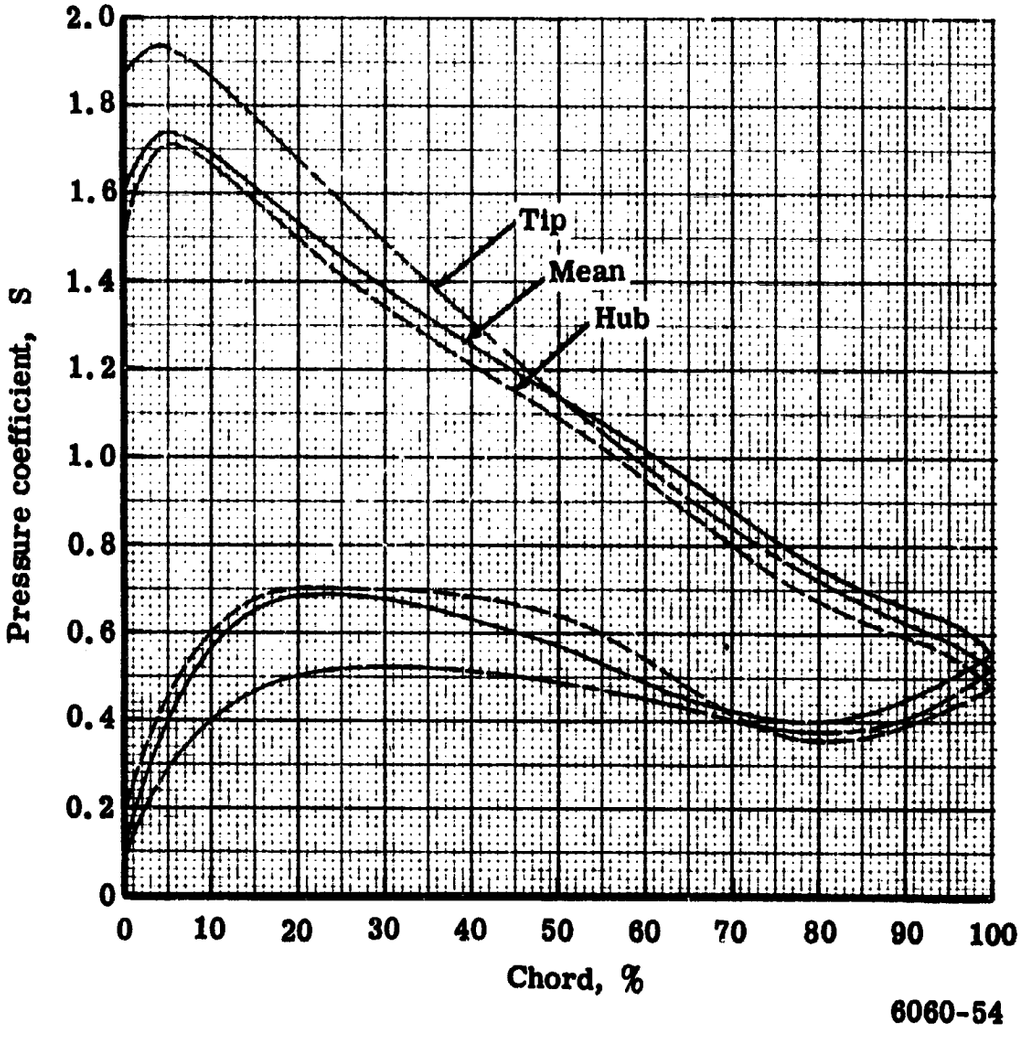

Figure 31. 0.65 D_f stator—pressure coefficient distribution (extrapolated from cascade data).

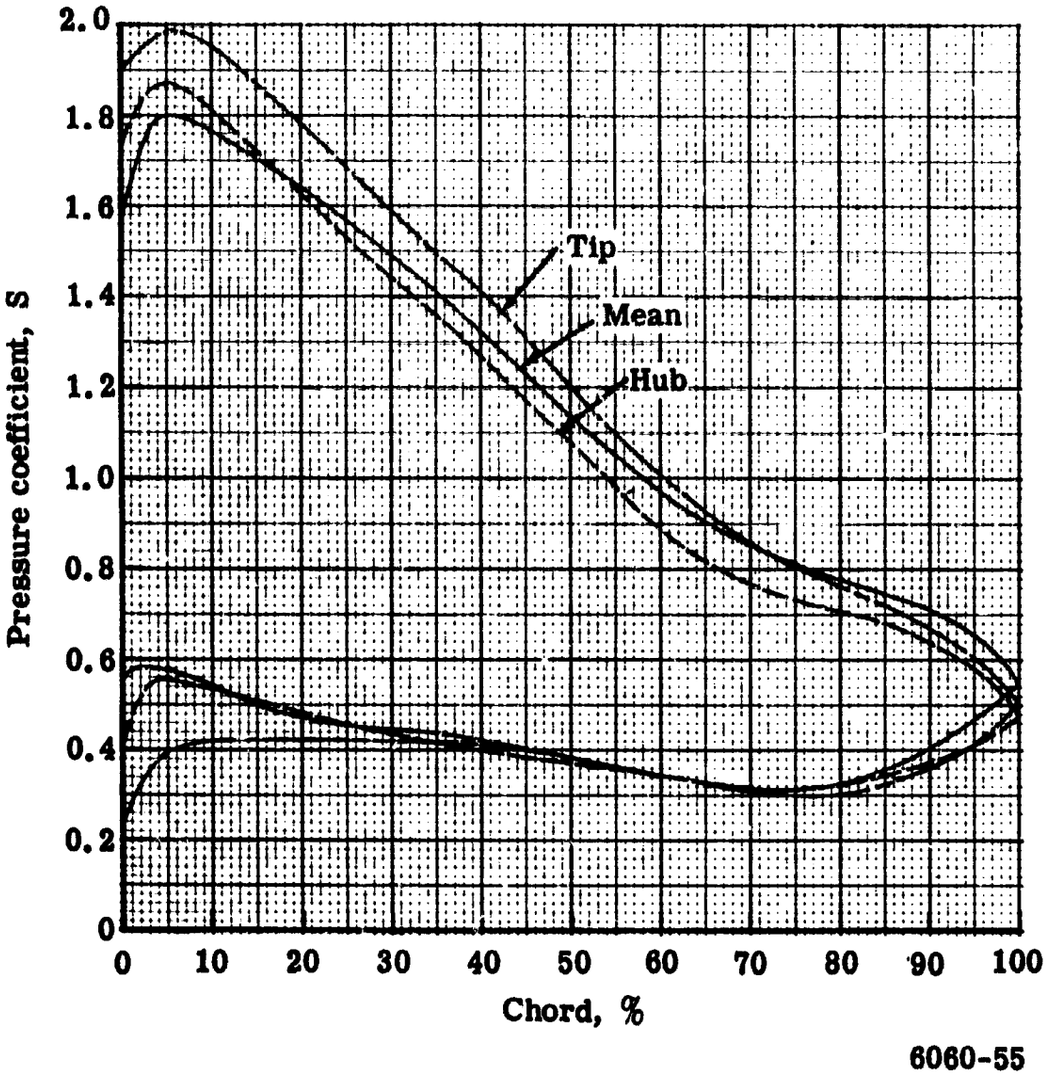

Figure 32. 0.75 D_f stator—pressure coefficient distribution (extrapolated from cascade data).

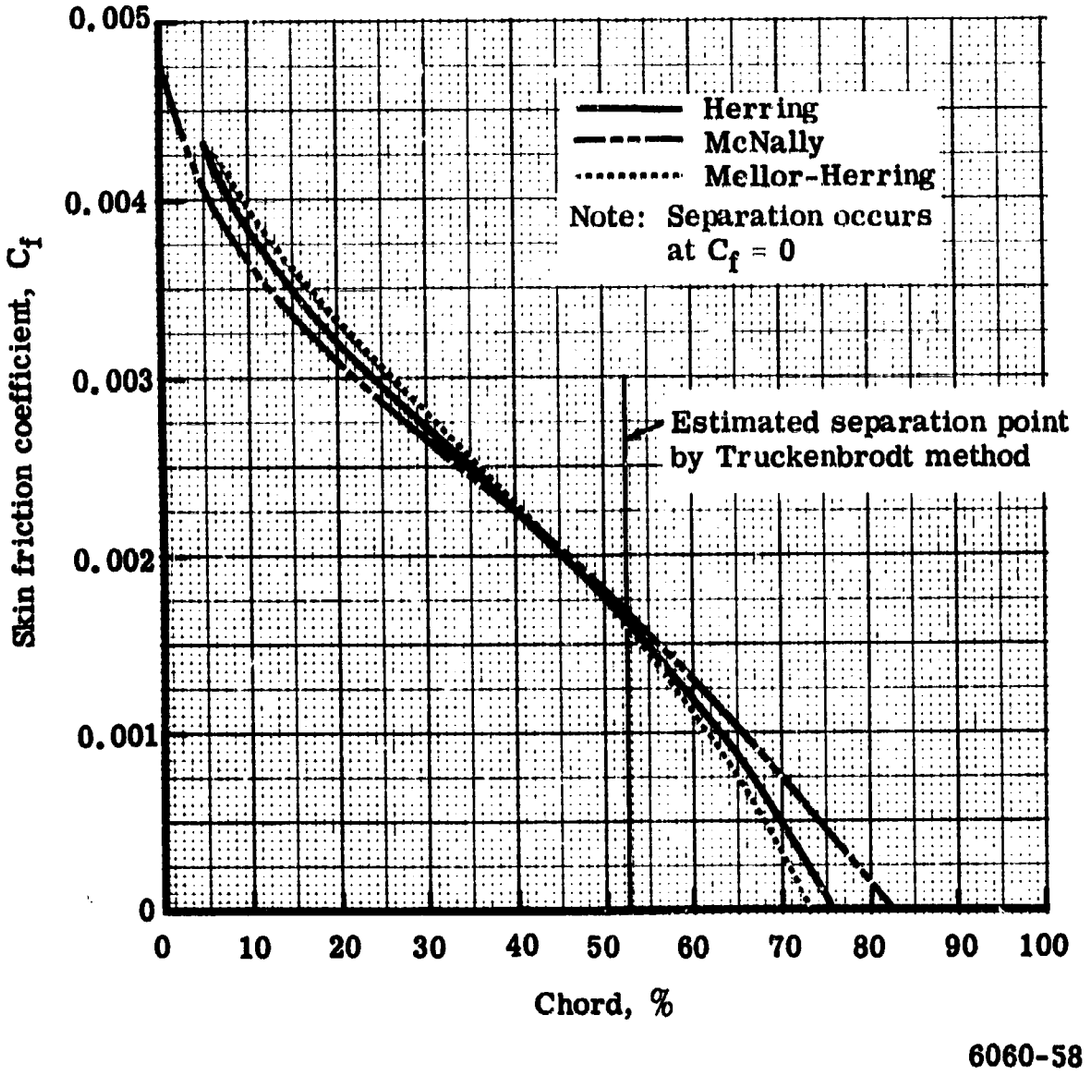

Figure 33. Comparison of the analytic methods used to predict boundary layer separation—0.65 D_f stator—10% annulus height.

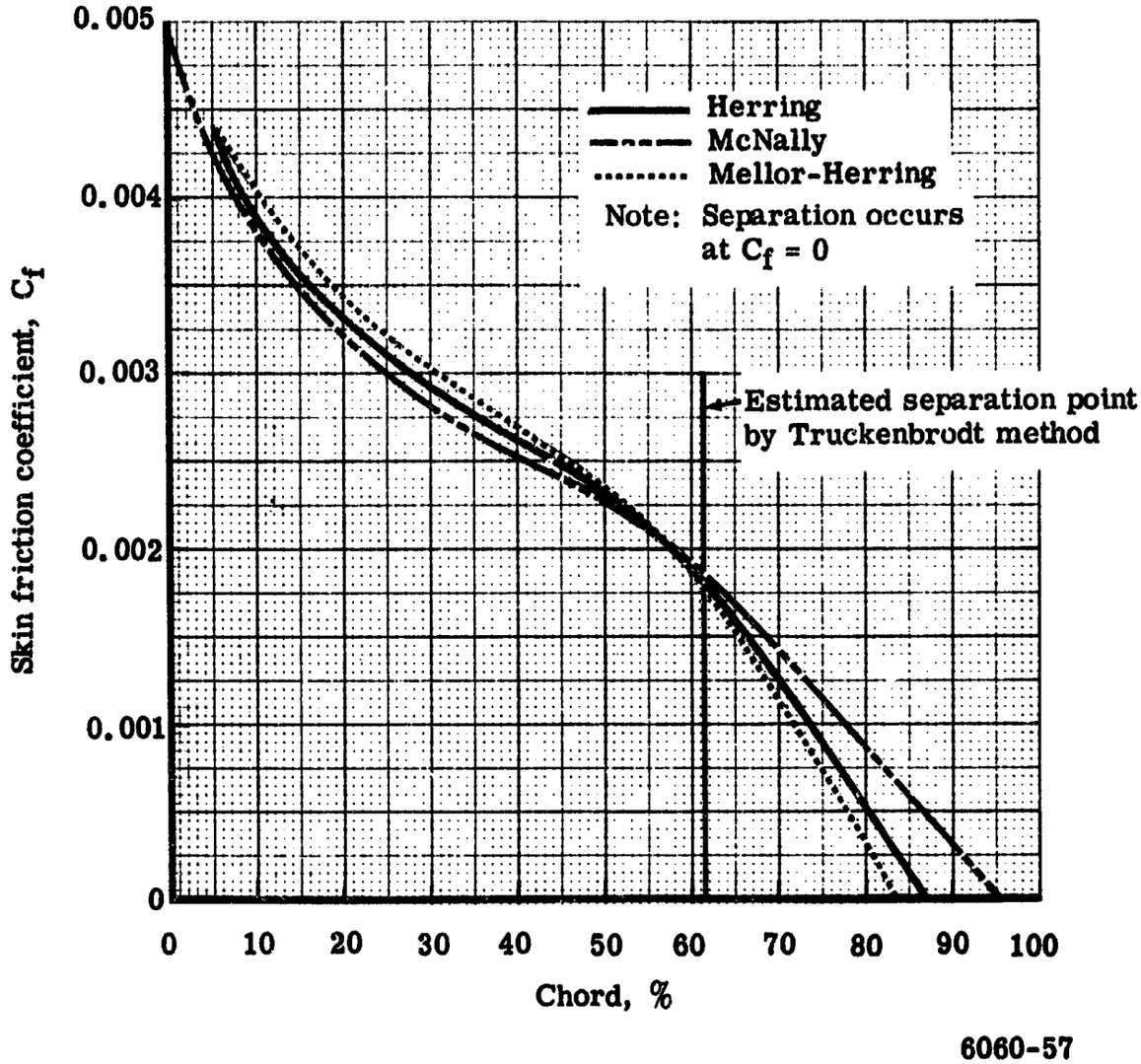

Figure 34. Comparison of the analytic methods used to predict boundary layer separation— 0.65 D_f stator—50% annulus height.

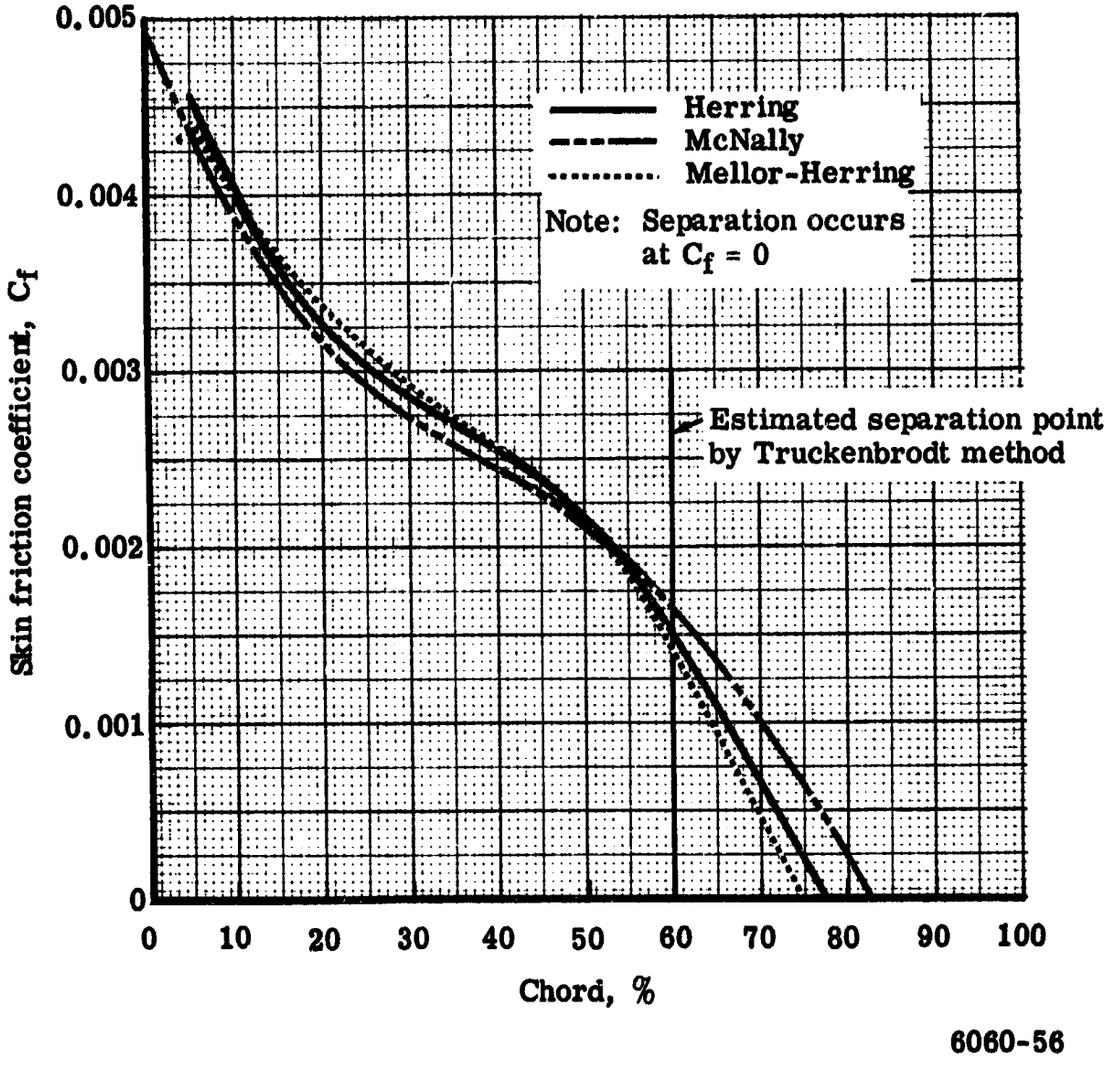

Figure 35. Comparison of the analytic methods used to predict boundary layer separation— 0.65 D_f stator—90% annulus height.

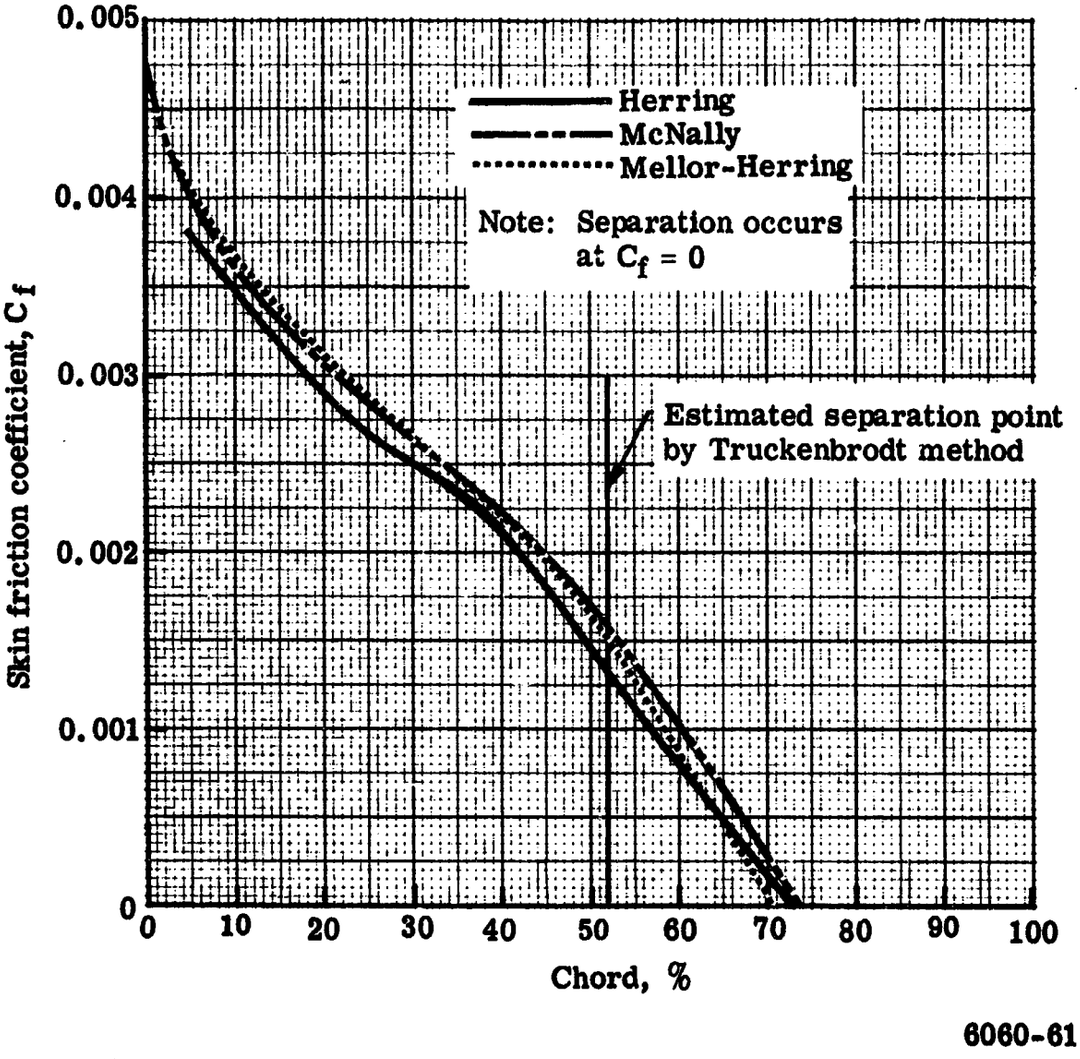

Figure 36. Comparison of the analytic methods used to predict boundary layer separation— 0.75 D_f stator—10% annulus height.

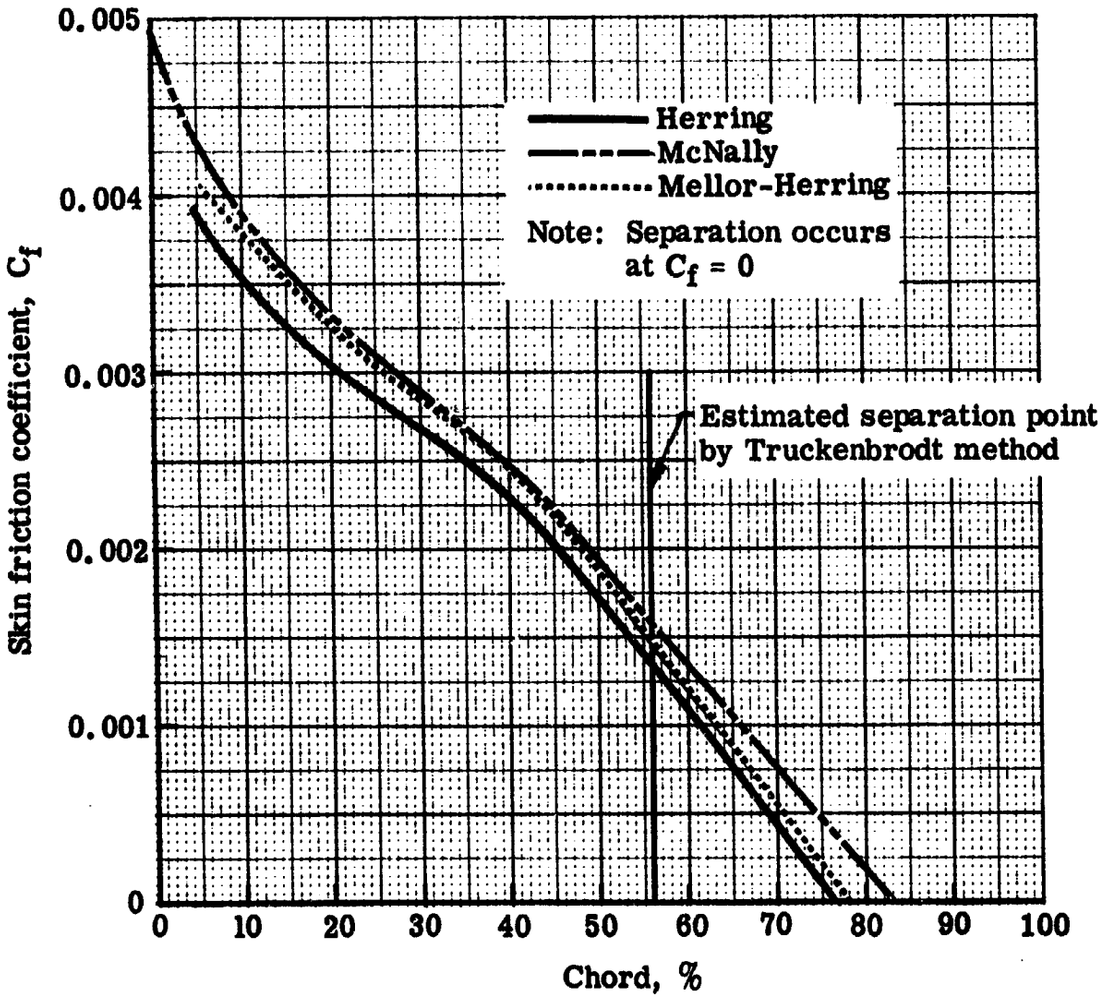

Figure 37. Comparison of the analytic methods used to predict boundary layer separation— 0.75 D_f stator—50% annulus height.

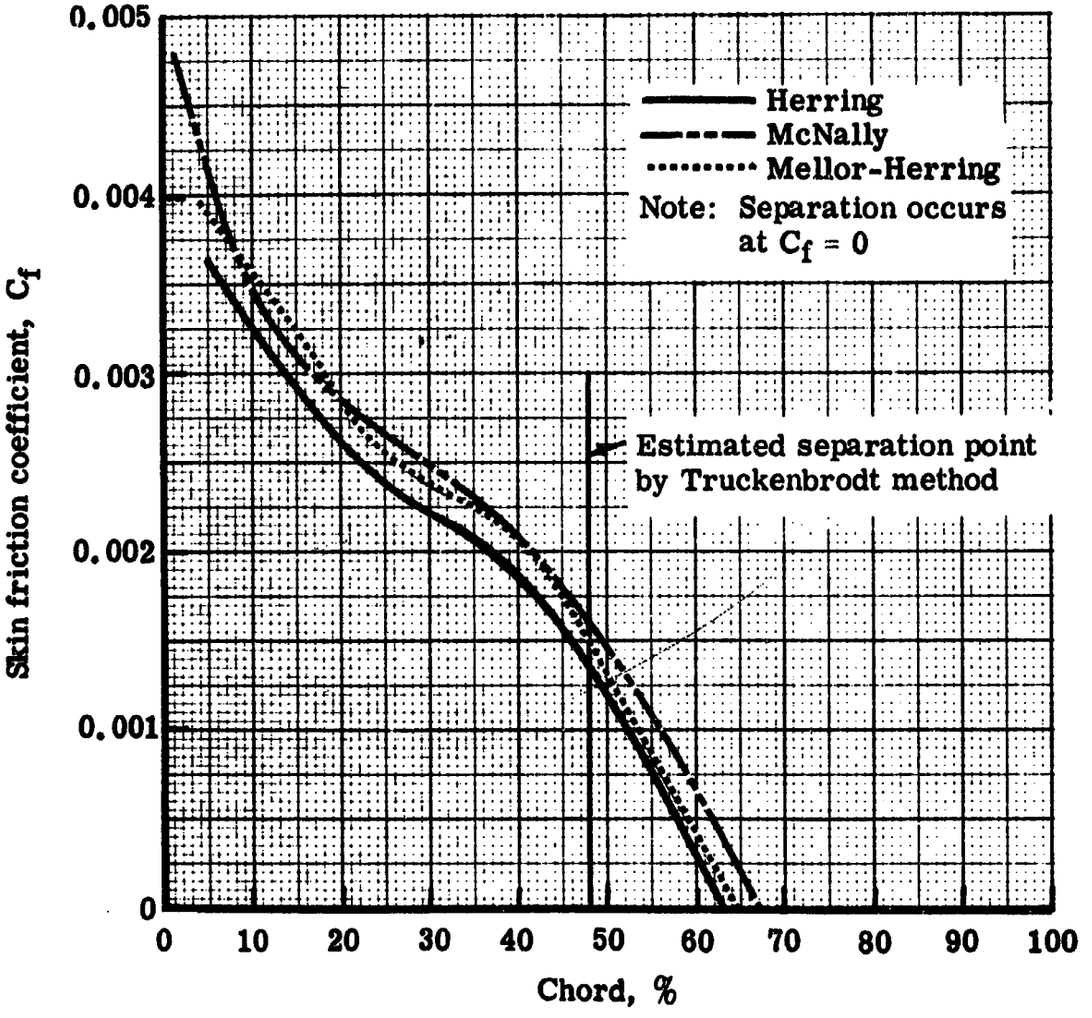

6060-59

Figure 38. Comparison of the analytic methods used to predict boundary layer separation— 0.75 D_f stator—90% annulus height.

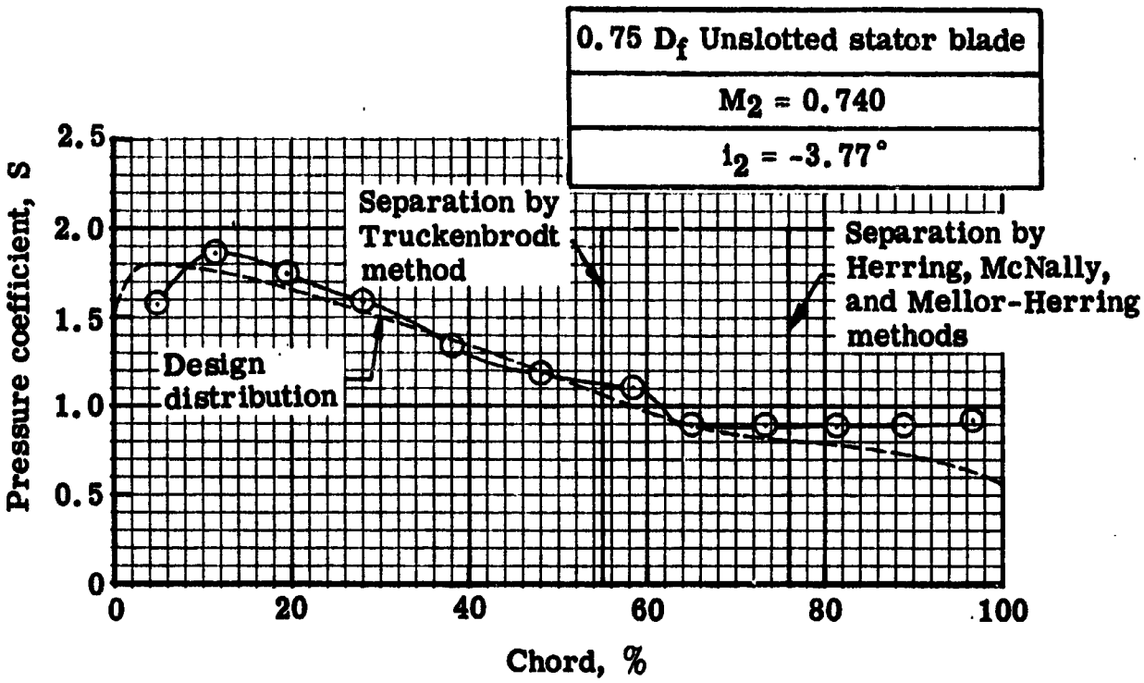

Figure 39a. 0.75 D_f stator—experimental pressure coefficient distribution—50% annulus height.

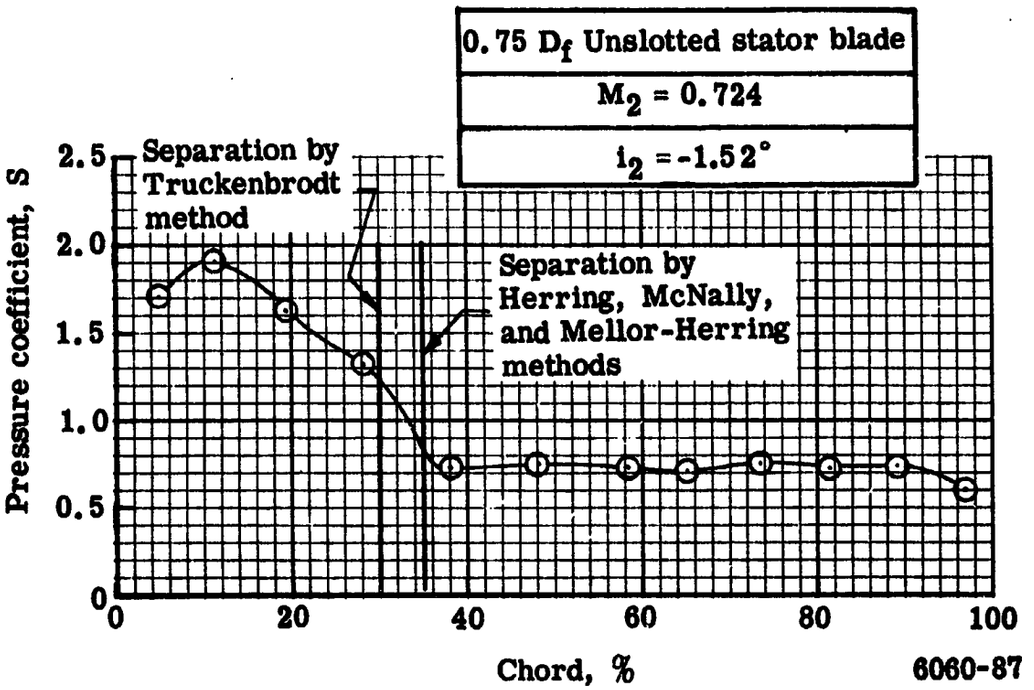

Figure 39b. 0.75 D_f stator—experimental pressure coefficient distribution—90% annulus height.

Table I.
Stator aerodynamic and blade geometric properties.

c = 3.00 inches, t/c = 10%

D_{1h}	R_3 (inches)	ϕ (degrees)	$\gamma°$ (degrees)	σ	i_2 (degrees)	$\delta_3°$ (degrees)	s (inches)	M_2	α_2 (degrees)	α_3 (degrees)
0.75	10.64	74.8	19.5	1.705	-3	17.9	1.759	0.748	56.9	-17.9
	11.66	72.2	18.4	1.556	↓	17.7	—	0.701	54.5	-17.7
	12.55	70.7	17.65	1.446	↓	17.7	2.075	0.666	53.0	-17.7
	13.82	70.2	17.0	1.313	↓	18.1	—	0.626	52.1	-18.1
	15.00	72.4	16.1	1.210	↓	20.1	2.480	0.600	52.3	-20.1
0.65	10.64	37.4	32.25	1.705	+3	9.3	1.759	0.748	50.9	13.5
	11.66	37.6	29.7	1.556	↓	9.3	—	0.701	48.5	10.9
	12.55	38.0	28.0	1.446	↓	9.5	2.075	0.666	47.0	9.0
	13.82	39.3	26.45	1.313	↓	10.2	—	0.626	46.1	8.8
	15.00	42.4	25.10	1.210	↓	11.6	2.480	0.599	46.3	3.9

6060-3

Table II.

Stator exit circumferential rake probe angles used for tests of stator blade configurations.

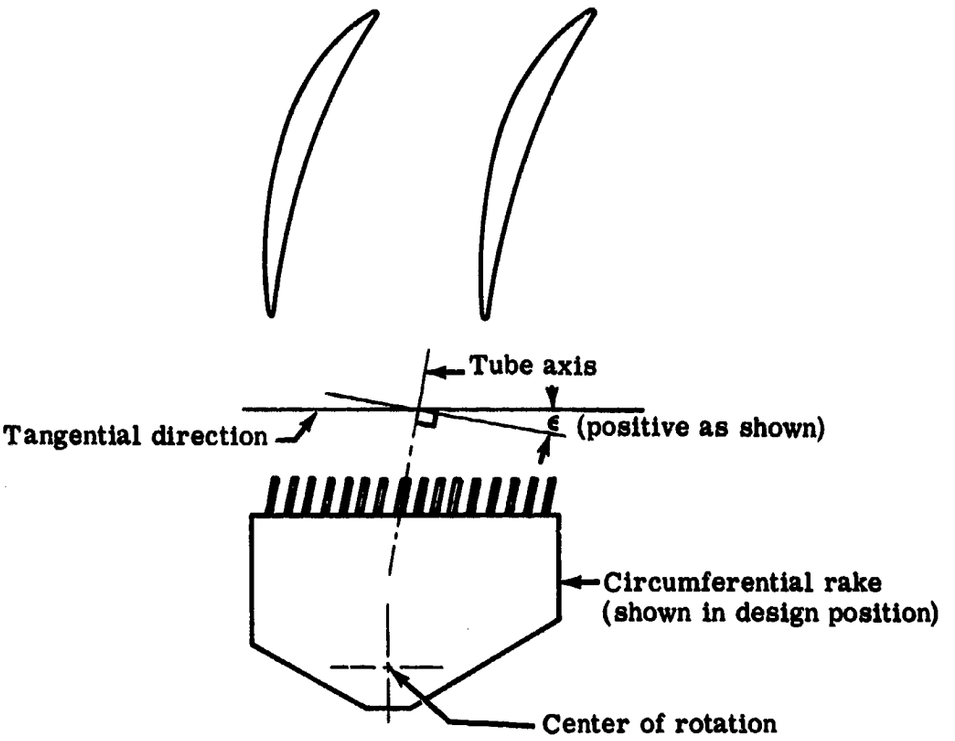

Stator configuration	Rake setting angle, ϵ
0.75 D_f unslotted [4]	-9° and -7°
0.75 D_f triple-slotted bleed [6]	-9°
0.75 D_f single-slotted blowing [3]	-7°
0.75 D_f double-slotted blowing [8]	-8°
0.65 D_f single-slotted bleed [5]	+19° and +28°
0.65 D_f single-slotted blowing [7]	+19°
Design rake angle for 0.65 and 0.75 D_f	9° 26'

Notes: (1) Superscripts denote references.

(2) The 0.75 D_f unslotted stator was tested twice and at slightly different rake angles. The 0.65 D_f single-slotted bleed stator also was tested twice. The initial rake setting angle was at 19°. Based on yaw probe measurements at Station 3, a 28° rake setting angle was selected for the second test.

6060-12

Table IIIa.

Blade element performance-0.75 D_f unslotted stator.

50% annulus height
Optimum wall bleed

$\%N/\sqrt{\theta}$	99.92	99.90	99.96	99.71	89.97	90.03	89.90	80.00
$W_a\sqrt{\theta}/\delta$	96.12	93.99	93.23	89.67	92.13	87.50	82.70	79.51
$R_{c,ST}$	1.25	1.34	1.35	1.40	1.19	1.27	1.31	1.21
$\eta_{ad,ST}$	77.06	81.48	86.72	87.25	76.94	88.62	87.88	91.27
β_2	41.954	49.582	49.433	51.497	40.783	46.379	51.132	46.412
β_3	-4.080	-4.430	-4.781	-4.430	-5.656	-5.131	-4.781	-5.481
V_2	821.67	798.74	792.02	765.61	730.20	712.34	705.07	633.82
V_3	628.26	533.81	490.61	467.64	544.53	467.27	427.36	425.58
$V_{z,2}$	611.06	517.87	515.08	476.63	552.91	491.43	442.45	437.00
$V_{z,3}$	626.67	532.21	489.90	466.24	541.87	465.40	425.87	423.64
$V_{\theta,2}$	549.31	608.11	601.65	599.14	476.96	515.68	548.96	459.09
$V_{\theta,3}$	-44.70	-41.24	-40.89	-36.12	-53.67	-41.79	-35.62	-40.65
M_2	0.7336	0.7032	0.7064	0.6895	0.6639	0.6419	0.6326	0.5735
M_3	0.5482	0.4590	0.4261	0.4094	0.4858	0.4123	0.3747	0.3792
$\Delta\beta_S$	46.033	54.012	54.214	55.927	46.439	51.510	55.913	51.894
$\bar{\omega}_3$	0.0601	0.0418	0.0435	0.0541	0.0436	0.0266	0.0340	0.0230
$D_{f,3}$	0.4896	0.6175	0.6658	0.6810	0.5098	0.6192	0.6854	0.6058
$\bar{\omega}_3 \cos\beta_3/2\sigma$	0.0211	0.0146	0.0153	0.0190	0.0153	0.0093	0.0119	0.0081
i_2	-10.75	-3.12	-3.27	-1.20	-11.92	-6.32	-1.57	-6.29
δ^*_3	13.670	13.320	12.969	13.320	12.094	12.619	12.969	12.269

6060-63

Table IIIa. (continued)

Blade element performance-0.75 D_f unslotted stator.

50% annulus height
Optimum wall bleed

$\%N/\sqrt{\theta}$	79.86	79.94	59.94	59.97	60.02
$W_a\sqrt{\theta}/\delta$	75.51	70.36	66.25	61.17	57.57
$R_{c,ST}$	1.23	1.26	1.09	1.11	1.12
$\eta_{ad,ST}$	90.28	86.19	85.86	88.97	86.91
β_2	49.050	53.450	39.879	44.552	48.749
β_3	-5.131	-4.956	-6.005	-5.481	-5.481
V_2	631.45	616.79	487.40	473.18	469.88
V_3	392.38	366.93	347.49	314.06	299.15
$V_{z,2}$	413.85	367.31	374.03	337.20	309.82
$V_{z,3}$	390.81	365.56	345.58	312.62	297.78
$V_{\theta,2}$	476.92	495.49	312.51	331.96	353.27
$V_{\theta,3}$	-35.09	-31.70	-36.36	-30.00	-28.57
M_2	0.5693	0.5535	0.4429	0.4286	0.4246
M_3	0.3477	0.3231	0.3129	0.2819	0.2677
$\Delta\beta_S$	54.181	58.406	45.885	50.033	54.230
$\bar{\omega}_3$	0.0306	0.0431	0.0283	0.0289	0.0241
$D_{f,3}$	0.6637	0.7056	0.5387	0.6053	0.6491
$\bar{\omega}_3 \cos\beta_3/2\sigma$	0.0107	0.0151	0.0099	0.0101	0.0084
i_2	-3.65	0.75	-12.82	-8.15	-3.95
δ^*_3	12.619	12.794	11.745	12.269	12.269

6060-64

Table IIIa. (continued)

Blade element performance-0.75 D_f unslotted stator.

50% annulus height

		Mean wall bleed		Minimum wall bleed	
$\%N/\sqrt{\theta}$	99.94	99.88	99.88	99.93	99.93
$W_a\sqrt{\theta}/\delta$	97.01	93.74	87.85	96.46	94.01
$R_{c,ST}$	1.23	1.35	1.40	1.23	1.34
$\eta_{ad,ST}$	70.12	85.31	85.05	69.08	84.53
β_2	42.122	48.182	53.596	42.489	49.181
β_3	-4.080	-4.781	-4.606	-4.080	-6.005
V_2	782.83	771.20	769.31	780.99	765.44
V_3	623.11	508.02	471.83	640.44	551.56
$V_{z,2}$	580.63	514.21	456.56	575.91	510.38
$V_{z,3}$	621.53	506.25	470.31	638.82	548.54
$V_{\theta,2}$	525.06	574.75	619.18	527.52	570.44
$V_{\theta,3}$	-44.33	-42.34	-37.89	-45.56	-57.71
M_2	0.7152	0.6971	0.6792	0.7148	0.6934
M_3	0.5570	0.4472	0.4055	0.5743	0.4882
$\Delta\beta_S$	46.202	52.963	53.202	46.568	54.186
$\bar{\omega}_2$	0.0650	0.0440	0.0593	0.0627	0.0395
$D_{f\,3}$	0.4598	0.6226	0.6870	0.4380	0.5680
$\bar{\omega}_3\cos\beta_3/2\sigma$	0.0228	0.0154	0.0208	0.0220	0.0138
i_2	-10.58	-4.52	0.90	-10.21	-4.52
δ^*_3	13.670	12.969	13.144	13.670	11.745

6060-65

Table IIIb.

Blade element performance-0.75 D_f triple-slotted bleed stator.

50% annulus height
Optimum wall bleed
Optimum stator bleed

$\%N/\sqrt{\theta}$	109.80	99.81	99.81	99.83	99.69	89.87	89.85	89.83
$W_a\sqrt{\theta}/\delta$	100.01	96.55	94.13	88.55	85.80	92.05	87.17	81.58
$R_{c,ST}$	1.40	1.21	1.35	1.40	1.42	1.19	1.28	1.32
$\eta_{ad,ST}$	79.63	65.74	86.66	84.05	83.22	73.76	88.29	88.25
β_2	51.424	43.729	50.652	56.297	58.994	40.034	48.347	54.657
β_3	-7.020	-6.451	-7.400	-7.210	-6.451	-7.939	-8.296	-7.580
V_2	900.06	803.44	784.65	775.70	746.17	717.43	703.44	697.04
V_3	556.07	599.78	486.14	437.96	421.62	518.49	430.83	400.95
$V_{z,2}$	561.24	580.58	497.48	430.43	384.37	549.31	467.52	403.21
$V_{z,3}$	551.90	595.98	482.09	434.50	418.95	513.52	426.32	397.44
$V_{\theta,2}$	703.65	555.38	606.78	645.32	639.55	461.48	525.60	568.58
$V_{\theta,3}$	-67.96	-67.39	-62.61	-54.97	-47.37	-71.61	-62.16	-52.89
M_2	0.7826	0.7321	0.7064	0.6925	0.6711	0.6625	0.6424	0.6343
M_3	0.4675	0.5334	0.4256	0.3794	0.3684	0.4690	0.3840	0.3559
$\Delta\beta_S$	58.444	50.180	58.052	63.507	65.445	47.972	56.643	62.237
$\bar{\omega}_3$	0.0245	0.0382	0.0172	0.0296	0.0506	0.0348	0.0253	0.0130
$D_{f\,3}$	0.6836	0.5260	0.6804	0.7528	0.7587	0.5386	0.6813	0.7383
$\bar{\omega}_3\cos\beta_3/2\sigma$	0.0086	0.0133	0.0060	0.0103	0.0177	0.0121	0.0088	0.0045
i_2	-1.28	-8.97	-2.05	3.60	6.29	-12.67	-4.35	1.96
δ_3	10.730	11.299	10.350	10.540	11.299	9.811	9.454	10.170

Table IIIb. (continued)

Blade element performance-0.75 D_f triple-slotted bleed stator.

50% annulus height
Optimum wall bleed
Optimum stator bleed

$\%N/\sqrt{\theta}$	89.87	79.93	79.90	79.87	59.94
$W_a\sqrt{\theta}/\delta$	79.23	85.30	78.87	73.90	56.43
$R_{c,ST}$	1.34	1.15	1.22	1.25	1.13
$\eta_{ad,ST}$	87.35	78.43	90.32	90.42	86.95
β_2	57.189	40.260	47.880	53.087	51.300
β_3	-7.400	-8.117	-8.296	-7.939	-8.830
V_2	703.71	652.73	633.79	624.52	467.50
V_3	394.14	448.94	402.02	356.49	276.15
$V_{z,2}$	381.32	498.11	425.07	375.09	292.30
$V_{z,3}$	390.86	444.45	397.82	353.08	272.87
$V_{\theta,2}$	591.45	421.83	470.11	499.33	364.85
$V_{\theta,3}$	-50.76	-63.39	-58.01	-49.24	-42.39
M_2	0.6385	0.5944	0.5728	0.5683	0.4208
M_3	0.3488	0.4027	0.3576	0.3181	0.2466
$\Delta\beta_S$	64.589	48.377	56.176	61.026	60.129
$\bar{\omega}_3$	0.0130	0.0373	0.0134	0.0146	0.0158
$D_{f\,3}$	0.7608	0.5736	0.6587	0.7380	0.7156
$\bar{\omega}_3 \cos\beta_3/2\sigma$	0.0045	0.0130	0.0047	0.0051	0.0055
i_2	4.49	-12.44	-4.82	0.39	-1.40
δ_3	10.350	9.633	9.454	9.811	8.920

6060-67

Table IIIb. (continued)

Blade element performance-0.75 D_f triple-slotted bleed stator.

50% annulus height
Optimum wall bleed
Mean stator bleed

$\%N/\sqrt{\theta}$	99.89	79.88	79.83	79.77	79.71	59.89	59.92	59.91
$W_a\sqrt{\theta}/\delta$	88.34	84.78	78.68	71.95	65.89	66.21	61.11	49.10
$R_{c,ST}$	1.40	1.16	1.22	1.25	1.27	1.09	1.11	1.15
$\eta_{ad,ST}$	84.13	81.16	91.19	88.92	84.22	85.64	90.44	85.43
β_2	56.814	38.804	48.347	55.289	59.435	37.202	45.140	59.083
β_3	-6.261	-6.641	-6.830	-6.830	-6.451	-8.652	-8.296	-6.830
V_2	763.46	644.33	625.02	624.90	618.77	486.94	473.16	471.23
V_3	437.04	465.47	402.04	361.61	351.79	333.44	300.62	261.63
$V_{z,2}$	420.12	502.12	415.40	355.84	314.66	387.85	333.76	242.11
$V_{z,3}$	434.43	462.35	399.19	359.05	349.56	329.65	297.47	259.77
$V_{\theta,2}$	637.48	403.78	467.01	513.69	532.79	294.42	335.39	404.27
$V_{\theta,3}$	-47.67	-53.83	-47.81	-43.01	-39.52	-50.16	-43.38	-31.12
M_2	0.6862	0.5915	0.5697	0.5576	0.5517	0.4390	0.4251	0.4206
M_3	0.3815	0.4207	0.3602	0.3166	0.3076	0.2977	0.2674	0.2309
$\Delta\beta_S$	62.876	45.445	55.178	62.119	65.886	45.855	53.436	65.913
$\bar{\omega}_3$	0.0416	0.0444	0.0188	0.0232	0.0342	0.0222	0.0195	0.0235
Df 3	0.7431	0.5273	0.6464	0.7346	0.7567	0.5640	0.6461	0.7697
$\bar{\omega}_3 \cos\beta_3/2\sigma$	0.0145	0.0155	0.0066	0.0081	0.0120	0.0077	0.0068	0.0082
i_2	3.91	-13.90	-4.35	2.59	6.73	-15.50	-7.56	6.38
δ^*_3	11.489	11.109	10.920	10.920	11.299	9.098	9.454	10.920

Table IIIc.

Blade element performance-0.75 D_f double-slotted blowing stator.

50% annulus height
Optimum wall bleed

$\%N/\sqrt{\theta}$	109.92	109.87	109.85	100.06	100.00	99.90	89.91	89.69
$W_a\sqrt{\theta}/\delta$	99.90	99.74	99.47	93.63	92.31	90.40	91.50	87.07
$R_{c,ST}$	1.25	1.39	1.43	1.36	1.38	1.39	1.20	1.27
$\eta_{ad,ST}$	61.09	79.88	84.04	86.15	87.04	86.91	75.65	87.13
β_2	43.816	49.231	52.402	50.680	52.020	53.863	43.087	49.329
β_3	-3.328	-1.842	-2.398	-1.842	-2.212	-2.212	-1.842	-1.842
V_2	884.92	888.54	884.79	804.67	804.17	803.44	743.21	735.42
V_3	667.92	585.22	533.44	502.07	489.14	480.92	559.81	487.66
$V_{z,2}$	638.53	580.23	539.83	509.88	494.88	473.80	542.78	479.29
$V_{z,3}$	666.80	584.91	532.98	501.81	488.77	480.56	559.52	487.41
$V_{\theta,2}$	612.67	672.94	701.03	622.51	633.86	648.86	507.69	557.79
$V_{\theta,3}$	-38.77	-18.81	-22.32	-16.14	-18.88	-18.57	-17.99	-15.67
M_2	0.7807	0.7753	0.7706	0.7024	0.7002	0.6970	0.6583	0.6430
M_3	0.5748	0.4960	0.4500	0.4263	0.4139	0.4056	0.4873	0.4179
$\Delta\beta_S$	47.144	51.073	54.800	52.522	54.232	56.076	44.929	51.171
$\bar{\omega}_3$	0.1018	0.0632	0.0643	0.0643	0.0581	0.0518	0.0892	0.0496
$D_{f\,3}$	0.5041	0.6151	0.6846	0.6551	0.6772	0.6935	0.4955	0.6111
$\bar{\omega}_3 \cos\beta_3/2\sigma$	0.0357	0.0222	0.0226	0.0226	0.0204	0.0182	0.0313	0.0174
i_2	-8.88	-3.47	-0.30	-2.02	-0.68	1.16	-9.61	-3.37
δ_3	14.422	15.908	15.352	15.908	15.538	15.538	15.908	15.908

Table IIIc. (continued)

Blade element performance-0.75 D_f double-slotted blowing stator.

50% annulus height
Optimum wall bleed

$\%N/\sqrt{\theta}$	89.93	79.93	79.92	80.00	79.90	59.97	59.96	59.93
$W_a\sqrt{\theta}/\delta$	82.27	83.92	77.55	75.13	70.16	65.07	59.52	56.47
$R_{c,ST}$	1.32	1.16	1.22	1.24	1.26	1.09	1.12	1.13
$\eta_{ad,ST}$	89.40	80.19	89.36	89.88	87.87	82.20	89.00	89.39
β_2	53.901	42.495	48.406	50.978	56.082	41.714	47.023	48.781
β_3	-1.842	-1.657	-1.287	-1.103	-1.657	-1.103	-0.734	-0.918
V_2	731.95	668.29	646.13	643.68	631.56	497.27	484.56	474.31
V_3	438.34	496.81	426.64	405.31	367.65	359.39	321.05	314.60
$V_{z,2}$	431.25	492.76	428.94	405.27	352.41	371.20	330.33	312.54
$V_{z,3}$	438.12	496.60	426.54	405.23	367.50	359.32	321.02	314.56
$V_{\theta,2}$	591.41	451.44	483.22	500.08	524.10	330.89	354.52	356.77
$V_{\theta,3}$	-14.09	-14.36	-9.58	-7.80	-10.63	-6.92	-4.11	-5.04
M_2	0.6369	0.5890	0.5655	0.5633	0.5502	0.4372	0.4243	0.4127
M_3	0.3732	0.4318	0.3674	0.3487	0.3144	0.3134	0.2786	0.2714
$\Delta\beta_S$	55.743	44.151	49.693	52.081	57.739	42.817	47.757	49.699
$\bar{\omega}_3$	0.0433	0.0950	0.0599	0.0517	0.0522	0.0791	0.0654	0.0540
$D_{f,3}$	0.6920	0.5011	0.6079	0.6478	0.7156	0.5161	0.5977	0.6049
$\bar{\omega}_3 \cos\beta_3/2\sigma$	0.0152	0.0334	0.0211	0.0182	0.0183	0.0278	0.0230	0.0190
i_2	1.20	-10.21	-4.29	-1.72	3.38	-10.99	-5.68	-3.92
δ^*_3	15.908	16.093	16.463	16.647	16.093	16.647	17.016	16.832

Table IIIc. (continued)

Blade element performance-0.75 D_f double-slotted blowing stator.

50% annulus height
Optimum wall bleed

$\%N/\sqrt{\theta}$	59.93	59.96
$W_a\sqrt{\theta}/\delta$	51.32	47.47
$R_{c,ST}$	1.15	1.15
$\eta_{ad,ST}$	88.38	83.93
β_2	55.861	59.708
β_3	-2.027	-1.287
V_2	473.65	485.12
V_3	285.59	274.12
$V_{z,2}$	265.81	244.70
$V_{z,3}$	285.41	274.05
$V_{\theta,2}$	392.03	418.89
$V_{\theta,3}$	-10.10	-6.16
M_2	0.4111	0.4219
M_3	0.2453	0.2359
$\Delta\beta_S$	57.889	60.995
$\bar{\omega}_3$	0.0622	0.0551
$D_{f\,3}$	0.6956	0.7430
$\bar{\omega}_3 \cos\beta_3/2\sigma$	0.0219	0.0194
i_2	3.16	7.01
δ^*_3	15.723	16.463

6060-71

Table IIId.

Blade element performance-0.75 D_f single-slotted blowing stator.

50% annulus height
Optimum wall bleed

$\%N/\sqrt{\theta}$	89.89	89.96	79.96	59.88	59.96	59.73
$W_a\sqrt{\theta}/\delta$	91.42	88.57	65.58	64.49	60.66	52.65
$R_{c,ST}$	1.19	1.25	1.27	1.09	1.11	1.14
$\eta_{ad,ST}$	74.46	84.31	84.30	80.21	85.19	90.22
β_2	44.547	48.979	58.319	39.958	44.743	54.115
β_3	0.000	-2.620	-8.640	0.476	-1.760	-3.480
V_2	731.22	734.39	632.05	488.47	487.68	475.89
V_3	547.12	499.34	363.32	361.70	339.59	291.60
$V_{z,2}$	521.13	482.01	331.94	374.43	346.39	278.95
$V_{z,3}$	547.12	498.81	359.19	361.69	339.43	291.06
$V_{\theta,2}$	512.95	554.07	537.86	313.71	343.29	385.57
$V_{\theta,3}$	0.00	-22.83	-54.58	3.00	-10.43	-17.70
M_2	0.6567	0.6428	0.5425	0.4367	0.4260	0.4154
M_3	0.4828	0.4282	0.3064	0.3208	0.2940	0.2520
$\Delta\beta_S$	44.547	51.599	66.959	39.482	46.503	57.595
$\bar{\omega}_3$	0.1137	0.0843	0.0786	0.0947	0.0910	0.0841
$D_{f\,3}$	0.4984	0.5963	0.7548	0.4832	0.5587	0.6852
$\bar{\omega}_3 \cos\beta_3/2\sigma$	0.0400	0.0296	0.0273	0.0333	0.0320	0.0295
i_2	-8.15	-3.72	5.62	-12.74	-7.96	1.41
δ^*_3	17.750	15.130	9.110	18.226	15.990	14.270

Table IIIe.

Blade element performance-0.65 D_f single-slotted blowing stator.

50% annulus height
Optimum wall bleed

$\%N/\sqrt{\theta}$	109.83	109.90	99.89	99.82	99.91	99.77	99.85	89.95
$W_a\sqrt{\theta}/\delta$	100.08	99.43	96.38	95.59	93.53	90.22	86.77	87.35
$R_{c,ST}$	1.43	1.45	1.27	1.32	1.36	1.39	1.41	1.27
$\eta_{ad,ST}$	80.82	82.99	75.04	82.87	85.43	85.34	84.44	84.56
β_2	52.281	53.141	47.124	49.190	52.788	53.885	56.532	49.986
β_3	23.000	23.000	25.924	25.064	24.204	25.064	24.376	24.376
V_2	864.59	862.38	817.03	802.12	795.22	731.25	752.01	723.66
V_3	553.97	528.47	621.56	574.18	519.48	464.16	437.42	512.62
$V_{z,2}$	528.94	517.30	555.92	524.23	480.92	460.48	414.71	465.29
$V_{z,3}$	509.93	486.46	559.02	520.11	473.81	420.45	398.43	466.93
$V_{\theta,2}$	683.91	690.00	598.75	607.11	633.32	631.12	627.33	554.25
$V_{\theta,3}$	216.45	206.49	271.73	243.24	212.98	196.63	180.53	211.57
M_2	0.7566	0.7534	0.7175	0.7066	0.6912	0.6799	0.6523	0.6340
M_3	0.4695	0.4469	0.5330	0.4939	0.4393	0.3927	0.3693	0.4398
$\Delta\beta_S$	29.281	30.141	21.200	24.126	28.584	28.821	32.156	25.610
$\bar{\omega}_3$	0.0582	0.0801	0.0735	0.0418	0.0624	0.0885	0.0925	0.0468
$D_{f\,3}$	0.5494	0.5843	0.3800	0.4437	0.5326	0.6014	0.6272	0.4581
$\bar{\omega}_3\cos\beta_3/2\sigma$	0.0188	0.0259	0.0232	0.0133	0.0200	0.0282	0.0296	0.0150
i_2	5.60	6.46	0.44	2.51	6.11	7.20	9.85	3.31
δ^*_3	14.550	14.550	17.474	16.614	15.754	16.614	15.926	15.926

6060-73

Table IIIe. (continued)

Blade element performance-0.65 D_f single-slotted blowing stator.

50% annulus height
Optimum wall bleed

$\%N/\sqrt{\theta}$	89.94	89.92	79.92	79.94	79.95	79.97	79.93	79.87
$W_a\sqrt{\theta}/\delta$	83.32	79.65	82.42	79.32	74.34	70.28	66.59	63.44
$R_{c,ST}$	1.31	1.33	1.18	1.21	1.24	1.26	1.27	1.28
$\eta_{ad,ST}$	87.78	87.83	83.70	86.96	88.49	87.25	85.74	83.70
β_2	52.682	55.725	45.916	48.381	52.164	55.434	57.503	58.651
β_3	23.344	23.344	24.720	24.892	23.688	23.688	25.236	25.064
V_2	701.19	706.18	654.85	646.77	638.86	622.38	626.48	627.80
V_3	456.89	409.62	500.63	473.90	426.29	367.79	357.78	360.33
$V_{z,2}$	425.09	397.69	455.59	429.56	391.88	353.11	336.58	326.61
$V_{z,3}$	419.49	376.09	454.76	429.88	390.37	336.80	323.63	326.40
$V_{\theta,2}$	557.65	583.55	470.39	483.51	504.55	512.51	528.38	536.15
$V_{\theta,3}$	181.04	162.31	209.36	199.47	171.26	147.76	152.54	152.64
M_2	0.6116	0.6140	0.5789	0.5660	0.5555	0.5389	0.5401	0.5395
M_3	0.3900	0.3484	0.4364	0.4084	0.3647	0.3126	0.3028	0.3040
$\Delta\beta_S$	29.338	32.381	21.196	23.439	28.476	31.746	32.267	33.587
$\bar{\omega}_3$	0.0598	0.0890	0.0619	0.0477	0.0444	0.0829	0.0868	0.0730
D_{f3}	0.5373	0.6297	0.3757	0.4217	0.5162	0.6151	0.6399	0.6408
$\bar{\omega}_3\cos\beta_3/2\sigma$	0.0193	0.0287	0.0198	0.0152	0.0143	0.0267	0.0276	0.0232
i_2	6.00	9.05	−0.76	1.70	5.48	8.75	10.82	11.97
δ^*_3	14.894	14.894	16.270	16.442	15.238	15.238	16.786	16.614

Table IIIe. (continued)

Blade element performance-0.65 D_f single-slotted blowing stator.

50% annulus height
Optimum wall bleed

$\%N/\sqrt{\theta}$	59.94	59.90	59.92	59.92	59.99
$W_a\sqrt{\theta}/\delta$	63.76	59.60	56.85	53.38	47.70
$R_{c,ST}$	1.10	1.12	1.13	1.14	1.15
$\eta_{ad,ST}$	83.85	86.99	88.37	90.85	82.89
β_2	44.263	48.842	50.962	53.773	58.030
β_3	24.032	24.376	25.064	24.376	25.408
V_2	493.39	476.93	472.88	468.46	468.06
V_3	376.21	343.14	333.33	320.92	279.63
$V_{z,2}$	353.34	313.89	297.84	276.86	247.83
$V_{z,3}$	343.60	312.55	301.95	292.31	252.58
$V_{\theta,2}$	344.36	359.08	367.30	377.90	397.06
$V_{\theta,3}$	153.21	141.62	141.21	132.45	119.98
M_2	0.4322	0.4191	0.4144	0.4094	0.4070
M_3	0.3269	0.2989	0.2895	0.2779	0.2409
$\Delta\bar{p}_S$	20.231	24.466	25.898	29.397	32.622
$\bar{\omega}_3$	0.0490	0.0541	0.0539	0.0452	0.0567
$D_{f,2}$	0.3737	0.4409	0.4632	0.4992	0.6107
$\bar{\omega}_3\cos\beta_3/2\sigma$	0.0157	0.0173	0.0172	0.0145	0.0180
i_2	-2.42	2.16	4.28	7.09	11.35
δ^*_3	15.582	15.926	16.614	15.926	16.958

6060-75

Table IIIf.

Blade element performance-0.65 D_f single-slotted bleed stator.

50% annulus height
Optimum wall bleed
Optimum stator bleed

$\%N/\sqrt{\theta}$	109.79	109.82	99.75	99.77	79.87	79.99	59.90	59.90
$W_a\sqrt{\theta}/\delta$	99.59	98.66	94.88	87.67	71.43	68.59	59.22	49.47
$R_{c,ST}$	1.44	1.46	1.35	1.39	1.26	1.27	1.12	1.15
$\eta_{ad,ST}$	82.62	83.38	87.95	83.97	91.49	88.10	93.01	88.10
β_2	51.311	52.217	49.328	54.721	52.142	54.471	47.547	55.945
β_3	17.291	18.678	16.772	19.026	15.736	18.678	15.736	16.599
V_2	867.82	867.26	803.31	768.49	621.44	624.79	479.59	462.92
V_3	551.35	532.26	497.33	442.27	337.01	350.57	308.34	254.97
$V_{z,2}$	542.47	531.35	523.53	443.85	381.38	363.08	323.72	259.23
$V_{z,3}$	526.43	504.22	476.18	418.11	324.38	332.10	296.78	244.34
$V_{\theta,2}$	677.38	685.43	609.27	627.35	490.65	508.47	353.86	383.53
$V_{\theta,3}$	163.87	170.46	143.51	144.19	91.40	112.27	83.62	72.84
M_2	0.7508	0.7512	0.7026	0.6650	0.5410	0.5436	0.4196	0.4027
M_3	0.4615	0.4444	0.4214	0.3712	0.2871	0.2986	0.2668	0.2190
$\Delta\beta_S$	34.020	33.539	32.557	35.695	36.406	35.792	31.811	39.346
$\bar{\omega}_3$	0.0132	0.0288	0.0077	0.0320	0.0067	0.0182	0.0278	0.0366
$D_{f\,3}$	0.5727	0.5951	0.5848	0.6456	0.6836	0.6619	0.5552	0.6852
$\bar{\omega}_3\cos\beta_3/2\sigma$	0.0044	0.0096	0.0026	0.0106	0.0023	0.0061	0.0094	0.0123
i_2	4.63	5.54	2.65	8.04	5.46	7.79	0.87	9.26
δ^*_3	8.841	10.228	8.322	10.576	7.286	10.228	7.286	8.149

6060-76

Table IIIf. (continued)

Blade element performance-0.65 D_f single-slotted bleed stator.

50% annulus height
Optimum wall bleed

	2/3 optimum stator bleed		1/3 optimum stator bleed		
$\%N/\sqrt{\theta}$	99.62	59.88	99.85	99.82	79.81
$W_a\sqrt{\theta}/\delta$	87.34	47.50	92.72	85.93	66.97
$R_{c,ST}$	1.40	1.15	1.37	1.40	1.26
$\eta_{ad,ST}$	84.31	86.61	87.21	82.53	84.48
β_2	54.516	55.174	51.515	54.973	55.248
β_3	19.200	22.214	17.291	20.621	19.911
V_2	764.86	473.02	795.91	776.48	629.21
V_3	459.73	274.12	511.03	462.27	374.48
$V_{z,2}$	443.98	270.14	495.30	445.66	358.67
$V_{z,3}$	434.15	253.78	487.93	432.65	352.10
$V_{\theta,2}$	622.81	398.30	623.02	635.85	516.98
$V_{\theta,3}$	151.19	103.64	151.89	162.81	127.54
M_2	0.6602	0.4083	0.6913	0.6654	0.5405
M_3	0.3863	0.2340	0.4317	0.3856	0.3161
$\Delta\beta_S$	35.316	32.959	34.225	34.352	35.337
$\bar{\omega}_3$	0.0413	0.0665	0.0200	0.0522	0.0389
$D_{f\,3}$	0.6158	0.6321	0.5661	0.6189	0.6225
$\bar{\omega}_3 \cos\beta_3/2\sigma$	0.0137	0.0216	0.0067	0.0172	0.0129
i_2	7.84	8.49	4.84	8.29	8.57
δ^*_3	10.750	13.764	8.841	12.171	11.461

6060-77

Table IV.

Stator blade element performance summary.

Design corrected speed
50% streamline blade element

Configuration	$i_{2,\ min}$ (deg)	$\varpi_{3,\ min}$	$D_{f_{3,\ min}}$	$\delta^{\circ}_{3,\ min}$ (deg)	$i_{2,\ neg}$ (deg)	$i_{2,\ pos}$ (deg)	$D_{f_{3,\ pos}}$	Δi_2 (deg)
0.75 D_f unslotted	-5.0	0.042	0.64	13.0	-14.4*	1.5	0.71*	15.9
0.75 D_f triple-slotted bleed								
Optimum bleed rate	-0.5	0.014	0.70	10.0	-13.5*	7.0	0.77	20.5
Mean bleed rate	-1.4	0.026	0.68	11.0*	-13.6*	6.3	0.76	19.9
Zero bleed rate	1.0	0.091	---	---	- 9.1	5.3	---	14.4
0.75 D_f single-slotted blowing	2.0	0.078	---	---	- 5.6	---	---	---
0.75 D_f Double-slotted blowing	1.2	0.052	0.70	15.5	- 6.8	4.9	0.74*	11.7
0.65 D_f Single-slotted bleed								
Optimum bleed rate	3.0	0.007	0.58	8.0	- 3.6	9.0*	0.68*	12.6
2/3 Optimum bleed rate	2.7	0.014	0.54	---	- 6.2*	8.8*	0.63*	15.0
1/3 Optimum bleed rate	2.0	0.010	0.52	8.0*	- 2.8*	8.4*	0.63	11.2
0.65 D_f single-slotted blowing	3.7	0.042	0.47	16.5	0*	8.0	0.62	8.0

*Values obtained by extrapolating data.